January 2015

Analysis and Energy Reduction of Humanoid Robot Motions – Stand Up and Sit Down

Ercan Elibol
University of South Florida, ercan@mail.usf.edu

Analysis and Energy Reduction of Humanoid Robot Motions – Stand Up and Sit Down

by

Ercan Elibol

A dissertation submitted in partial fulfillment
of the requirements for the degree of
Doctor of Philosophy in Electrical Engineering
Department of Electrical Engineering
College of Engineering
University of South Florida

Co-Major Professor: Wilfrido Moreno, Ph.D.
Co-Major Professor: Alfredo Weitzenfeld, Ph.D.
Paris Wiley, Ph.D.
Ismail Uysal, Ph.D.
Rob Hooker, Ph.D.
Fernando Falquez, Ph.D.
William S. Quillen, Ph.D.

Date of Approval:
June 9, 2015

Keywords: joint, power, center of mass, center of pressure, biped

DEDICATION

I would like to dedicate this work to my family

ACKNOWLEDGMENTS

I would like to express my appreciation and gratitude to Dr. Alfredo Weitzenfeld and Dr. Wilfrido Moreno for their guidance, inspiration, and vision in helping me to complete this dissertation. It was a privilege to work under their direction.

I would like to thank Juan Calderon and Martin Llofriu for their support and encouragement in helping me achieve this objective.

I would like to thank my family for their unconditional support and encouragement.

I would like to acknowledge that this work is funded by NSF IIS Robust Intelligence research collaboration grant #1117303 at University of South Florida and University of Arizona entitled “Investigations of the Role of Dorsal versus Ventral Place and Grid Cells during Multi-Scale Spatial Navigation in Rats and Robots,” and supported in part by the “Agencia Nacional de Investigación e Innovación (ANII)”.

TABLE OF CONTENTS

LIST OF TABLES

LIST OF FIGURES

ABSTRACT

This research studies the electrical power reduction and control analysis of various motion tasks of a humanoid robot. These motions include standing up and sitting down. Each motion's tasks have their stable and unstable phases throughout the complete motion cycle. Unstable phases can be caused by gravity forces and improper handling of the upper body of the humanoid robot leaning too forward or backward. Even though most of the dynamic motions seem to be accomplished very simply by humans; standing up and sitting down could create challenges for humanoid robots. Some of the critical challenges researches face are: dynamic nature of motions, humanoid robot joint coordination, whole body balance, stability of the model, limited energy source, energy saving techniques and modeling. Dynamic motions of humanoid robots can be modeled and analyzed to reduce electrical power use. In order to accomplish such energy savings, a researcher needs to study the kinematics, dynamics of a humanoid, and motion tasks with given constraints. The robot in this research is modeled as a planar humanoid robot. All motion tasks of a humanoid robot are characterized in terms of motion variables. These motion variables include joint angular positions, joint angular velocity, joint angular acceleration, humanoid robot center of mass (CoM) position, velocity and acceleration change and center of pressure (CoP) position change. All mathematical models are completed so that electrical power analysis of each task produce comparable results. Humanoid robot joint cost functions related to energy consumption are used to define joint input electrical power used, joint mechanical power used, joint mechanical power dispersion and joint power loss due to torque required.

In this research, a 4-link 3-joint humanoid is modeled for standing up and sitting down tasks. For each task, kinematics and dynamics models are created, motion constraints are found, energy and power usage analysis for whole robot and for individual joint motors are accomplished. By finding the best energy usage per motion variable, humanoid robot used less input electrical power to accomplish the motion task.

CHAPTER 1: INTRODUCTION

In the last few decades, robotic research and advancement have extended from traditional industrial manipulators to contain autonomous humanoid robots. Advancement in humanoid robots have produced many significant accomplishments. These advancements are due to improvements in other areas, such as computer technology, motor actuation and control, sensor technologies and other enabling technologies. Research being developed on humanoid robots and other legged robots has been growing. Humanoid research includes many areas from different disciplines contributing to the development of the overall autonomous humanoid research.

A robot in general can be a complex mechanical system to work with. A humanoid robot's dynamic and kinematic complexities are even bigger than most of the service they render compared to other mobile robots. Humanoid robots need to be autonomous all the time. New materials, technologies and chemistry have allowed the development of better subsystems of humanoid robots. For example, battery units now weigh less, are smaller in size and last longer in general usage. Even though results obtained are improving, they are not enough for an autonomous humanoid robot to perform complex for an extended period of time before the need to recharge the battery. Dynamic actions are the most energy consuming tasks for a humanoid. Inevitably, there is a need to determine what is the humanoid robot's least possible use of energy to complete a given task. As the energy efficiency increases, the autonomy of the humanoid robot will also increase.

Overall humanoid robot mechanical design and control is an important criteria for better energy usage. After a humanoid robot is put together physically, the motion task quality is dependent on the controller. A well designed humanoid robot control system prevents the robot from unstable motions, configurations, deliver energy efficient motions with better joint velocities, trajectories, and adapt to environmental changes and disturbances.

Using limited energy provided to a humanoid robot by a battery unit is a challenging problem. Autonomous humanoid robot are made of many different parts. Sensors such as vision, infrared, force

sensing sensors and sonar; collect environmental data and transmit the data to the robot controllers. DC motors transform the electrical energy to mechanical energy, which enables the humanoid to accomplish its dynamic motions, such as standing up, walking, and sitting down. Energy consumption of a humanoid robot happens not only because of dynamic motion creation and execution but also because of the humanoid robot's other subcomponent power demands for sensing, controlling and communicating between parts. Despite this fact it is important to investigate that all components can be managed to reach reduced energy consumption, since DC motor activation and control consumes the most energy required by many dynamic and static motions tasks. [1]

Most of the energy consumption of a joint DC motor depends on the motor angular velocity, angular acceleration and angular deceleration. Each joint has a different energy consumption profile depending on the dynamic motions and given motion variables. Each joint energy consumption profile is studied for energy performance used, lost energy, current consumption and input power demand.

Energy consumption saving is particularly important in humanoid robots having extensive degrees of freedoms (DoF) where even a simple humanoid robot can consist of over 10 DC motors between its ankles and hip [2] [3]. This complexity of the humanoid robots makes it critical to model new strategies to study and optimize the energy consumption since energy usage increases with increasing autonomy of humanoid robots. [4]

In this research, part of the problem is to model the angular position and angular velocity of joints so that each joint electrical power consumption and overall humanoid electrical power consumption can be minimized for any dynamic tasks. In order to accomplish modeling of velocity and acceleration of the joints, their power consumptions are modeled first. Humanoid motions are characterized by these motion variables to search for values that will reduce the electrical power consumption, establish a relationship between these motion variable and individual joint energy performances for further analysis. If a humanoid robot realizes a particular tasks, it should consume minimal electrical power in total and each individual joint should operate with minimal electrical power required due to the fact that battery is only a limited energy source. On the other hand if humanoid robots use different motion variable for certain tasks in order to accomplish shorter or longer motion task times, its individual joint energy consumption and overall energy consumption will be different each time those motion variables change. In order to achieve a desired energy

consumption level, a researcher needs to take many dynamic and non-linear variables caused by motions into account and find a tradeoff point with better electrical power usage efficiency for individual joints and whole humanoid robot, as well as motion task accomplishment times (faster or slower).The desired performance of the given task will critically effect the humanoid robot power demand and energy consumption during each task.

The motion of standing up from crouch position and sitting down seem like an apparent simple and everyday motion for humans, but it is a difficult dynamic motion for biped robots. Accomplishment of these motion tasks necessitate the humanoid balance, control of the biped's CoM location and CoP location as it stands over in a small support area between both feet. It is the goal of this research study to have such a motion and better understanding of biped's dynamic, kinetic complexities and postural capabilities to analyze and reduce the humanoid's energy usage. The feet contact forces of the humanoid are recorded as it executes the motions. The CoM location of a humanoid robot represents a crucial factor, which is used as a guide for the robot. [5]

With the aim of analyzing the energy efficiency, the balance of the humanoid robot during standing up, sitting down, humanoid CoM and humanoid CoP positions are taken into consideration. A controller model that accounts for the constraints of location of CoM and CoP is presented. These constraints are used by the humanoid robot balancing and at the same time achieve better electrical power efficiency with this balanced body structure. A balanced humanoid with proper torso placement over ankles, proper positioning of CoM and CoP in humanoid robot support area, a better electrical power efficient model that saves overall energy, is achieved. The humanoid robot will avoid violating the CoM and CoP constraint by using torques required for each joint. These torques are also directly affected by other joints angular positions and angular velocities. The torques required by the controller for balancing, define the proper location of the CoM and CoP.

In general, simplified models of humanoid robots that are used to analyze the characteristics of dynamic motions have been utilized in many research topics and applications. All the models created for the kinematics and dynamics of a humanoid robot, constraints of the motions, trajectory generation and tracking, and error compensation for positions; are used in correlation with the dynamics of the humanoid robot that were not modeled. Results of these models are the undertakings driving dynamic humanoid

robots that can accomplish standing up or sitting down. All those findings face many problems which make it necessary to analyze the energy saving techniques.

Balancing is another important control problem. It is possible to achieve the balance by adjusting the CoP and CoM and at the same time ensuring that the humanoid maintains its balance. The control of humanoid standing by ankle joint approach keeps all joints fixed with the exception of the ankle joint, and balances the humanoid like an inverted pendulum. The control of hip joint approach is accomplished mainly by using the hip joints. This control can cause a relocation of the CoM backward or forward.

It is the intent of this research to investigate humanoid motions with a desired energy consumption with proper dynamic motion balance. The direction of this research is to provide alternative models to analyze and control the energy consumption on joint level as well as on humanoid robots overall. Once each joint can be analyzed independently, the energy demands of each joint can be evaluated under different dynamic conditions. With this information from each joint actuator of humanoid robots, and different dynamic motion variables, motion tasks performance expectations can be adjusted to achieve increased energy efficiency by preferred energy consumption indexes.

Energy efficient motions find the joint trajectories and determine the velocities. There may be multiple trajectories to accomplish the same motion. This study focuses on comparing the energy used by joints. Energy efficiency can be obtained by finding better joint trajectories, and velocities, without repeated accelerations. If a humanoid robot has a short trajectory that includes several accelerations, energy usage can increase. A longer trajectory could require reduced energy if there is not too much acceleration.

Experiments are setup and completed on a physical robot, Aldebaran NAO v4, which is actuated by DC motors, and has joint reduction gears, joint position, current sensors, and foot force sensitive resistors under each foot. In order to apply controllers and constraints, NAO is given the joint trajectory and angular velocity data for each task. During each task all power and energy related data is collected from the robot for further analysis. Three main joints studied with the real robots are ankle, knee and hip joints. This humanoid robot is modeled after a planar robot, 4 links for standing up and sitting down task.

1.1 Motivation

Robots have been widely used in the industrial fields and in the last couple of decades there is an increasing interest in humanoid robot design and in a variety of industries and academic fields. Using

humanoid robots with enhanced autonomous abilities in service areas, and manipulation of industrial productions are some of the future possibilities. With its ever increasing processing power and dynamic abilities, a humanoid robot will have an intelligent autonomy to interact within the environment. With its human-like appearance, a humanoid robot can easily replace many jobs that humans do every day. There is an increasing research community about the humanoid robot modeling, design and application. Different research areas are focusing on control, programming, and electrical subsystems designs. With ever increasing difficulty of its structure and control models, there is always a very critical energy consumption problem with all autonomous humanoid robots. With its limited energy resource, humanoid robots will need to use minimal electrical power with all tasks it will accomplish, and it will need to be intelligent enough to decide its motion parameters for better energy usage. In this research, the humanoid robot minimal electrical power usage is studied for certain dynamic motions.

1.2 Objective

The main objective of this dissertation is to contribute to the analysis and reduction of electrical power consumption by offering a control and analysis method to achieve simplified models that can be utilized for humanoid robot overall electrical power consumption and joint individual electrical power consumption.

First objective is to model dynamic motions of the humanoid robot with joint absolute and relative angle values. The dynamic modeling describes the motions of the humanoid robot.

Second objective is to define constraints for humanoid robot kinematic relationships between body parts, which includes feet, legs, and torso. Control algorithm is used for regulating the robot motions for analyzing the prescribed motions.

Third objective is to analyze the dynamic motions in terms of their effect on electrical power consumption per joints and on the whole humanoid robot body. With changing motion variables, electrical power consumption will change, this will provide a per joint electrical power analysis for better assessment.

Objectives of this research study can be summarize as follows:

- The improvement of the electrical power usage analysis of the humanoid robot overall and its joint DC motors individually. This improvement is based on the fact that effects of dynamic motions of multiple degrees of freedom on energy consumption is too complex to model and analyze.

- Humanoid robot dynamic motions are characterized in terms of motion variables, such as joint position, joint angular velocity and acceleration, center of mass position, CoM angular velocity and acceleration, CoP position
- Define constraints for motion variables so that humanoid robot will not violate the limits imposed for balance and stability
- In order to achieve better electrical power efficiency, search for motion variables for standing up, sitting down tasks
- Define cost functions that are defined to analyze the joint current consumption, joint input electrical power consumption, joint produced mechanical power, joint mechanical power dispersion over time, joint produced torque, joint energy loss due to torque produced
- Experiment findings on a real robot

1.3 Contribution of This Research

This research proposes an approach for the analysis and reduction of the electrical power used per joints and overall humanoid robot. Some key contributions are summarized below.

- Control aspect of the kinematic and dynamic motions for sitting down, standing up are developed
- Dynamical model is used for standing up (4-link 3-joints model)
- Development of an energy analysis method for individual joints to analyze the effect of the dynamic nature of the humanoid robot motions
- Development of an energy analysis method for the whole humanoid robot to see the effect of the motion variables on the overall energy usage
- The improvement of the electrical power usage analysis of the humanoid robot overall and its joint DC motors individually by finding the best motion variables based on the fact that effects of dynamic motions of multiple degrees of freedom on energy consumption is too complex to model and analyze

1.4 Definitions of Some Terms

The following list show some of terms used throughout the dissertation.

- Center of Mass (CoM): the mean location point of the overall weight of the humanoid
- Center of Pressure (CoP): a point where total sum of pressure acts under the foot in support area.

- Kinematic: the motion of links and joints
- Dynamic: the motion of links and joints under the action of torques
- Torque: the rotational force developed in the DC motor due to the applied electrical input power.
- Humanoid: a biped robot resembling a human in its shape
- Autonomous Robot: a robot acting independently.
- Electrical Power: the product of voltage and current at the motor input.
- Mechanical Power: the output from a DC motor, which is the product of torque and velocity.
- Degree of freedoms (DoF): a direction in which a motion can occur
- Joint: a point on the robot where two links joins together, it also represents a degree of freedom.

1.5 Organization of This Dissertation

This research includes different sections. Chapter 2 includes the literature review, Chapter 3 includes the 4-link planar humanoid model for standing up sitting down (such as humanoid dynamical modeling, center of mass location analysis, center of pressure location analysis with movement synthesis, and effective energy utilization analysis), Chapter 4 presents the model tracking control, Chapter 5 presents the mechanical and electrical power performance and evaluation, Chapter 6 presents the joint motor dynamics and control, , Chapter 7 presents the experimental setup and the results, Chapter 8 presents minimizing energy consumption with Q learning algorithm for standing up and sitting down motions, Chapter 9 shows the conclusion.

CHAPTER 2: LITERATURE REVIEW

2.1 Energy Saving Researches

Human locomotion does not seem difficult to accomplish for humans. Standing up and sitting down can become real challenges when they are implemented by humanoid robots. Operating the humanoid robot subsystems in harmony with efficient performance of the motion can be a big challenge where the weight of individual body parts, weight of the humanoid robot and individual power consumption of the parts play important roles. [6]

Efficient use of limited energy on a humanoid robot is critical because of power demand increases with robotics application especially in autonomous humanoid robotic areas. Depending on the desired performance of the tasks and environmental conditions, power demand will change. Power saving techniques have been a research topic for mobile robots for some time. Some studies try to minimize the total power usage by predicting the power usage for specific tasks and using an electrical power saving control for components [4], and some other studies worked with power management units for their mobile robots for fast charging and power management approach [7]. A conservation technique is proposed for a wheeled robot by introducing power usage reduction techniques with power controlling model and motion planning to minimize the amount of energy usage in [1].

The concept of optimization of power management of the processor is studied in [8]. Power consumption used for robot's computation for path planning, sensing algorithms, completing a task, and optimization of motor power usage couple each other. According to the study, controlling the joint motor speed and the operational frequency of the robot's CPU processor all together can provide an overall increased performance for the robot.

Study [9] attempts to limit the humanoid electrical current for each motor. This constrains how tightly the joint can follow the generated motion. The research presented uses the reduced joint dc motor electrical stiffness during humanoid motions.

The energy consumption of a DC motor is heavily effected by its angular velocity and acceleration. The problem of energy efficient navigation is presented in study [10]. An established model for the energy consumption of a DC motor is obtained. A wheeled robot is studied to reduce the electrical power used during the travel along the provided trajectory on a flat surface with an optimal velocity. Power consumption is modeled in order to compute the velocity and acceleration profile.

For humanoid robot locomotion, study [11] suggests key considerations for different energy consumption. Study remarks that mean mechanical power is the result of the torque of joint motor and load angular velocity. Even though mean power demand may be small and occur during locomotion of the humanoid robot, joints instantaneous power demand can reach high values. Study establishes an additional optimization objective relating distribution of instantaneous power around the mean power required. Mean torque consumption is an important energy consumption key indication that shows the torque consumption of all joint over a period.

There are different approaches to energy utilization based control. In some motion task studies, humanoid gaits require bended knees for better balance. This causes knee joint motors to be constantly engaged which increases the joint current consumption. Torque at the hip joints can be a driving force of body during tasks. With different motion parameters at different tilting forward angles by the humanoid torso, it was observed that energy consumption also increased. The method in study [12] is based on accurate control of actuators which give full control and applicability with expenditure of energy consumption. In that study, a model of the control system from a view point of less energy consumption is achieved by introducing and changing a control gain from the relationship between the desired energy consumption and current energy consumption. According to that study, most energy efficient walk is the passive dynamic walk, where motions depend on the relationship between gravity potential effect and the robots mechanical structure. On the other hand, stable humanoid motion tasks require actuator systems and precise control. If a robot walks without any desired performance, it should walk with minimum energy consumption, if the robot walks with desired performance, it should change its walking motion to wider step size while consuming extra energy.

In order to accomplish reduced energy usage with the genetic algorithm, study [13] used fitness functions to analyze the relationship between walking distance and energy consumption while keeping knee

joints straightforward on the stance leg to gauge the reduced energy usage. In most humanoid gaits, the robot's upper body is often kept in the vertical position to decrease overall energy consumption because location of the mean weight of the humanoid is located in the torso. This technique decreases the current consumption in ankle and hip joints, but knee joint current consumption might increase.

Different approaches have been offered to address the humanoid balance and stability problem during dynamic tasks in literature. In [5], standing up from the sitting position on a chair by using data, the has been collected from prior human demonstrations, was accomplished by a humanoid robot. In that research, a stable humanoid motion of standing up is achieved and human-like movement and speed are simulated. In study [14], an inverted pendulum model that finds the motions of how to stand up using a tiered reinforcement learning technique is shown, where a hierarchical architecture is applied on a three-links two-joints robot.

In most humanoid gaits, the robot's upper body is often kept in the vertical position to decrease energy usage since the location of the mean point of the humanoid weight is in the robot's torso. Hip joints play a critical part in reducing the biped energy utilization. Study in [15] proposed a motion generation technique for a humanoid to produce steady movement by using consumed energy as a condition, and generating a series of joint motions with a feedback technique to increase the humanoid stability.

2.2 Inverted Pendulum Researches

A humanoid robot model can be modeled as an inverted pendulum. This model simplifies the humanoid model. Researchers in [16] shows that a human reacts to forces by moving its ankle joint during a vertical stance position. This model has been frequently used to research bipedal posture, where the humanoid robot has motions in the sagittal plane direction. The ankle joint manages the torque to control the biped vertical position for balancing. [17] [18] [19] [20]

Stepping forward to escape falling is studied in [21] using Lagrangian dynamics to drive feedback control of computed constraint forces. Linear Inverted Pendulum Model is studied for bipedal locomotion research in [22] where a humanoid motion as a linear dynamic system is studied. This is also known as the cart on a table model.

The research in [23] uses the inverted pendulum model to describe humanoid robot balance and stability. The hip joint torque control approach and ankle joint torque control approach, [24], have been key

explanations of balance control in humans. Study [25] claims that ankle strategy and hip strategy take place together. The CoM position is considered as an important indicator of humanoid balance. It was also mentioned in [26] that usage of CoM velocity in addition to its location can be a better indicator of stability.

2.3 Zero Moment Point

Study [27] first published the idea of the ZMP applied to a biped for balance. Other researches on robot balance and stability are done by similar studies in [28] [29].

ZMP is a common stability criteria for humanoid dynamic balance. The published works show zero moment point used as a guide for ensuring stable motions [30]. Zero moment point ensures stability by keeping the moment of the humanoid's forces within the geometrical area of both feet. The most commonly used modeling method for a biped is the Linear Inverse Pendulum Model (LIPM) which simplifies the dynamics of a humanoid maintaining the control over the robots center of gravity (CoG) for a stable locomotion [31][32]. In order to generate a control model for locomotion, LIPM and zero moment point can be combined. In humanoid motions, when walking with a single support period, the ZMP is positioned in the middle of the support area. [33][34]

Zero moment point focuses on implementing dynamic balancing by ensuring that the moment of the forces of the humanoid remain within the humanoid's foot support area [35]. As a consequence, the contact forces from the humanoid are canceled by the ground's reaction force. The ZMP principle is well described in [36] which is focused on demonstrating humanoid motion. The zero moment point method considers dynamic and static forces. Humanoids commonly have kinematic redundancy, where there exist different connections from the ZMP reference trajectory to the joint motions. [37][38]

2.4 Center of Mass and Center of Pressure Researches

Humanoid kinematic modeling is essential for reducing the complexity of controlling the dynamic stability of a humanoid. Center of mass, center of pressure location and movement synthesis permits the controller to generate a sequence of motions and the overall robot motion can be efficiently optimized by the control techniques. Supposing that the robot's CoM is concentrated somewhere close in the torso, the humanoid model is estimated as a point mass, and a stable reference motion trajectory can be designed without comprehensive control participation. [39]

The CoP denotes the point of a matching force, which is the total of the pressure forces under the foot. It measures the inclination for the feet to rotate and leave the horizontal base. Many humanoid projects used CoP as a reference point. Although the meaning and practicality of the center of pressure has been questioned in [40], CoP is the primary measure of balance and stability for some humanoid robots [41].

2.5 Simplified Humanoid Robot Model

The purpose of the modeling of humanoid is to provide a proper description of the robot in mathematical form. Some of the real effects of the humanoid may not be taken into consideration so that a simple model can be built. If the motions require very slow velocity, inertia tensor effect in the equations of motions will not have much effect on the overall model. One of the most common simplification is to simplify the rigid links as bodies with individual center of masses on humanoid robot. By doing that, some rotational dynamics are dismissed, and do not affect the model result. DC motor actuation, joint frictions, impact of the motions, electrical losses are important effects which change with the physical humanoid robot.

2.6 Inverted Pendulum Model

The inverted pendulum method has a model which relies on feedback control [39] [42]. This model is used for bipedal control because a human walking motion can be modeled as an inverted pendulum model for the single support part. This simplified model is used to understand the dynamics in the system and determine the reference trajectories that meet with the natural dynamics [43].

By using the method, the humanoid kinematics and dynamics are estimated by an inverted pendulum. The mean mass location of the robot is considered in the robot trunk, the base of the pendulum matches with the support foot, Figure 2.1. Because this method is flexible and gait patterns can be computed online, it is used in many humanoids, such as Honda Asimo [44], HRP-2 [45], and UT-Theta [46]. See Figure 2.1 for reference.

In order to drive the equations of the motions, angular momentum of the mass and its derivative are written as follows in equations (2.1) and (2.2).

$$L_0 = mr^2\dot{\theta} \tag{2.1}$$

$$\dot{L}_0 = mr^2\ddot{\theta} \tag{2.2}$$

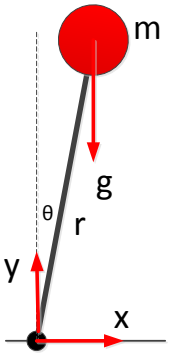

Figure 2.1 Figure of inverted pendulum method

Simplifying the equations by removing accelerations, equations (2.3) and (2.4) are obtained.

$$\dot{L}_0 = mgrsin\theta \tag{2.3}$$

$$\ddot{\theta} = \frac{g}{r} sin\theta \tag{2.4}$$

With the aim of using this model in humanoid robots, center of pressure model is used, which is described as forces acting on the feet do not cause any moment or force. This inverted pendulum model becomes useful when the humanoid robot point mass is located over the center of pressure and humanoid total mass positon is in the same position as center of mass.

2.7 Linear Inverted Pendulum Model

In this model, humanoid robot point mass is moving in parallel to the ground. Support does not have any mass and does not apply any torques at the base.

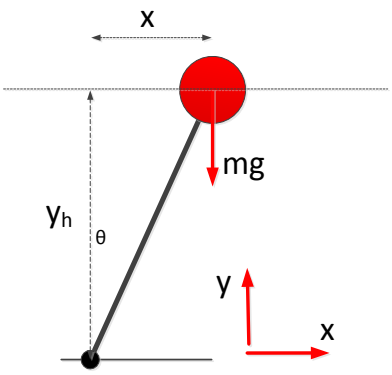

Figure 2.2 Model of linear inverted pendulum moving parallel to the ground

Vertical forces is shown in equation (2.5)

$$F_y = -mg \tag{2.5}$$

F_x is obtained by the geometric constraints imposed on the movement of the pendulum

$$\frac{F_x}{F_y} = \frac{x}{y_h} \tag{2.6}$$

Replacing equations (2.5) and (2.6) to eliminate F_y and solving for F_x

$$F_x = -\frac{mgx}{y_h} \tag{2.7}$$

The dynamics in x direction is summarized as

$$F_x = m\ddot{x} \tag{2.8}$$

Finally F_x is eliminated with equations (2.7) and (2.8)

$$\ddot{x} + x\frac{x}{y_h} = 0 \tag{2.9}$$

These calculations are simplified from the references to allow better understanding of the model. [39]

CHAPTER 3: PLANAR HUMANOID ROBOT

Dynamic modeling used in this research is to define the establishments of control algorithms of the humanoid robot motions, which are constrained in the sagittal plane, and require the humanoid robot to be modeled as planar.

3.1 Modeling of Humanoid During Standing Up and Sitting Down

The positions of the planar humanoid model for standing up and sitting motions as well as inverse pendulum model are shown in Figure 3.1. The CoM of every link is positioned at the center. The first joint of the model matches to the ankle joint, the second joint matches to the knee and the third one matches to the hip joint. Humanoid model motion starts with the crouch position as shown in Figure 3.1a, pushes its torso upward with balance and stability control with the aim of minimal energy usage (Figure 3.1b), and in the final position, it stands straight up trying to balance similar to an inverted pendulum model.

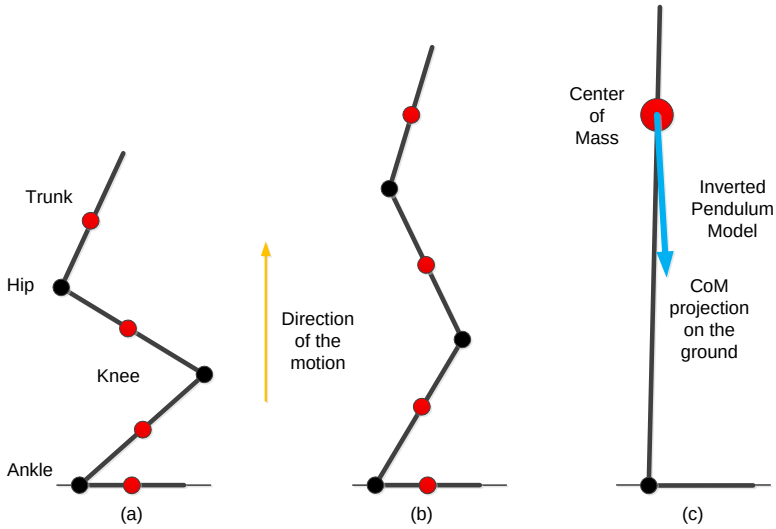

Figure 3.1 (a) and (b) show model for robot during standing up (c) shows model for stand position

3.2 Humanoid Robot Model Dynamic and Kinetic Analysis

This model consists of 4 rigid links, link 3 represents upper body, link 2 represents the thigh, link 1 shows the shank, and link 0 shows the foot, (Figure 3.2). These links are connected by rotational joints. Following assumptions are made: The foot of the model stays horizontal at all times and its weight is added

to link 1. This model represents one side of a humanoid biped model, and both sides are symmetric (left and right). This model is constrained only in the sagittal plane, friction between the humanoid feet and the horizontal surface is satisfactory enough to stop any slippage; internal friction of these joints is not taken into consideration during the model analysis.

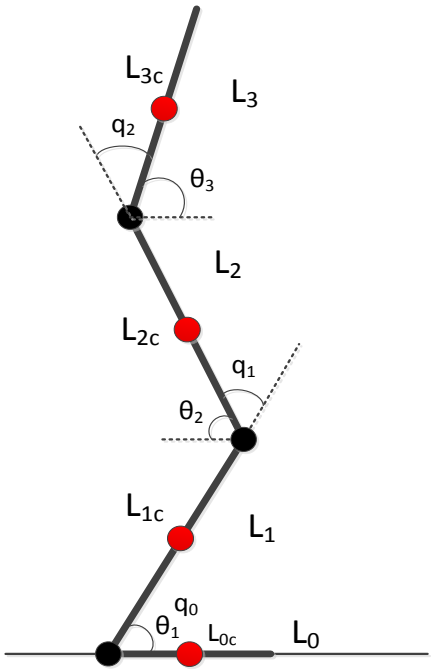

Figure 3.2 4-link planar model represented with link's center of mass (red circles) and joints (black circles)

3.3 Kinematic Model

Kinematic model of the system is defined by the CoM of every link denoted by x_{ic} which is in x direction and y_{ic} which is in y direction as shown below in equation (3.1)

$$\begin{aligned} x_{1c} &= L_{1c}\cos\theta_1 \\ y_{1c} &= L_{1c}\sin\theta_1 \\ x_{2c} &= L_1\cos\theta_1 - L_{2c}\cos\theta_2 \\ y_{2c} &= L_1\sin\theta_1 + L_{2c}\sin\theta_2 \\ x_{3c} &= L_1\cos\theta_1 - L_2\cos\theta_2 + L_{3c}\cos\theta_3 \\ y_{3c} &= L_1\sin\theta_1 + L_2\sin\theta_2 + L_{3c}\sin\theta_3 \end{aligned} \tag{3.1}$$

where L_i shows the length of the every link for the model, θ_i shows the absolute angular rotation about each joint and L_{ic} shows the center of mass location for every link from respective joint points where $i = 1,2,3$.

3.4 Center of Mass Location of the Biped Model

Coordinate of the CoM of the humanoid robot in general terms can be shown as in the following equations (3.2) and (3.3).

$$C_{CoM} = \frac{\sum m_i c_i}{\sum m_i} = \frac{\sum m_i c_i}{M} \tag{3.2}$$

$$c_i = \begin{bmatrix} x_{cm} \\ y_{cm} \end{bmatrix} \tag{3.3}$$

where m_i is each link mass, c_i is the absolute position of CoM link. CoM of the model can be expanded to be shown as the following in x and y direction as in following equations (3.4) and (3.5)

$$x_{cm} = \frac{m_1 x_{1c} + m_2 x_{2c} + m_3 x_{3c}}{m_1 + m_2 + m_3} \tag{3.4}$$

$$y_{cm} = \frac{m_1 y_{1c} + m_2 y_{2c} + m_3 y_{3c}}{m_1 + m_2 + m_3} \tag{3.5}$$

3.5 Ground Location Prediction of the Center of Mass

Development of a successful motion without falling over requires correct position data of the humanoid's CoM during implementation of motions. The humanoid's CoM must be placed above the feet during the motions to accomplish the balance. If the mass values and link CoM locations are known, the total center of mass location of the model can be found via forward kinematics [47][48].

Exact CoM trajectory management is an important factor for successful motions [49]. Therefore, in this work, the objective is not only to optimize the total energy usage, but also accurately estimate and control the humanoid's CoM motion so that its center of mass will move along the estimated trajectory which is verified experimentally.

A motionless upright humanoid simply experiences forces created by gravity. Gravitational forces are substituted by a virtual force at the CoM of the humanoid. The location vector of the humanoid's CoM can be defined with equation (3.2).

The ground location prediction of the CoM,$\mathrm{C_{FCoM}}$, is derived from $\mathrm{C_{CoM}}$, consequently it realizes the relation in equation (3.6). If $\mathrm{C_{FCoM}}$ is in the support polygon, the motionless biped will stay as it is. See Figure 3.3. [50]

$$\sum_{i=1}^{n} \left((C_{FCoM} - P_i) \times m_i g \right) = 0 \tag{3.6}$$

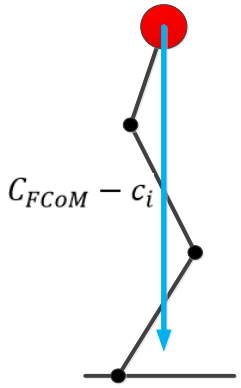

Figure 3.3 The ground location prediction of center of mass

3.6 CoM Linear Velocity of Links of the Model

CoM Linear velocity of every link is written as following from equations (3.1). For link1, location of CoM is defined by

$$x_{1c} = L_{1c}\cos\theta_1 \quad y_{1c} = L_{1c}\sin\theta_1 \tag{3.7}$$

Linear velocity of CoM of the link 1 is

$$v_{c1} = \begin{bmatrix} -L_{1c}\sin\theta_1 \\ L_{1c}\cos\theta_1 \end{bmatrix}\dot{\theta}_1 \tag{3.8}$$

For link 2, location of CoM is

$$x_{2c} = L_1\cos\theta_1 - L_{2c}\cos\theta_2 \qquad y_{2c} = L_1\sin\theta_1 + L_{2c}\sin\theta_2 \tag{3.9}$$

Linear velocity of CoM of the link 2 is

$$v_{c2} = \begin{bmatrix} -L_1\sin\theta_1 \\ L_1\cos\theta_1 \end{bmatrix}\dot{\theta}_1 + \begin{bmatrix} L_{2c}\sin\theta_2 \\ L_{2c}\cos\theta_2 \end{bmatrix}\dot{\theta}_2 \tag{3.10}$$

For link 3, location of CoM is

$$x_{3c} = L_1\cos\theta_1 - L_2\cos\theta_2 + L_{3c}\cos\theta_3 \qquad y_{3c} = L_1\sin\theta_1 + L_2\sin\theta_2 + L_{3c}\sin\theta_3 \tag{3.11}$$

Linear velocity of the link 3 CoM is

$$v_{c3} = \begin{bmatrix} -L_1\sin\theta_1 \\ L_1\cos\theta_1 \end{bmatrix}\dot{\theta}_1 + \begin{bmatrix} L_2\sin\theta_2 \\ L_2\cos\theta_2 \end{bmatrix}\dot{\theta}_2 + \begin{bmatrix} -L_{3c}\sin\theta_3 \\ L_{3c}\cos\theta_3 \end{bmatrix}\dot{\theta}_3 \tag{3.12}$$

3.7 Dynamic Model – Equations of Motions

Simplification of the complex nature of the humanoid robot is useful to develop further control strategies. Even with simplifications, dynamics that are not modeled can produce different results with each motion. With the rigid links of the humanoid robot, classic mechanics can be applied to the robot model. Rigid links are supposed to be compliant during all motions.

Dynamic equations of the biped model will be calculated by Euler-Lagrange's Equations which is shown in the following general form in equation (3.13)

$$\frac{d}{dt}\left(\frac{\partial \mathcal{L}}{\partial \dot{\theta}_i}\right) - \frac{\partial \mathcal{L}}{\partial \theta_i} = \tau_i \tag{3.13}$$

where $\mathcal{L}$ represents the Lagrangian equation and τ_i represents the torque for each joint, which includes the control torques, forces, and friction effects. This equation can be formed in the following equation (3.14)

$$\mathcal{L} = K_E - P_E \tag{3.14}$$

where K_E represents the kinetic energy and P_E represents the potential energy of every link. Substituting this into the above equation (3.13), we get the following formula

$$\frac{d}{dx}\left(\frac{\partial (K_E - P_E)}{\partial \dot{\theta}_i}\right) - \frac{\partial (K_E - P_E)}{\partial \theta_i} = \tau_i \tag{3.15}$$

The final form of the Euler-Lagrange equation is as following

$$\frac{d}{dx}\left(\frac{\partial K_E}{\partial \dot{\theta}_i}\right) - \frac{\partial K_E}{\partial \theta_i} + \frac{\partial P_E}{\partial \theta_i} = \tau_i \tag{3.16}$$

Kinetic and potential energy is written in the following forms

$$K_E = \sum_{i=1}^{4} K_{E_i} = \sum_{i=1}^{4} \left(\frac{1}{2} m_i v_{ci}^2 + \frac{1}{2} I_i \dot{\theta}_i^2\right) = \sum_{i=1}^{4} \left(\frac{1}{2} m_i v_{ci}^2 + \frac{1}{2} I_i w_{ci}^2\right) \tag{3.17}$$

where I_i represents the Inertia of each link

$$P_E = \sum_{i=1}^{4} P_{E_i} = \sum_{i=1}^{4} m_i g y_{ic} \tag{3.18}$$

where g shows the gravitational acceleration. Following equations show the relationship between linear velocity and angular velocity with Jacobian matrix.

$$v_{ci} = J_L^{(i)} \dot{\theta} \tag{3.19}$$

$$w_{ci} = J_A^{(i)} \dot{\theta} \tag{3.20}$$

$J_L^{(i)}$ and $J_A^{(i)}$ represents the Jacobian matrices for linear velocity and angular velocity of link *i*, respectively. Total Potential Energy of the 4 link model is found to be the following equation (3.21).

$$\begin{aligned} P_E = {} & m_1 g L_{1c} \sin\theta_1 + m_2 g L_1 \sin\theta_1 + m_3 g L_1 \sin\theta_1 + m_2 g L_{2c} \sin\theta_2 + m_3 g L_2 \sin\theta_2 \\ & + m_3 g L_{3c} \sin\theta_3 \end{aligned} \tag{3.21}$$

Total Kinetic Energy of the 4 link model is found to be the following equation

$$K_E = \frac{1}{2}m_1 {L_{1c}}^2 {\dot{\theta}_1}^2 + \frac{1}{2}I_1\dot{\theta}_1^2 + \frac{1}{2}m_2 {L_1}^2 {\dot{\theta}_1}^2 + \frac{1}{2}m_3 {L_1}^2 {\dot{\theta}_1}^2 + \frac{1}{2}m_2 {L_{2c}}^2 {\dot{\theta}_2}^2 + \frac{1}{2}I_2\dot{\theta}_2^2 + \frac{1}{2}m_3 {L_2}^2 {\dot{\theta}_2}^2$$
$$+ \frac{1}{2}m_3 {L_{3c}}^2 {\dot{\theta}_3}^2 + \frac{1}{2}I_3\dot{\theta}_3^2 + m_2 L_1 L_{2c}\cos(\theta_1+\theta_2)\,\dot{\theta}_1\dot{\theta}_2$$
$$+ m_3 L_1 L_2 \cos(\theta_1+\theta_2)\,\dot{\theta}_1\dot{\theta}_2 + m_3 L_2 L_{3c}\cos(\theta_3+\theta_2)\,\dot{\theta}_2\dot{\theta}_3 \quad (3.22)$$
$$+ m_3 L_1 L_{3c}\cos(\theta_1-\theta_3)\,\dot{\theta}_1\dot{\theta}_3$$

Torque for link 1 is

$$\tau_1 = \left(m_1 {L_{1c}}^2 + I_1 + m_2 {L_1}^2 + m_3 {L_1}^2\right)\ddot{\theta}_1 + \left(m_2 L_1 L_{2c}\cos(\theta_1+\theta_2) + m_3 L_1 L_2\cos(\theta_1+\theta_2)\right)\ddot{\theta}_2$$
$$+ m_3 L_1 L_{3c}\cos(\theta_1-\theta_3)\,\ddot{\theta}_3$$
$$+ \left(-m_2 L_1 L_{2c}\sin(\theta_1+\theta_2) - m_3 L_1 L_2\sin(\theta_1+\theta_2) + m_2 L_1 L_{2c}\sin(\theta_1+\theta_2)\right.$$
$$\left. + m_3 L_1 L_2\sin(\theta_1+\theta_2)\right)\dot{\theta}_1\dot{\theta}_2 + \left(-m_3 L_1 L_{3c}\sin(\theta_1-\theta_3)\right. \quad (3.23)$$
$$\left. + m_3 L_1 L_{3c}\sin(\theta_1-\theta_3)\right)\dot{\theta}_1\dot{\theta}_3 - m_2 L_1 L_{2c}\sin(\theta_1+\theta_2)\,{\dot{\theta}_2}^2$$
$$- m_3 L_1 L_2\sin(\theta_1+\theta_2)\,{\dot{\theta}_2}^2 + m_3 L_1 L_{3c}\sin(\theta_1-\theta_3)\,{\dot{\theta}_3}^2 + m_1 g L_{1c}\cos\theta_1$$
$$+ m_2 g L_1\cos\theta_1 + m_3 g L_1\cos\theta_1$$

Torque for link 2 is

$$\tau_2 = \left(m_2 {L_{2c}}^2 + I_2 + m_3 {L_2}^2\right)\ddot{\theta}_2 + m_3 L_2 L_{3c}\cos(\theta_3+\theta_2)\,\ddot{\theta}_3$$
$$+ \left(m_2 L_1 L_{2c}\cos(\theta_1+\theta_2) + m_3 L_1 L_2\cos(\theta_1+\theta_2)\right)\ddot{\theta}_1$$
$$+ \left(-m_2 L_1 L_{2c}\sin(\theta_1+\theta_2) - m_3 L_1 L_2\sin(\theta_1+\theta_2) + m_2 L_1 L_{2c}\sin(\theta_1+\theta_2)\right.$$
$$\left. + m_3 L_1 L_2\sin(\theta_1+\theta_2)\right)\dot{\theta}_1\dot{\theta}_2 + \left(-m_3 L_2 L_{3c}\sin(\theta_3+\theta_2)\right. \quad (3.24)$$
$$\left. + m_3 L_2 L_{3c}\sin(\theta_3+\theta_2)\right)\dot{\theta}_2\dot{\theta}_3 - m_3 L_1 L_2\sin(\theta_1+\theta_2)\,{\dot{\theta}_1}^2$$
$$- m_2 L_1 L_{2c}\sin(\theta_1+\theta_2)\,{\dot{\theta}_1}^2 - m_3 L_2 L_{3c}\sin(\theta_3+\theta_2)\,{\dot{\theta}_3}^2 + m_2 g L_{2c}\cos\theta_2$$
$$+ m_3 g L_2\cos\theta_2$$

Torque for link 3 is

$$\tau_3 = m_3 L_1 L_{3c}\cos(\theta_1-\theta_3)\,\ddot{\theta}_1 + m_3 L_2 L_{3c}\cos(\theta_3+\theta_2)\,\ddot{\theta}_2 + \left(m_3 {L_{3c}}^2 + I_3\right)\ddot{\theta}_3$$
$$+ \left(-m_3 L_2 L_{3c}\sin(\theta_3+\theta_2) + m_3 L_2 L_{3c}\sin(\theta_3+\theta_2)\right)\dot{\theta}_2\dot{\theta}_3$$
$$+ \left(m_3 L_1 L_{3c}\sin(\theta_1-\theta_3) + m_3 L_1 L_{3c}\sin(\theta_1-\theta_3)\right)\dot{\theta}_1\dot{\theta}_3 \quad (3.25)$$
$$- m_3 L_2 L_{3c}\sin(\theta_3+\theta_2)\,{\dot{\theta}_2}^2 - m_3 L_1 L_{3c}\sin(\theta_1-\theta_3)\,{\dot{\theta}_1}^2 + m_3 g L_{3c}\cos\theta_3$$

Equations of motions (3.13) for the model can be rearranged into the following general form shown in equation (3.26)

$$D(\theta)\ddot{\theta} + H(\theta, \dot{\theta})\dot{\theta} + G(\theta) = T_\theta \tag{3.26}$$

where $D(\theta)$ represents the inertia matrix, $H(\theta, \dot{\theta})$ represents the centrifugal and Coriolis forces matrix, $G(\theta)$ represents the matrix of gravitational forces, T_θ represents the vector torques required at the humanoid joints. Vectors $\theta, \dot{\theta}, \ddot{\theta}$ represent each joint's rotational position, velocity and acceleration respectively. Inertia matrix $D(\theta)$ is shown below, this matrix is a 3×3 matrix which defines the kinetic energy of the every link.

$$D(\theta)\ddot{\theta} = \begin{bmatrix} D_{11} & D_{12} & D_{13} \\ D_{21} & D_{22} & D_{23} \\ D_{31} & D_{32} & D_{33} \end{bmatrix} \ddot{\theta} \tag{3.27}$$

$H(\theta, \dot{\theta})$ matrix groups together Coriolis and centrifugal inertia terms.

$$H(\theta, \dot{\theta})\dot{\theta} = \begin{bmatrix} 0 & h_{122} & h_{133} \\ h_{211} & 0 & h_{233} \\ h_{311} & h_{322} & 0 \end{bmatrix} \dot{\theta} \tag{3.28}$$

Gravitational torques matrix $G(\theta)$ represents the terms of gravity for every link of the model.

$$G(\theta) = \begin{bmatrix} G_1 \\ G_2 \\ G_3 \end{bmatrix} \tag{3.29}$$

And T is the actuating torque control required by each joint during motions.

$$T_\theta = \begin{bmatrix} T_{\theta_1} \\ T_{\theta_2} \\ T_{\theta_3} \end{bmatrix} \tag{3.30}$$

Equation (3.31) shows how equation (3.26) is actually related to every link by its angular rotational value. For example for link 1, it is shown as below

$$D(\theta_1)\ddot{\theta_1} + H(\theta_1, \dot{\theta_1})\dot{\theta_1} + G(\theta_1) = T_{\theta_1} \tag{3.31}$$

where θ_1 shows the link 1 absolute rotational displacement with respect to the horizontal plane. In matrix form, θ is shown below

$$\theta = \begin{bmatrix} \theta_1 \\ \theta_2 \\ \theta_3 \end{bmatrix} \tag{3.32}$$

To model the control properly, relative angles (q) between every joints need to be used in the model formulations.

With this information, equation of motions is modified as in equation (3.33), see Figure 3.2 for all relative angles q between each links. Equation of motions with relative angles is shown below.

$$D_q(q)\ddot{q} + h_q(q,\dot{q})\dot{q} + G_q(q) = T_q \tag{3.33}$$

where q in matrix form can be shown as following

$$q = [q_0 \quad q_1 \quad q_2]^T \tag{3.34}$$

Here, $q_0, q_1$and q_2 are the relative joint angles between links. The relationship between relative angles (q) and absolute angles (θ) are formulated as following in equation (3.35).

$$\begin{aligned} q_0 &= \theta_1 \\ q_1 &= \pi - \theta_1 - \theta_2 \\ q_2 &= \pi - \theta_2 - \theta_3 \end{aligned} \tag{3.35}$$

Relationship between relative angles between joints and the joint angles with respect to the ground is shown below in equation (3.36). [51]

$$T_{\theta_i} = \sum_{j=0}^{2} \tau_j \frac{\partial q_j}{\partial \theta_i} \tag{3.36}$$

where T_{θ_i} shows the torque defined by the equations of motion and τ_j shows the individual link driving torques. $i = 1,2,3$ and $j = 0,1,2$. For every link, equation (3.36) can be expanded by using equation (3.34) as following in equation (3.37).

$$\begin{aligned} T_{\theta_i} &= \tau_j \frac{\partial q_0}{\partial \theta_i} + \tau_j \frac{\partial q_1}{\partial \theta_i} + \tau_j \frac{\partial q_2}{\partial \theta_i} \\ T_{\theta_1} &= \tau_0 \frac{\partial(\theta_1)}{\partial \theta_1} + \tau_1 \frac{\partial(\pi - \theta_1 - \theta_2)}{\partial \theta_1} + \tau_2 \frac{\partial(\pi - \theta_2 - \theta_3)}{\partial \theta_1} \\ T_{\theta_2} &= \tau_0 \frac{\partial(\theta_1)}{\partial \theta_2} + \tau_1 \frac{\partial(\pi - \theta_1 - \theta_2)}{\partial \theta_2} + \tau_2 \frac{\partial(\pi - \theta_2 - \theta_3)}{\partial \theta_2} \\ T_{\theta_3} &= \tau_0 \frac{\partial(\theta_1)}{\partial \theta_3} + \tau_1 \frac{\partial(\pi - \theta_1 - \theta_2)}{\partial \theta_3} + \tau_2 \frac{\partial(\pi - \theta_2 - \theta_3)}{\partial \theta_3} \end{aligned} \tag{3.37}$$

Matrix in equation (3.38) shows the relation between torques of individual links and the torque defined by the equations of motion

$$T_\theta = \begin{bmatrix} 1 & -1 & 0 \\ 0 & -1 & -1 \\ 0 & 0 & -1 \end{bmatrix} \begin{bmatrix} \tau_0 \\ \tau_1 \\ \tau_2 \end{bmatrix} \tag{3.38}$$

In the following equation (3.39), T_{q_i} represents the generalized torques corresponding to the relative angles displacements where $i = 1,2,3$.

$$T_{q_i} = \tau_i \tag{3.39}$$

where τ_i is the actual driving torque at the joints. Angle movement (θ_i) of every link can be expressed in terms of q_i values in equation (3.40)

$$\begin{aligned} \theta_1 &= q_0 \\ \theta_2 &= \pi - q_0 - q_1 \\ \theta_3 &= q_0 + q_1 - q_2 \end{aligned} \tag{3.40}$$

Equation (3.36) can be rewritten as following in equation (3.141) where $i = 0,1,2$.

$$T_{q_i} = \sum_{j=0}^{2} \tau_{\theta_j} \frac{\partial q_j}{\partial q_i} \tag{3.41}$$

Generalized torques from the actual driving torque at the joints is calculated as following in equation (3.42).

$$\begin{aligned} T_{q_i} &= \tau_{\theta_1} \frac{\partial q_1}{\partial q_i} + \tau_{\theta_2} \frac{\partial q_1}{\partial q_i} + \tau_{\theta_3} \frac{\partial q_1}{\partial q_i} \\ T_{q_0} &= \tau_{\theta_1} \frac{\partial (q_0)}{\partial q_0} + \tau_{\theta_2} \frac{\partial (\pi - q_0 - q_1)}{\partial q_0} + \tau_{\theta_3} \frac{\partial (q_0 + q_1 - q_2)}{\partial q_0} \\ T_{q_1} &= \tau_{\theta_1} \frac{\partial (q_0)}{\partial q_1} + \tau_{\theta_2} \frac{\partial (\pi - q_0 - q_1)}{\partial q_1} + \tau_{\theta_3} \frac{\partial (q_0 + q_1 - q_2)}{\partial q_1} \\ T_{q_2} &= \tau_{\theta_1} \frac{\partial (q_0)}{\partial q_2} + \tau_{\theta_2} \frac{\partial (\pi - q_0 - q_1)}{\partial q_2} + \tau_{\theta_3} \frac{\partial (q_0 + q_1 - q_2)}{\partial q_2} \end{aligned} \tag{3.42}$$

From equations in (3.42), the torque values for the equation of motions can be found in equation (3.43).

$$\begin{aligned} T_{q_0} &= T_{\theta_1} - T_{\theta_2} + T_{\theta_3} \\ T_{q_1} &= -T_{\theta_2} + T_{\theta_3} \\ T_{q_2} &= -T_{\theta_3} \end{aligned} \tag{3.43}$$

From equation (3.33), equations of motion are expressed in the following forms.

Equations of motion for link 1 is

$$\begin{aligned} \Lambda_{11}\ddot{\theta}_1 + \Lambda_{12}\ddot{\theta}_2 + \Lambda_{13}\ddot{\theta}_3 + h_{q0} + G_{q0} &= \tau_0 \\ A_{1j} &= \Pi_{1j} - \Pi_{2j} + \Pi_{3j} \end{aligned} \tag{3.44}$$

$$h_{q0} = \Gamma_1 - \Gamma_2 + \Gamma_3$$

$$G_{q0} = \Upsilon_1 - \Upsilon_2 + \Upsilon_3$$

Equations of motion for link 2 is

$$\begin{aligned} \Lambda_{21}\ddot{\theta}_1 + \Lambda_{22}\ddot{\theta}_2 + \Lambda_{23}\ddot{\theta}_3 + h_{q1} + G_{q1} &= \tau_1 \\ \Lambda_{2j} &= -\Pi_{2j} + \Pi_{3j} \\ h_{q1} &= -\Gamma_2 + \Gamma_3 \\ G_{q1} &= -\Upsilon_2 + \Upsilon_3 \end{aligned} \tag{3.45}$$

Equations of motion for link 3 is

$$\begin{aligned} \Lambda_{31}\ddot{\theta}_1 + \Lambda_{32}\ddot{\theta}_2 + \Lambda_{33}\ddot{\theta}_3 + h_{q2} + G_{q2} &= \tau_3 \\ \Lambda_{3j} &= -\Pi_{3j} \\ h_{q2} &= -\Gamma_3 \\ G_{q2} &= -\Upsilon_3 \end{aligned} \tag{3.46}$$

Equations of motion in terms of relative angles are shown in equation (3.47) by using equation (3.31).

$$D_q(q)\ddot{q} + H_q(q,\dot{q})\dot{q} + G_q(q) = T_q \tag{3.47}$$

where D_q, H_q, $G_q$and $T_q$are shown below in equations (3.48-3.51).

$$\begin{aligned} D_q(i,1) &= \Lambda_{i1} - \Lambda_{i2} + \Lambda_{i3} \\ D_q(i,2) &= -\Lambda_{i2} + \Lambda_{i3} \\ D_q(i,3) &= -\Lambda_{i3} \end{aligned} \tag{3.48}$$

$$H_q = \left[h_{q0}, h_{q1}, h_{q2}\right]^T \tag{3.49}$$

$$G_q = \left[G_{q0}, G_{q1}, G_{q2}\right]^T \tag{3.50}$$

$$T_q = \left[T_{q0}, T_{q1}, T_{q2}\right]^T \tag{3.51}$$

where $i = 1,2,3$.

3.8 Jacobian Matrix

The torque applied on the humanoid robot links by the electrical motors are shown in equation (3.52)

$$T = J^T \left(\frac{d}{dx} \left(\frac{\partial L}{\partial \dot{\theta}_i} \right) - \frac{\partial L}{\partial \theta_i} \right) \tag{3.52}$$

where J shows the Jacobian matrix in terms of joint displacements in equation (3.53).

$$J = \begin{bmatrix} \frac{\partial x_{1c}}{\partial \theta_1} & \frac{\partial y_{1c}}{\partial \theta_1} \\ \frac{\partial x_{2c}}{\partial \theta_2} & \frac{\partial y_{2c}}{\partial \theta_2} \\ \frac{\partial x_{3c}}{\partial \theta_3} & \frac{\partial y_{3c}}{\partial \theta_3} \end{bmatrix} \tag{3.53}$$

3.9 CoM Velocity of CoM of Humanoid Robot

Velocity of the CoM of the humanoid robot model can be formulized as in equation (3.54)

$$v_c = \frac{dC_{om}}{dx} = \frac{\sum m_i v_i}{\sum m_i} = \frac{P}{M} \tag{3.54}$$

where P is linear momentum and M is total mass of the system and v_i is the absolute velocity of the CoM of every connected link.

$$P = \sum P_i = \sum m_i v_i \tag{3.55}$$

3.10 CoM Average Angular Velocity of Humanoid Model

Biped CoM average angular velocity can be found by the following equation (3.56)

$$W_{CoM} = \frac{\sum I_i w_i}{\sum I_i} \tag{3.56}$$

where I_i is inertia matrix of ith body link, and w_i is angular velocity of ith link.

3.11 Link Angular Acceleration of Humanoid Model

Equation of motions of every joint actuator is shown by equation (3.31). Acceleration of every link can be formulized as in the following equation (3.57).

$$\ddot{q} = D_q(q)^{-1} \left(T_q - H_q(q, \dot{q})\dot{q} - G_q(q) \right) \tag{3.57}$$

The value of acceleration for every joint will be dependent on effects from other joints and applied torques. Equation (3.56) will represent the joint angular positions, accelerations which are affected by other link dynamics.

3.12 Angular Momentum of the Humanoid

The humanoid has zero moment if sum of the resulting external forces and moments, which is calculated for its general CoM is zero, and provides rotational stability.

The amount of deviation of humanoid's angular momentum is a consequence of external moment on the humanoid robot, which is rotationally stable and does not fall over. In that case, angular momentum amount variation of the CoM is zero. Humanoid robot angular momentum is conserved during all motions. External force or moments can result from ground contacts, unpredicted instabilities and gravity. Angular momentum is shown by the following equation (3.58)

$$L = \sum_{i}^{n} I_i w_i + m_i C_{CoM} \mathrm{x} v_c \tag{3.58}$$

where I_i is inertia tensor of i^{th} body link, w_i is angular velocity of i^{th} link, C_{CoM} is the position of the CoM and v_c is the velocity of the CoM.

Angular momentum of a humanoid robot near the end of link i can be found by the following expression in equation (3.59)

$$L_i = L + m[(y_{cm} - y_i)\dot{x}_{cm} - (x_{cm} - x_i)\dot{y}_{cm}] \tag{3.59}$$

where x_{cm} and y_{cm} is the location of link CoM in x and y direction, x_i and y_i is the location of humanoid's CoM, $\dot{x}_{cm}$ and $\dot{y}_{cm}$ show the velocities of CoM of links.

From above expression, torque for a link i can be estimated as following

$$\tau = \frac{dL}{dt} = I\frac{dW}{dt} \tag{3.60}$$

This shows relations between angular momentum and torque/acceleration for every joint. Angular Momentum around a joint can also be estimated by the following equation (3.61).

$$\frac{\partial K_E}{\partial \dot{\theta}_i} = m_i \dot{q}_i \tag{3.61}$$

where $\frac{\partial K_E}{\partial \dot{\theta}_i}$ is from the equations of motion which was calculated previously. It represents the force caused by the kinetic energy of the model.

3.13 Total Rotational Inertia

Biped's total rotational inertia can be found by the following equation (3.62)

$$I = \sum I_i + m_i(c_i - c) \tag{3.62}$$

where I_i is link rotational inertia and c_i and c are the distance of every link CoM to the humanoid CoM.

3.14 Center of Pressure

The center of pressure represents a location in supporting area of the humanoid robot that the entire amount of the pressure forces C_F producing a force, see Figure 3.4.

During humanoid motion, the parts of the humanoid that are effected by contact forces are the biped's feet. [50]

A pressure area shown in Figure 3.4 remains. The resultant of this pressure area with n contact locations in normal direction given below.

$$C_{FN} = \sum_{i=1}^{n} F_{Pi} \tag{3.63}$$

The location of the CoP is calculated with the equation (3.64):

$$CoP = \frac{\sum_{i=1}^{n} L_{FNi} F_{Pi}}{C_{FN}} \tag{3.64}$$

where L_{FNi} is the distance of every force vector to the origin. If the center of pressure is outside the support area, the biped tends to tip over.

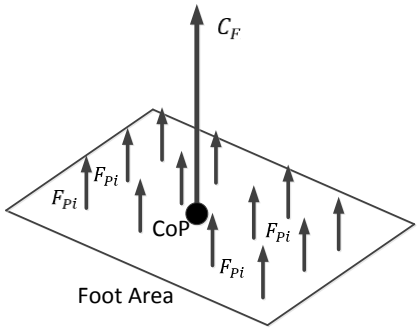

Figure 3.4 Position of center of pressure and contact forces

CHAPTER 4: MODEL TRACKING CONTROL

4.1 Zero Moment Point

Throughout the motions of the robot, humanoid can have either of its feet on the ground or both. Humanoid balance is supported by the single and double supporting legs, and thus the ZMP criteria must be applicable in both cases.

The ZMP of a robot can be hard to keep and changes throughout any motion. The ZMP point of a humanoid robot can be defined with the use of the equations below. [50]

$$x_{zmp} = \frac{MgCoM_x - \dot{L_y}}{Mg + \dot{P}}$$
$$y_{zmp} = \frac{MgCoM_y - \dot{L_x}}{Mg + \dot{P}} \quad (4.1)$$

where M is total mass of the biped, P linear momentum, L angular momentum.

$$P = \sum_{i=1}^{n} m_i \, v_{ci} \quad (4.2)$$

$$L = \sum_{i=1}^{n} (v_{ci} \times m_i v_{ci} + I_i w_i) \quad (4.3)$$

where m_i is humanoid individual link weight, v_{ci} is the link linear velocity, I_i is link inertia, and w_i is link angular velocity.

The above equations (4.1) – (4.3) demonstrate how the location of the ZMP is reliant on the position of the humanoid. The ZMP calculations consider the influence of every link. The mass of the robot and its links are accounted for with the m_i term. The position of the link CoM are represented with the variables CoM.

The resulting values for the x_{zmp} and y_{zmp} must stay within the positions for the robot to remain stable. If the position of the ZMP moves outside of the foot's region, then control models are required to return position to the proper position. This method for defining the robot's present ZMP can be very computationally significant.

4.2 Balance Control with ZMP

Postural Control and trajectory generation of a humanoid can be modelled by proportional-derivative control of the joint torques to increase the stability [52]. Torque from motion of equations (3.26) is shown in generalized formula form in equation (4.4)

$$D(q)\ddot{q} + H(q,\dot{q})\dot{q} + G(q) = \tau \tag{4.4}$$

where $D(q)$ is the inertia matrix, $h(q,\dot{q})$ represents the centrifugal and Coriolis forces matrix, $G(q)$ is the matrix of gravitational forces, τ represents the vector of external forces and torques required at the joints. Vectors $q, \dot{q}, \ddot{q}$ show position, velocity and joint acceleration respectively.

These generalized equation of motions can be shown in terms of state vector $\begin{bmatrix} q^T & \dot{q}^T \end{bmatrix}^T$.

$$\frac{d}{dx}\begin{bmatrix} q \\ \dot{q} \end{bmatrix} = \begin{bmatrix} \dot{q} \\ D_q(q)^{-1}\left(T_q - H_q(q,\dot{q})\dot{q} - G_q(q)\right) \end{bmatrix} \tag{4.5}$$

Position control of the links can be formulated by giving a desired position q_d and find the torque τ to make the positions q close to the preferred position as much as possible. Main goal is to find the torque τ for position control so that humanoid joints follow the trajectories with minimal error.

$$\lim_{t\to\infty} q(t) = q_d \tag{4.6}$$

where q_d represents the desired joint positions. Equation (4.6) can be written as in equation (4.7) and (4.8).

$$\lim_{t\to\infty} q_e(t) = 0 \tag{4.7}$$

$$q_e(t) = q(t) - q_d \tag{4.8}$$

If position error dynamics is shown to be zero, $\begin{bmatrix} {q_e}^T & \dot{q}^T \end{bmatrix}^T = 0$, then we can say that control is asymptotically stable. Calculation of τ involves a nonlinear vector function of $q, \dot{q}$ and $\ddot{q}$. Usually robot joints have sensors which will allow measurements of q and $\dot{q}$.

These values can be used by the controller function mentioned above. Even though measurement of the acceleration $\ddot{q}$ will have high sensitivity to the noise, with the proper filtering, the values can be used in calculations.

The position error control is based on derivation of the positional error and determination of control parameters. This enables reduction of the error for joints. The positional error is calculated and reduced for every joints independently.

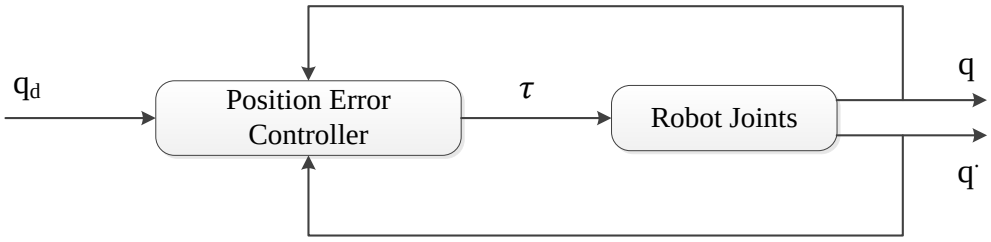

Figure 4.1 Simple diagram for the position error controller closed-loop controller for robot joints

Separate controllers can be established as there are degrees of freedom that exist in a robot. The positional error q_e is enlarged by proportional position gain K_p, which is a diagonal matrix of the gains of joints controllers. A velocity closed loop can add damping to the controller in order to minimize the position errors that are related to the overshoots of the joints and not stopping at desired positions. This is shown by K_d, which is a diagonal matrix of velocity gains.

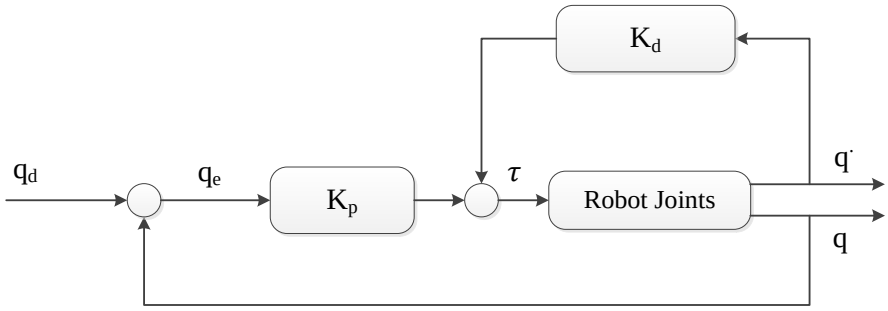

Figure 4.2 PD positon error control with damping

Controller is shown in the following form in equation (4.9) for the above diagram

$$\tau = K_p q_e + K_d \dot{q} \tag{4.9}$$

The controller using Lyapunov second method will be used to study the stability of the system is shown below in equation (4.10)

$$\tau = D(q)\ddot{q_d} + H(q,\dot{q})\dot{q_d} + G(q) - K_p q_e - K_d \dot{q} \tag{4.10}$$

where $K_p = {K_p}^T > 0$ and $K_d = {K_d}^T > 0$. Position, velocity and joint acceleration error relation with actual and desired values shown below respectively in equation (4.11)

$$\begin{aligned} q_e &= q - q_d \\ \dot{q_e} &= \dot{q} - \dot{q_d} \\ \ddot{q_e} &= \ddot{q} - \ddot{q_d} \end{aligned} \tag{4.11}$$

Acceleration with error values can be shown using the motion of equations and above equations.

$$\ddot{q_e} = D(q)^{-1}\left(T - H(q,\dot{q})\dot{q} - G(q)\right) - \ddot{q_d} \tag{4.12}$$

$$D(q)\ddot{q_e} = T - H(q,\dot{q})\dot{q} - G(q) - D(q)\ddot{q_d}$$

$$\dot{q} = \dot{q_e} + \dot{q_d}$$

$$D(q)\ddot{q_e} = T - H(q,\dot{q})(\dot{q} + \dot{q_d}) - G(q) - D(q)\ddot{q_d}$$

$$T = D(q)\ddot{q_d} + H(q,\dot{q})\dot{q_d} + G(q) - K_p q_e - K_d\dot{q} \tag{4.13}$$

$$D(q)\ddot{q_e} = D(q)\ddot{q_d} + H(q,\dot{q})\dot{q_d} + G(q) - K_p q_e - K_d\dot{q} - H(q,\dot{q})\dot{q} - H(q,\dot{q})\dot{q_d} - G(q) - D(q)\ddot{q_d}$$

$$D(q)\ddot{q_e} = -K_p q_e - K_d\dot{q} - H(q,\dot{q})\dot{q}$$

$$D(q)\ddot{q_e} + K_p q_e + K_d\dot{q} + H(q,\dot{q})\dot{q} = 0$$

Above position error dynamics formula needs to be stable around $q_e(t) = 0$. To prove the stability of equation (4.13), a Lyapunov candidate function will be used, which is the total energy associated with the closed loop. [53]

$$\vartheta = \frac{1}{2}\,\dot{q}_e^T D(q)\dot{q}_e + \frac{1}{2} q_e^T K_p q_e \tag{4.14}$$

To demonstrate the stability, equation (4.14) candidate function time derivative needs to be less than or equal to zero.

$$\dot{\vartheta} = \frac{1}{2}\ddot{q}_e^T D(q)\dot{q}_e + \frac{1}{2}\,\dot{q}_e^T D(\dot{q})\dot{q}_e + \frac{1}{2}\,\dot{q}_e^T D(q)\ddot{q}_e + \frac{1}{2}\dot{q}_e{}^T K_p q_e + \frac{1}{2} q_e{}^T K_p \dot{q}_e \tag{4.15}$$

$$\dot{\vartheta} = \ddot{q}_e^T D(q)\dot{q}_e^T + \frac{1}{2}\,\dot{q}_e^T D(\dot{q})\dot{q}_e + \dot{q}_e^T K_p q_e = \dot{q}_e^T\left(\ddot{q}_e^T D(q) + \frac{1}{2}\,D(\dot{q})\dot{q}_e + K_p q_e\right) \tag{4.16}$$

After working on the equation (4.15) and (4.16), following result is obtained in equation (4.17).

$$\dot{\vartheta} = -\dot{q_e}^T(K_d\dot{q}) \tag{4.17}$$

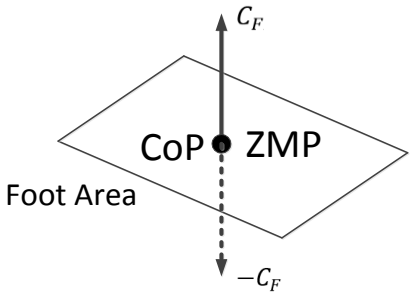

Figure 4.3 Dynamically stable correlation between ZMP and center of pressure

In order to reach dynamic stability, the ZMP needs to exist in the support area during the humanoid motions.

During double support period, the CoP point, which represents the resulting force, locates individually under every feet. ZMP overlaps with CoP if the humanoid robot has the dynamic stability.

If the humanoid robot has dynamic stability, the location of the ZMP can be located with the center of pressure using force sensors under the feet [50]. To have the model stabilize ZMP needs to stay in the support polygon region that is found by three pressure points at a minimum.

4.3 Balancing Techniques

One of the balance techniques is the ankle joint control approach, which is regulated by executing control of the torque of the ankle. The inverse pendulum model is used to better model the motions of the humanoid, which are used to design the ankle joint control approach. The results determine that the ankle joint control approach can function accurately for small forces and that additional controllers can be used to advance humanoid balance capability to optimize the energy usage and provide balance during motions.

The other control approach implements hip joint control by handling the hip joint torque. The required torque of hip joint is applied nearer to the CoM of the humanoid. The hip joint control approach can cause larger torques so it is used for recovering from unbalanced postures compared to the ankle approach for better energy usage. The model was derived from the kinematics model with a linear inverse pendulum joined with a damping spring factor [54]. The ankle recovery is practical for small forces but it can easily fail after a certain threshold. The hip recovery is practical for bigger forces than the ankle recovery and has a fast recovery time for unbalanced humanoids.

CHAPTER 5: MECHANICAL, ELECTRICAL POWER PERFORMANCE AND EVALUATION

To demonstrate the results of the kinematics, dynamics and task motion trajectories in the humanoid mechanical power consumption, average mechanical power is calculated for every joint.

$$P_{avm} = \left|\tau_{ij}\dot{q}_{ij}\right| \tag{5.1}$$

For joint j of the leg i, the mechanical power is calculated as the result of the joint torque and the load angular velocity. The overall average power is calculated by taking average value of the equation (5.1) delivered over a period T for all joints.

$$P_{avm}(t) = \frac{1}{T}\sum_{i,j}\int_0^T \left|\tau_{ij}(t)\dot{\theta}_{ij}(t)\right| dt \tag{5.2}$$

where τ_i represents the required joint torque and $\dot{\theta}_i$ represents the load angular velocity. A sudden very high power demand may occur with humanoid joints during motions. Even though the average value of power usage can be small, whereas the peak can actually be very high. The standard deviation of mechanical power quantity can be used to assess the distribution around the mechanical absolute power.

$$P_{sd}(t) = \sqrt{\frac{1}{T}\int_0^T [P_i(t) - P_{avm}(t)]^2 dt} \tag{5.3}$$

where P_i is shown as in equation (5.4).

$$P_i = \sum_i \tau_{ij}\dot{q}_{ij} \tag{5.4}$$

P_i represents the instantaneous mechanical power [11]. For a humanoid robot, the energy lost due to mean torque consumption for a joint is

$$E_{Lost} = \frac{1}{T}\int_0^T \tau^T \tau dt \tag{5.5}$$

For all joints of humanoid, energy loss due to the torque required is

$$E_{lost}(t) = \frac{1}{T}\sum_{i}\int_{0}^{T}[\tau_i(t)]^2\,dt \tag{5.6}$$

The function for mechanical power consumption is calculated from previous equations in equation (5.7)

$$E_t(t) = P_{avm}^t(t) + P_{sd}^t(t) + E_{lost}^t(t) \tag{5.7}$$

where $P_{avm}^t(t)$, $P_{sd}^t(t)$, and $E_{lost}^t(t)$ represent the average absolute joint mechanical power, average joint mechanical power deviation, and mean joint torque usage, respectively.

The electrical input power consumed by the geared dc motors installed at every leg joint can be evaluated. Ignoring the effect of rotor inertia, break-away torque, and motor armature inductance [55], the total energy deduced by the applied voltages V_a and currents $i(t)$ is given by

$$E = \int_T {V_a}^T I_a dt = \sum \int_T (\tau_m w_m + i^2 R_m + \tau_{load} w_{load} + \tau_{loss} w_m) dt \tag{5.8}$$

$$V_a = I_a R_m + V_{EMF} + L\frac{dl_a}{dt} \tag{5.9}$$

$$\tau_m = I_a . k_t = \tau_{shaft} + \tau_{gm} \tag{5.10}$$

$$I_a = \frac{\tau_{shaft}}{k_t} + \frac{\tau_{gm}}{k_t} \tag{5.11}$$

$$V_a = I_a R_m + V_{EMF} \tag{5.12}$$

V_a is input voltage to the motor, I_a is motor armature current, R_m is motor armature resistance, V_{EMF} is electromagnetic force voltage across the motor, L is motor inductance, τ_m is motor torque, k_t is torque constant, τ_{shaft} is motor shaft torque, τ_{gm} is gearbox torque. Power consumed by motor is written as in equation (5.13)

$$P_{IN} = V_{in} i = i(I_a R_m + V_{EMF}) = I_a^2 R_m + I_a V_{EMF} \tag{5.13}$$

$$\begin{aligned} P_{IN} &= I_a^2 R_m + \left(\frac{\tau_{shaft}}{k_t} + \frac{\tau_{gm}}{k_t}\right) V_{EMF} \\ &= \frac{\tau_{shaft}^2}{k_t^2} R_m + \frac{\tau_{gm}^2}{k_t^2} R_m + 2\frac{\tau_{shaft}\tau_{gm}}{k_t^2} R_m + \frac{\tau_{shaft}}{k_t} V_{EMF} + \frac{\tau_{gm}}{k_t} V_{EMF} \end{aligned} \tag{5.14}$$

$$P_{INi} = \frac{\tau_{shafti}^2}{k_{ti}^2} R_{mi} + \frac{\tau_{gmi}^2}{k_{ti}^2} R_{mi} + 2\frac{\tau_{shafti}\tau_{gmi}}{k_{ti}^2} R_{mi} + \frac{\tau_{shafti}}{k_{ti}} V_{EMFi} + \frac{\tau_{gmi}}{k_{ti}} V_{EMFi} \tag{5.15}$$

Since objective is to minimize the overall energy utilization, above equations is written in equation (5.16) – (5.18).

$$\min_{\tau} \sum \left[c^T \tau + \frac{1}{2} \tau^T \tau \right] \tag{5.16}$$

$$c = \begin{bmatrix} \frac{\tau_{shaft1}^2}{k_{t1}^2} R_{m1} + \frac{\tau_{gm1}^2}{k_{t1}^2} R_{m1} + 2 \frac{\tau_{shaft1} \tau_{gm1}}{k_{t1}^2} R_{m1} + \frac{\tau_{shaft1}}{k_{t1}} V_{EMF1} + \frac{\tau_{gm1}}{k_{t1}} V_{EMF1} \\ \ldots. \\ \frac{\tau_{shaftn}^2}{k_{tn}^2} R_{mn} + \frac{\tau_{gmn}^2}{k_{tn}^2} R_{mn} + 2 \frac{\tau_{shaftn} \tau_{gmn}}{k_{tn}^2} R_{mn} + \frac{\tau_{shaftn}}{k_{tn}} V_{EMFn} + \frac{\tau_{gmn}}{k_{tn}} V_{EMFn} \end{bmatrix} \tag{5.17}$$

$$\tau = \begin{bmatrix} \tau_1 \\ \ldots \\ \tau_n \end{bmatrix} \tag{5.18}$$

Here, w_m and τ_m are the joint velocity and joint torque vector of the link; $R_m$is the armature resistance of the motor of the i joint. Total input energy consumption of the all joints can be shown by equation (5.19)

$$E_{Total} = \sum E_i \tag{5.19}$$

5.1 Energy Efficiency of the Center of Mass

A cost of transport can be defined for a biped system to analyze the energy efficiency when different motion parameters are used in equation (5.20)

$$C_E = \frac{E}{Mgh} \tag{5.20}$$

where E is the total energy used, M represents the humanoid overall weight, g represents the gravitational constant, h represents the distance for biped that changed the location of CoM in vertical direction. Cost will be dependent on the total energy usage where specific motion parameters are employed for every joint.

5.2 Power Flow Inside a DC Motor

DC motor power demand is shown by input power, P_{IN}, Figure 5.1. This power is directly related with the current consumption of the motor. P_{IN} is the electrical power provided to the joint motor. This electrical power is converted to mechanical power and during this conversion there happens some electrical losses, mainly due to armature current.

$P_{elec\ loss}$ shows the electrical losses due to armature resistance. P_{mag} is power developed by the motor which produces power out (P_{mech}) and rotational losses (P_{loss}). P_{loss} shows the losses due to friction of mechanical parts, magnetic inefficiencies of the material, losses coupling brushes and commutator. P_{mech} shows the mechanical power produced by the joint motor to handle the load attached to end of the motor.

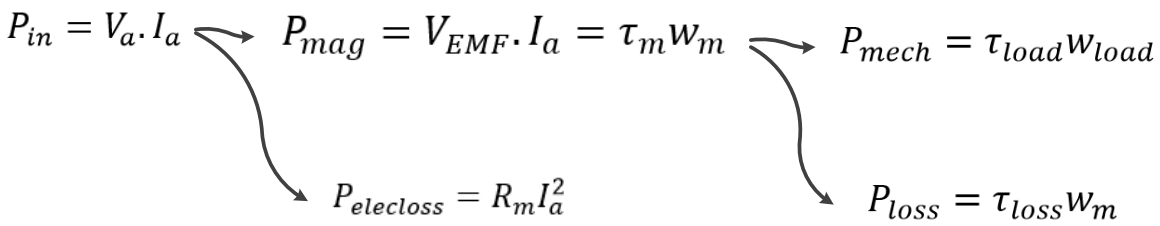

Figure 5.1 Power flow and losses in a DC motor. P_{IN} provides the electrical power and P_{mech} represents the mechanical power produced by a joint

CHAPTER 6: JOINT MOTOR DYNAMICS AND CONTROL

The differential equations of the dynamics of n degree of freedom humanoid biped robot are obtained as following in equation (6.1)

$$D(q)\ddot{q} + H(q,\dot{q})\dot{q} + G(q) = \tau \tag{6.1}$$

where τ is defined as the generalized force or torque acting at the joint which is produced by an actuator. Study of humanoid dynamics provides torque requirement imposed by humanoid joints which actuator have to supply.

It is essential to show the actuator dynamics along with humanoid kinematics and dynamics. Motor dynamics will be studied in two stages. In the first stage, only mechanical part will be described and in the second stage electrical part will be shown. Mechanical and electrical sections will be joined later. End result will be then coupled with humanoid dynamics.

6.1 Mechanical Analysis

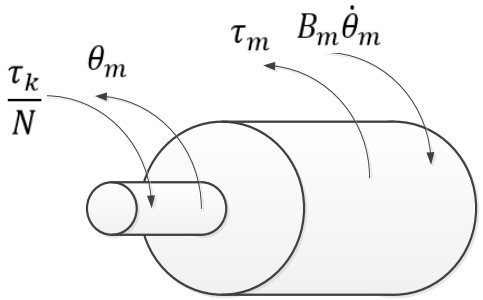

Figure 6.1 DC motor armature diagram without any load

Torque supplied by DC motor will be used to overcome against the load torque from humanoid joint and damping torque.

$$I_m\ddot{\theta}_m + B_m\dot{\theta}_m + \frac{\tau_k}{N} = \tau_m \tag{6.2}$$

$$\tau_m = k_m l_a \tag{6.3}$$

$$I_m\ddot{\theta}_m + B_m\dot{\theta}_m + \frac{k_t}{N} = \tau_m = k_m l_a \tag{6.3a}$$

where τ_m represents the torque supplied by the motor, $\frac{\tau_k}{N}$ represents the load coming on joint motor due to humanoid joint, I_m represents the inertia of the motor, $\ddot{\theta}_m$is motor acceleration, B_m motor damping constant, $\dot{\theta}_m$ is motor velocity, l_a is armature current, k_m is motor constant, k_t is torque constant, N is gear ratio.

6.2 Electrical Analysis

Whenever a conductor moves in a magnetic field, a voltage is generated across its terminals. This voltage is known as back electromagnetic force (emf) which is proportional to velocity of the conductor in the field (ω) and the magnetic flux ∅, $V_{EMF} \propto \emptyset\omega$

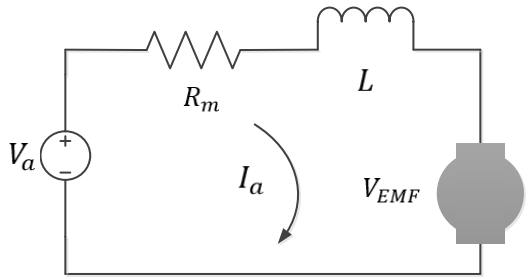

Figure 6.2 DC motor electrical circuit diagram

$$V_{EMF} = k_E \emptyset \omega \tag{6.4}$$

where V_{EMF} is emf voltage, ∅ is flux, ω is the angular velocity of the motor armature, with permanent magnet stator flux ∅ is constant,

$$V_{EMF} = k_E \dot{\theta}_m \tag{6.5}$$

where k_E is back emf constant. This voltage will tend to oppose the current flow in the conductor which needs to be taken into account.

$$V_a = I_a R_m + V_{EMF} + L\frac{dl_a}{dt} \tag{6.6}$$

where V_{EMF} is the back emf, and $L\frac{dl_a}{dt}$ is usually small and it is neglected. Elimination of current I_a from above mechanical and electrical equations (6.2-6.4)

$$I_m\ddot{\theta}_m + B_m\dot{\theta}_m + k_t g_k = k_m\frac{V - k_E\dot{\theta}_m}{R_m} \tag{6.7}$$

$$g_k = \frac{1}{N_k} \tag{6.8}$$

Rearranging and introducing subscripts corresponding to k^{th} joint, equation (6.9) is obtained.

$$I_m\ddot{\theta}_{mk} + \left(B_m + \frac{k_E k_m}{R_m}\right)\dot{\theta}_{mk} = \frac{k_m}{R_m}V_k - k_t g_k \tag{6.9}$$

Humanoid dynamics and actuator dynamics are combined in order to get a relationship between them. Humanoid dynamical equation is

$$D(q)\ddot{q} + H(q,\dot{q})\dot{q} + G(q) = \tau \tag{6.10}$$

which is a vector matrix equation.

$$\sum_j D_{kj}(q)\ddot{q}_j + \sum_{i,j} H_{kj}(q)\dot{q}_i\dot{q}_j + \frac{\partial PE}{\partial q_k} = \tau_k \tag{6.11}$$

where

$$G(q) = \frac{\partial PE}{\partial q_k} \tag{6.12}$$

which corresponds to one joint of the humanoid robot, where $k = 1,2,\ldots n$. The following equation (6.13) shows the actuator dynamics equation.

$$I_m\ddot{\theta}_{mk} + \left(B_m + \frac{k_E k_m}{R_m}\right)\dot{\theta}_{mk} = \frac{k_m}{R_a}V_k - k_t g_k \tag{6.13}$$

By substituting equation (6.11) τ_k into equation (6.13), equation (6.14) is obtained.

$$I_m\ddot{\theta}_{mk} + \left(B_m + \frac{k_E k_m}{R_m}\right)\dot{\theta}_{mk} = \frac{k_m}{R_a}V_k - \left\{\sum_j D_{kj}(q)\ddot{q}_j + \sum_{i,j} H_{kj}(q)\dot{q}_i\dot{q}_j + \frac{\partial PE}{\partial q_k}\right\}g_k \tag{6.14}$$

Here generalized coordinate of joints are expressed as in equation (6.15)

$$q_k = g_k\theta_{mk} = \frac{\theta_{mk}}{N_k} \tag{6.15}$$

where $k = 1,2,\ldots n$ and

$$\ddot{q}_k = g_k\ddot{\theta}_{mk} = \frac{\ddot{\theta}_{mk}}{N_k} \tag{6.16}$$

After rearranging equation (6.14) by equations (6.15) and (6.16), equation (6.17) is obtained.

$$[I_m + r_k^2 d_{kk}(q)]\ddot{\theta}_{mk} + \left[B_m + \frac{k_E k_m}{R_m}\right]\dot{\theta}_{mk} = \frac{k_m}{R_m}V_k - \left[\sum_{j,k} D_{kj}(q)\ddot{q}_j + \sum_{i,j} H_{ikj}(q)\dot{q}_i\dot{q}_j + G_k\right]g_k \tag{6.17}$$

The effective inertia for the motor is shown in equation (6.18).

$$I_{eff} = I_m + g_k^2 d_{kk}(q) \tag{6.18}$$

The effective damping in the motor is shown in equation (6.19).

$$B_{eff} = B_m + \frac{k_E k_m}{R_m} \tag{6.19}$$

Every joint of the humanoid is controlled independently, the coupling effects due to motion of other links needs to be separated and treated as a disturbance. That's why the terms representing coupled inertias, Coriolis forces and Centripetal terms are separated and grouped under name D_k.

$$D_k = \sum_{j,k} D_{kj}(q)\ddot{q}_j + \sum_{i,j} H_{ikj}(q)\dot{q}_i\dot{q}_j + G_k \tag{6.20}$$

This term is a disturbance to the controller.

$$I_{eff}\ddot{\theta}_{mk} + B_{eff}\dot{\theta}_{mk} = KV_k - D_k g_k \tag{6.21}$$

$$K = \frac{k_m}{R_m} \tag{6.22}$$

This is a linear differential equation (6.21) of system along with nonlinear disturbance $D_k g_k$. Humanoid and actuator dynamics equation reduced to linear form with nonlinear terms grouped as a disturbance. I_{eff} is assumed to be constant but it is function of generalized coordinates.

6.3 Joint DC Motor Model

Torque produced by motor can be formulized by the following equation (6.23). With this formula, applied voltage caused an increase in motor torque. If the angular velocity increases, the motor torque decreases.

$$\tau_m = \frac{k_t}{R_m}V_a - \frac{{k_t}^2}{R_m}w_m \tag{6.23}$$

Electrical input power provided to the motor is shown below in equation (6.24).

$$P_{in} = V_a . l_a \tag{6.24}$$

Power developed magnetically by motor armature is

$$P_{mag} = V_{EMF} . l_a \tag{6.25}$$

Power dissipated in the DC motor armature is

$$P_{elecloss} = R_m {l_a}^2 \tag{6.26}$$

Putting two equations (6.27) and (6.26) together, dissipated power can written as in equation (6.28)

$$\tau_m = i . k_t \tag{6.27}$$

$$P_{elecloss} = \frac{R_m}{{k_t}^2}{\tau_m}^2 \tag{6.28}$$

$$k_m = \frac{k_t}{\sqrt{R_m}} \tag{6.29}$$

where k_m represents motor constant, which symbolizes that effectiveness of electric power conversion to torque produce by motor. For steady state condition V_L voltage can be ignored, and V_a is written as the following equation (6.30).

$$V_a = V_R + V_{EMF} = R_m \frac{\tau_m}{k_t} + k_e w_m \tag{6.30}$$

Mechanical power provided by the joint motor is result of its required torque and load angular speed. Mechanical power from the motor is

$$P_{mech} = \tau_m w_m = (\frac{k_t}{R_m} V_a - {k_m}^2 w_m) w_m \tag{6.31}$$

Total power is the sum of the power to overcome friction and the power to accelerate the load. If it is an idealized DC motor without power loss during electrical power into mechanical power conversion, electrical power should be equal to mechanical power.

$$P_{in} = V_{EMF} l_a = \tau_m w_m = k_t l_a w_m \tag{6.32}$$

Following torque equation can be created by taking into consideration the mechanical properties of the motor in equation (6.33)

$$T_m = T_{\dot{w}} + T_w + T_L \tag{6.33}$$

where T_m represents electromagnetic torque, $T_{\dot{w}}$ represents motor inertial torque, T_w represents motor damping torque, and T_L represents load torque. Motor electromagnetic torque is proportional to the motor torque as shown in equation (6.27). The motor's angular acceleration creates an inertial torque.

$$T_{\dot{w}} = I \frac{\partial w_m(t)}{\partial t} \tag{6.34}$$

where I represents the moment of inertia of motor rotor and joined load link. T_w is proportional to the motor rotor velocity.

$$T_w = f w_m(t) \tag{6.35}$$

where f shows viscous friction or viscous damping in the motor. Substituting (6.33) and (6.34) into (6.33) the second differential equation of the model is obtained in equation (6.36).

$$k_t l_a(t) = I\frac{\partial w_m(t)}{\partial t} + f w_m(t) + T_L \tag{6.36}$$

Therefore, the Laplace transform can be implemented on equations (6.30) and (6.36)

$$V_{in} = k_t w_m(s) + l_a(s)(R_m + sL) \tag{6.37}$$

$$k_t i(t) = (f + sJ) w_m(s) + T_L \tag{6.38}$$

From (6.37) and (6.38), a joint model is obtained

$$w_m(s) = \frac{k_t^2}{(R_m + sL)(f + sI) + k_t^2} V_{in}(s) - \frac{R_m + sL}{(R_m + sL)(f + sI) + k_t^2} T_L(s) \tag{6.39}$$

Figure 6.3 shows a diagram of the obtained dynamical model in equation (6.39)

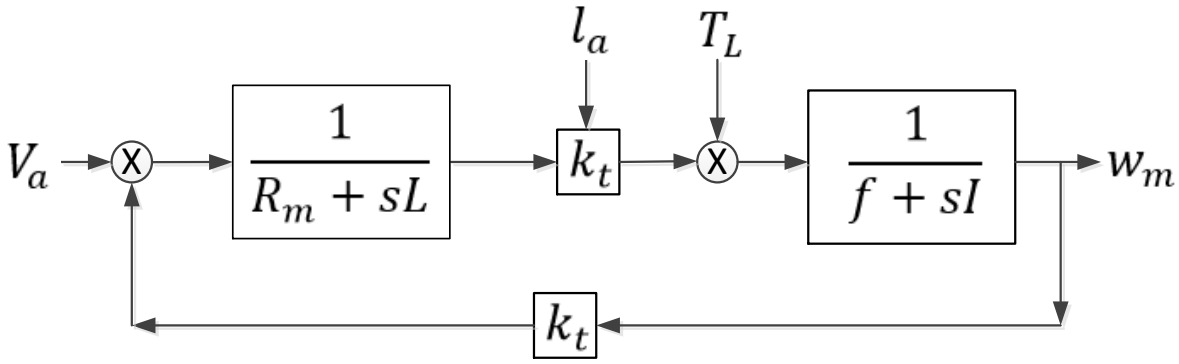

Figure 6.3 Joint DCM motor model

Transfer function can be shown in the following equation (6.40), since current is used to control the system.

$$w_m(s) = \frac{k_t}{(f + sI)} l_a(s) - \frac{1}{(f + sI)} T_L(s) \tag{6.40}$$

Transfer function first component is affected by the rotor current, second component is affected by torque of the motor load. Humanoid robot motions and mass of the load link affect the load torque and the moment of the inertia. Dynamics of the above function is affected by the inertial value. Load torque can be seen as a disturbing influence for motor velocity and motor current.

6.4 Trajectory Tracking

Linear differential equation of system along with nonlinear form with disturbance is shown below.

$$I_{eff}\ddot{\theta}_{mk} + B_{eff}\dot{\theta}_{mk} = KV_k - D_k g_k \tag{6.41}$$

In this method along with feed forwarding the information calculation of d_k term in above equation is done which contains terms representing Coriolis, Centripetal, and gravity.

$$D_k = \sum_{j,k} D_{kj}(q)\ddot{q}_j + \sum_{i,j} H_{ikj}(q)\dot{q}_i\dot{q}_j + G_k \tag{6.42}$$

The following Figure 6.4 shows the trajectory tracking control mechanism. Output is the joint angular position and the joint angular velocity.

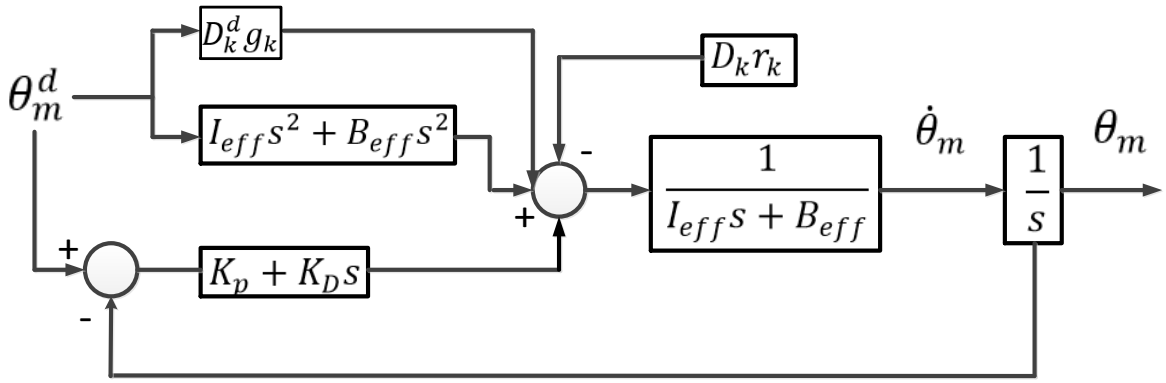

Figure 6.4 Trajectory tracking control mechanism

Controller equation is shown below in equation (6.43).

$$KV_k = I_{eff}\ddot{\theta}^d + B_{eff}\dot{\theta}^d + K_p(\theta^d - \theta_m) + K_D\left(\dot{\theta}^d - \dot{\theta}_m\right) + D_k^d g_k \tag{6.43}$$

Substituting this controller, equation (6.44) is obtained.

$$I_{eff}\ddot{e} + \left(B_{eff} + K_D\right)\dot{e} + K_p e = -\left(D_k - D_k^d\right)g_k \tag{6.44}$$

where

$$e(t) = \theta_m - \theta^d \tag{6.45}$$

where θ^d represents the desired angular rotation of the joint, and θ_m represents the joint actual angular rotation. The tracking error can be reduced but calculation of nonlinear terms representing Coriolis, centripetal, gravitational which will rise complexity of the controller.

CHAPTER 7: EXPERIMENTS ON REAL ROBOT – STANDING UP AND SITTING DOWN

The goal of the experiments is to analyze the controllers formulated previously and find the minimum energy consumption during the standing and sitting down motions, which are realized by different motion variable and within motion constraints. In order to compare energy usage for motions with different angular velocities, fully actuated humanoid robot accomplished the given joint trajectories with different task times. During every individual motion experiment, all data related to the robots motion, such as joint rotation, velocity, foot contact forces, battery voltage and current, is recorded.

7.1 Robot Used in Experiments

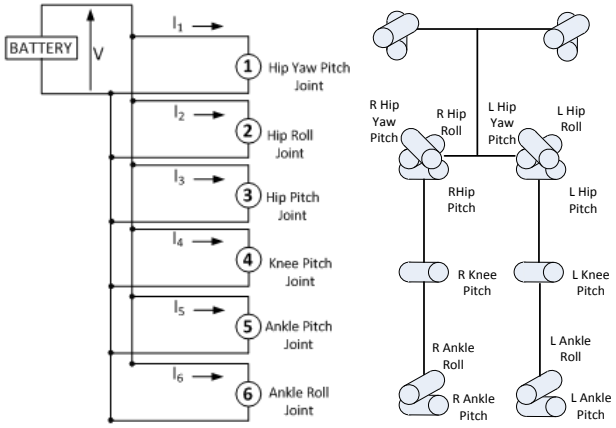

Figure 7.1 (Left) Electric diagram of lower body NAO joints, (Right) diagram showing joints relative location.

Nao V4.0 humanoid is used for all experiments. Figure 7.1 shows the humanoid robot structure, relative location of the joints and electric diagram of a leg. Three main joints studied in the experiments are ankle pitch, knee pitch and hip pitch joints. This robot is modeled as a 4-link planar robot, and it is assumed that both sides of the robot (left and right) are identical.

7.2 Standing Up and Sitting Down Motion

The humanoid is in crouch position initially. Its next motion is to stand up while maintaining its balance. During this experiment, humanoid will obey the constraints (CoM, CoP) previously discussed, it tries to keep its torso vertical to the ground, and it does not lift any feet off the ground. When humanoid

reaches its next motion, as seen in Figure 9.2c, it tries to find the best location for CoM and CoP, balance itself and provide the most stable stance, and also tries to produce the most energy efficient stance by analyzing its own CoM and CoP. Next phase of this experiment for humanoid is to go back to its original crouch position from the stand position. It tries sitting down until it is in crouch position. Same constraints and objectives are still valid. Robot keeps its balance.

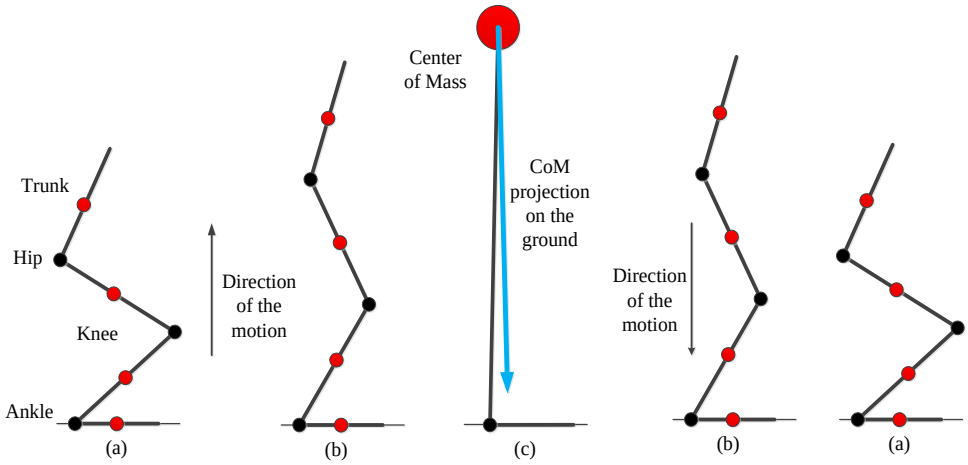

Figure 7.2 Model of standing up and sitting down

7.3 Process Used to Find the Minimum Energy Usage

Figure 7.3 shows the process flow for successful standing up and sitting down motions with minimum acceleration, minimum mechanical power loss, minimum electrical loss and minimum electrical current usage. Humanoid starts its motions with a reference angular velocity and joint trajectories. After these velocities and trajectories are applied to the joint motors, constraints are verified that, these limitations values are not violated which can cause humanoid to fall over. Some motion durations can be very short which will cause very high speed standing up and sitting down motion, or they can be very slow which will take a very long time to finish. DC motors will draw input current, voltage and electrical power depending on its electrical and mechanical loads and electrical and mechanical losses. These values will differ with different angular velocities, different trajectories and motion task time required.

Decision making process will choose the minimum electrical input current, power for a successful motion task. At the same time, process will choose the minimum possible electrical losses and required mechanical torque and power to accomplish the motion task. With these new values, all motion values will be reevaluated and checked again for a successful motion task until minimum values for losses, current, input power are reached while maintaining the enough mechanical torque and power from DC motors.

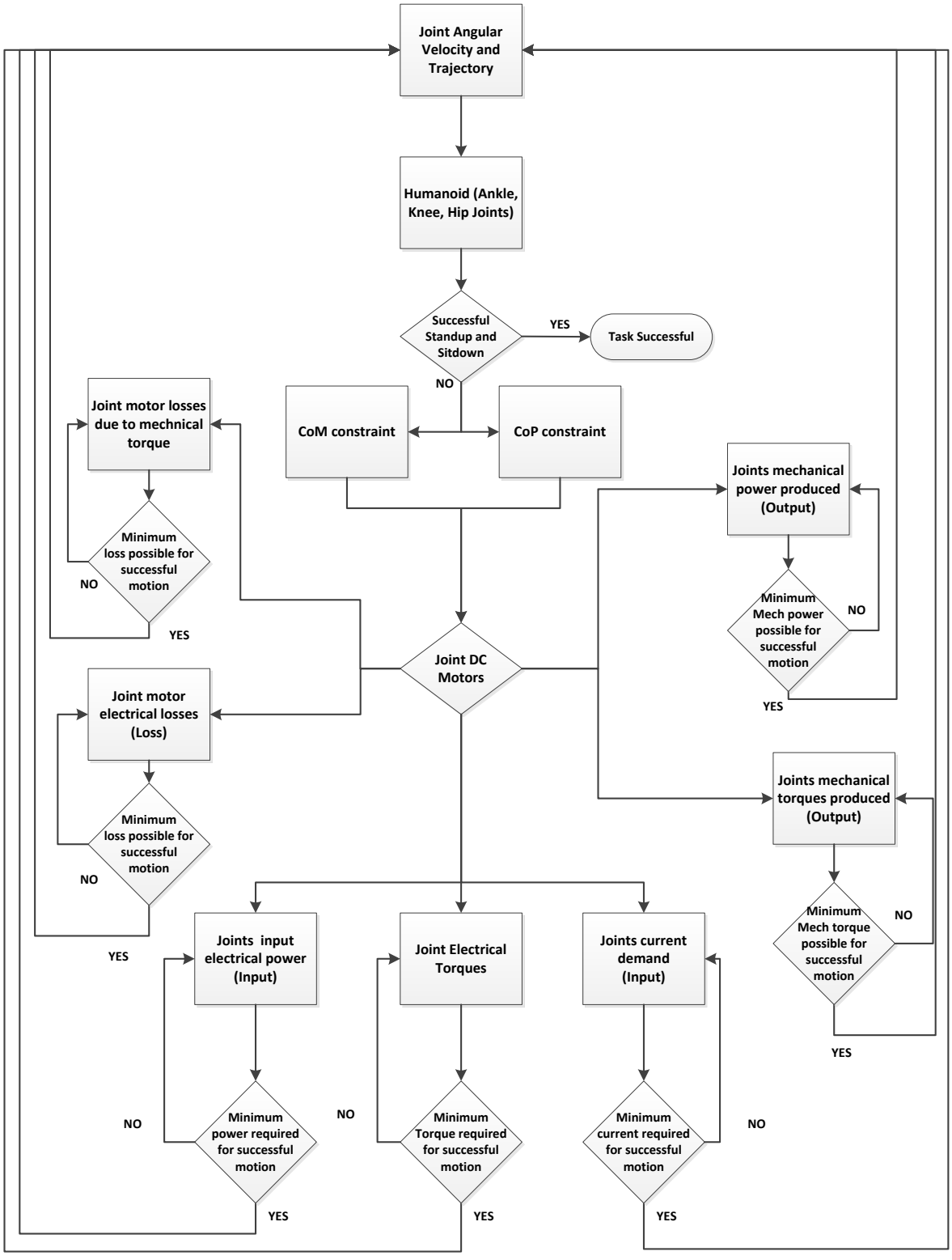

Figure 7.3 Decision making process for lower energy usage per joints

It is the goal of this particular test to find the best angular velocity of joint trajectories to obtain minimum energy consumption. In order to accomplish this, robot tries different trajectories and joint angular velocities. Every joint angular velocity and trajectory will have a power consumption or energy expenditure profile depending on the humanoid's dynamics. This information is used by the process to find the best acceptable velocity and trajectory with minimum power consumption for this particular task.

There are some assumptions that are needed be defined. Torso of the humanoid will be in a vertical position, there might be small changes in the torso angle but algorithm will try to find the best energy efficient angle by moving backward or forward during standing up or sitting down. Humanoid will have enough friction under each foot so that it will not slip and fall down.

There are location constraints for ground projection of CoM and CoP of the humanoid which will be explained and tested in another section. Another constraint is the angular and linear velocity of the humanoid CoM.

To evade the humanoid fall due to high angular speeds, robot will find the best angular and linear velocity value of center of mass for minimum energy usage. Process used to approximate the robot model analyzes the kinematics and dynamics of the real humanoid robot, estimates the torques that are required by every joints. This torque information is used when motor mechanical power is estimated per joint.

Robot will save all related information for every joint locally to analyze data later offline. After analysis of this data, once a best match is found for velocity and trajectory for best energy usage, it will attempt the test again to verify the same results. Data is collected and analyzed by using Python and Matlab programs. There is a Naoqi module running in Nao's main CPU processor to record all the data from all joints during the tests. This includes system time, joint angular positions, joint current consumptions, robot's battery voltage and current demand.

Robot is managed over an Ethernet network from a Microsoft Windows 7 machine running a Python (version 2.7) codes for all the motion related tasks. Matlab program is used to analyze the data.

7.4 Comparison of the Joint Angular Positions

Figure 7.4 shows the angular positions for knee, hip and ankle joints. As seen in the above graph, knee pitch joint cover larger angular difference in radians (from 2.1 rad to -0.06 rad) compared to other two joints for standing up motion.

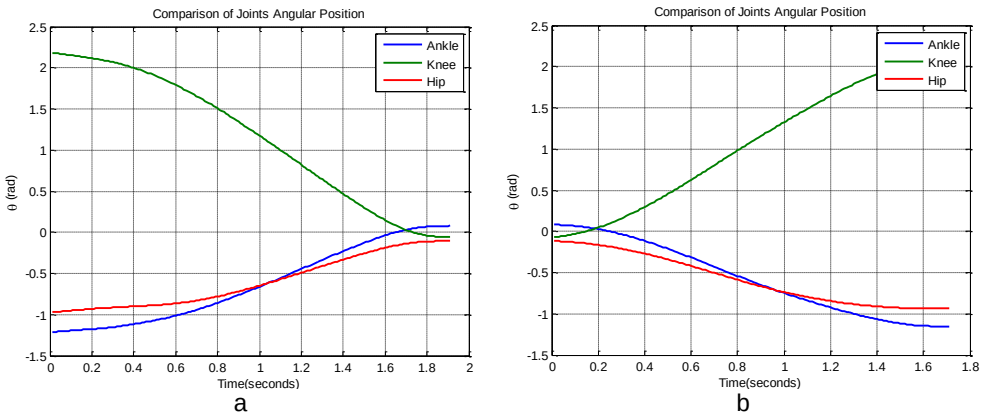

a b

Figure 7.4 Standing up trajectories and sitting down trajectories for joints

Hip pitch joint rotates (from -0.92 to -0.1) which is the least amount of rotation amongst these three joints for standing up. Ankle joint only rotates from -1.16 rad to 0.08 rad for standing up. Three joints use the same amount of rotation backwards when the humanoid is sitting down as seen in the Figure 7.4b.

7.5 Joint Angular Trajectories Duration

Following Table 7.1 shows the joint angle interpolation with time for each motion task. Three different task durations are used to compare the results. Every joint trajectory is required to finish its angular rotation in these times. Following results are compared with each other by referencing this angular speeds and task times.

Table 7.1 Joint angular trajectories duration

Joint Motion Time (sec)	1	6
Knee Pitch Angular Velocity (rad/sec)	2.13	0.35
Ankle Pitch Angular Velocity (rad/sec)	1.23	0.2
Hip Pitch Angular Velocity (rad/sec)	0.80	0.13

7.6 Joint Angular Velocity Comparison

Figure 7.5 shows the joint angular velocities. In Figure 7.5a, knee joint has the highest angular velocity and the hip has the lowest angular velocity. This same characteristic is valid for the other graph Figure 7.5b. This is because of the angular rotation time that knee pitch joint needs to finish. Of course, with shorter motion completion time, knee has the highest of angular velocity among all other joints and motion times. Hip pitch joint tries to balance the upper body vertically during this test. That's why it does not cover a wide angular trajectory and its angular velocity is minimal.

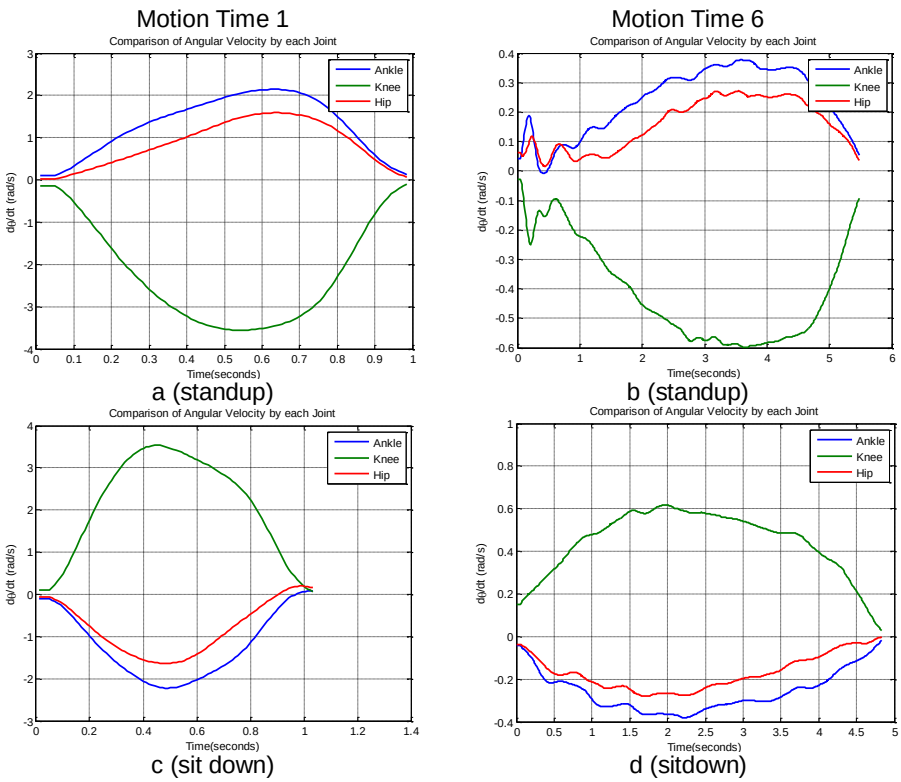

Figure 7.5 Angular velocities of each joints

7.7 Joint Accelerations

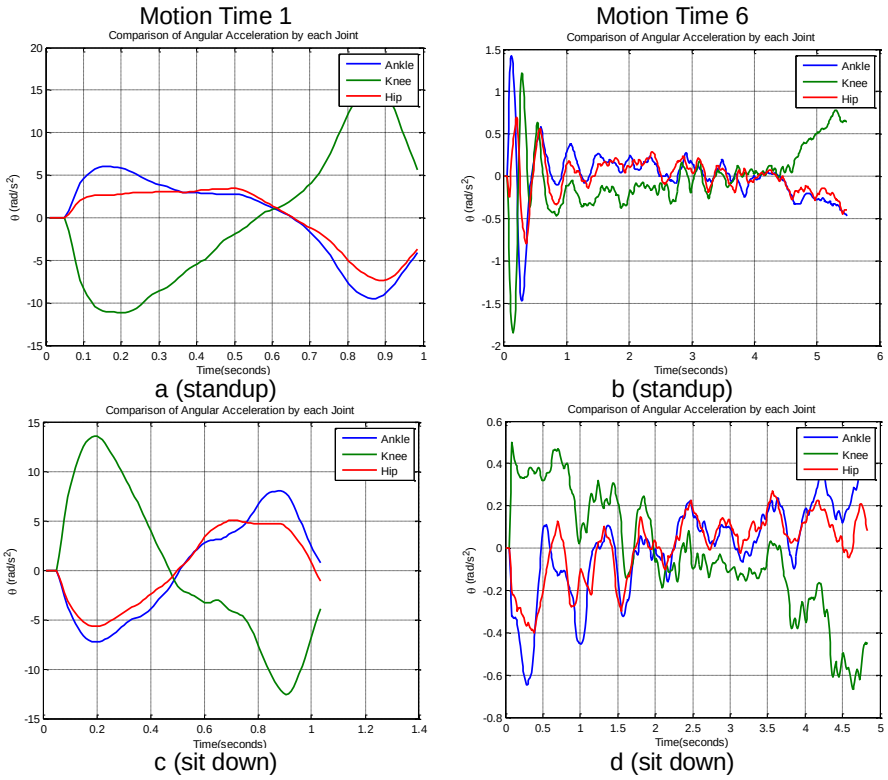

Figure 7.6 Joint accelerations

Figure 7.6 shows the joint accelerations. Knee joint has the highest acceleration, see Figure 7.6a. Knee joint uses 15% more acceleration while standing up with fast motion, and 178% more acceleration with very slow motion. Reason for the difference is that standing up requires the motion against the gravity.

7.8 Comparison of Link CoM Angular Velocity

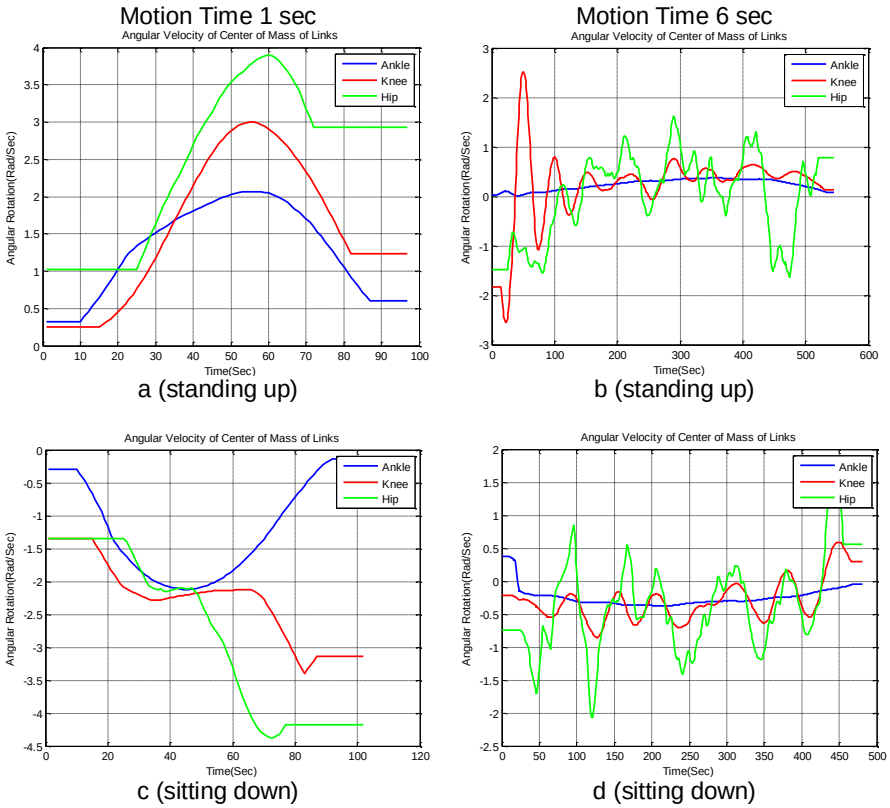

Figure 7.7 Link CoM angular and linear velocities

During standing up motion, hip pitch link CoM has the highest angular velocity, see Figure 7.7a. Ankle pitch link CoM has the lowest angular velocity. Even though knee joint needs to rotate a wider angle than the other two joints, its link CoM has a lower angular velocity value. With slowest test time (motion time 6 sec), knee joint CoM has the biggest angular velocity and ankle pitch CoM joint has the lowest angular velocity.

For sitting down motion, hip pitch link CoM has the biggest angular acceleration, and ankle pitch link CoM has the lowest angular acceleration. This is because of the hip link CoM angular rotation is bigger than the other two joints. See Figure 7.8 which shows the location displacement of each CoM. This graph shows only the sitting down motion but up and down trajectories are same, it is intended to only show the angular displacement and its effect on the velocity of every link CoM.

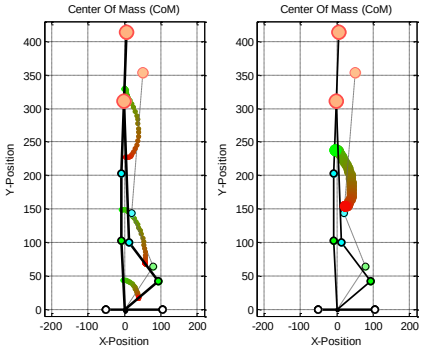

Figure 7.8 CoM location change

During sitting down motion with longer time period (6 sec), Figure 7.7d shows that hip pitch link CoM has the highest angular velocity change. Ankle pitch link CoM angular velocity is very close to zero. Motion control during sit down position tries to balance the upper body during very slow motion, that's why, graph shows the control signals are have big spikes.

7.9 Comparison of Link CoM Linear Velocity

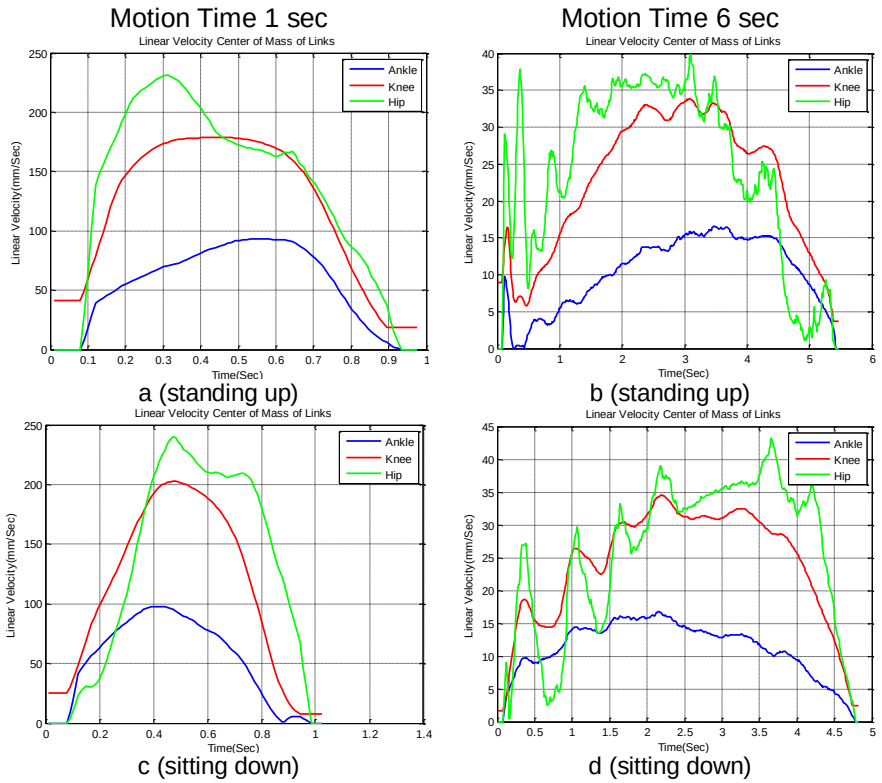

Figure 7.9 Comparison of linear velocities

As for the linear velocity of the CoM for every link, they have the very similar relationship, see Figure 7.9. Hip CoM has the highest linear velocity for standing up and sitting down for the same reason, it rotates a bigger angle in order to comply with the control signal. Signals shown for slower speed (6 sec)

has a lot spikes, it is because of the controller is trying to balance the upper body and knee joint for very slow speed with dynamic disturbances from other links, it is constantly sending commands to the joints to increase or decrease the angular velocities to comply with the constraints. Whereas with high speed test, every link CoM needs to get to their position in given short time, that's why command signals are applied more efficiently to check the position and velocity.

7.10 Link CoM Accelerations

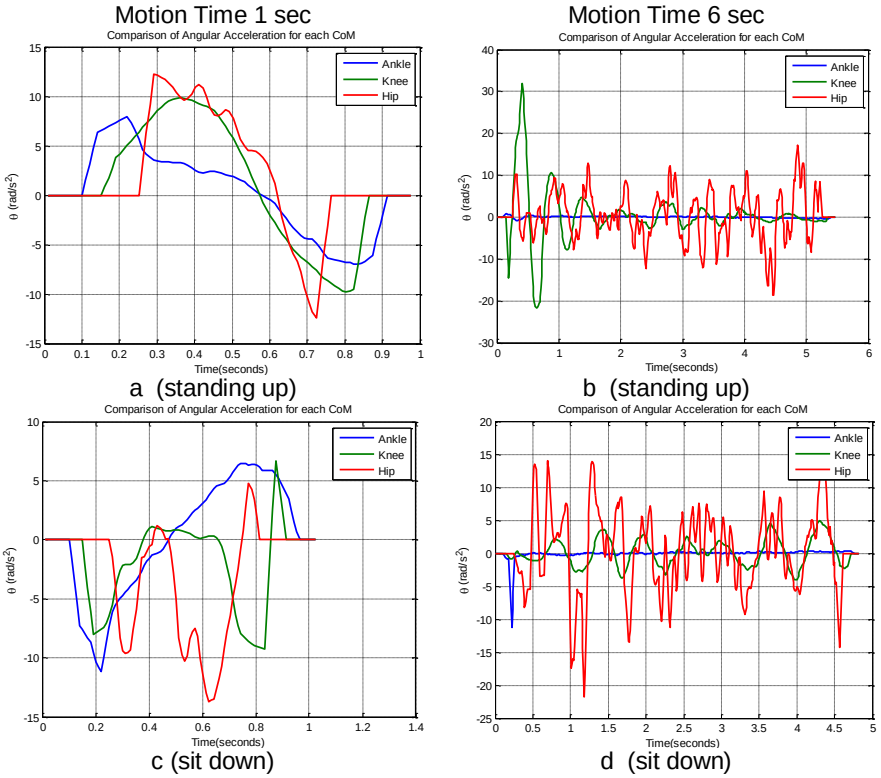

Figure 7.10 Link CoM accelerations

Figure 7.10 shows the angular acceleration of each CoM. For standing up and sitting down, hip link CoM has the highest angular acceleration, since this link CoM has the highest angular velocity, this results makes sense. In given test time, this link need to cover the biggest angular rotation, that's why it used the biggest angular acceleration and angular velocity. See Figure 7.10a and c.

For longer test time (6 sec), during standing up, even though knee link CoM uses bigger angular acceleration spike as seen in Figure 7.10b, it slowly become less. Hip link CoM on the other hand has a steady acceleration during standing up. Ankle link CoM has a fluctuating angular acceleration value around value zero. Similar results are seen on Figure 7.10d for sitting down. Hip has the highest angular acceleration, knee has oscillation like pattern and ankle has very small acceleration.

7.11 CoM Position Location

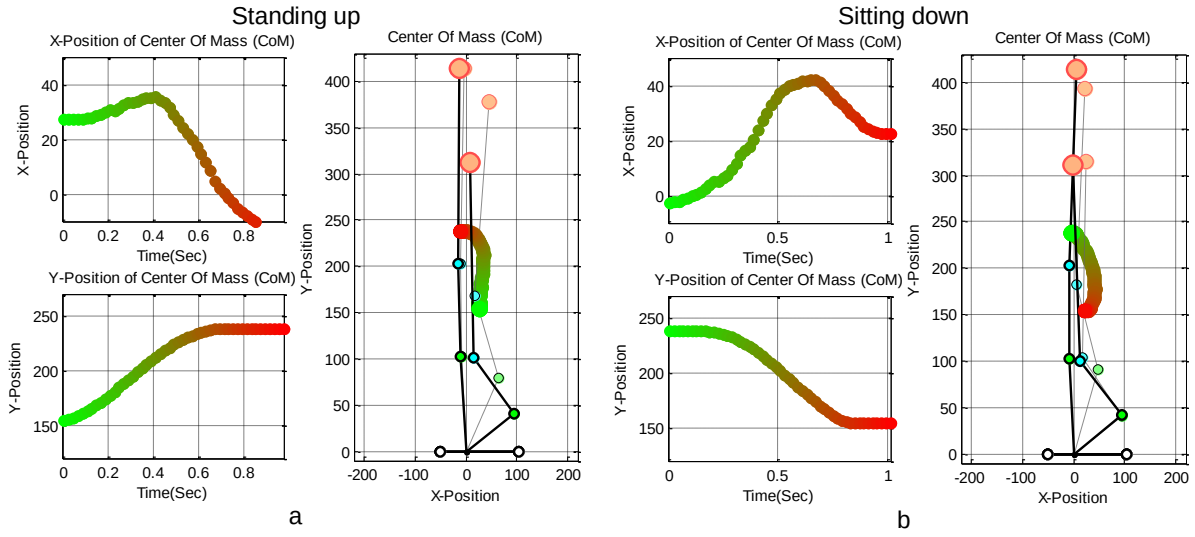

Figure 7.11 The CoM location change in x and y direction

Above Figure 7.11a shows the complete stand up and Figure 7.11b shows sitting down movement. This CoM represents the humanoid whole body center of mass. While the robot is sitting it is around 150mm from the ground, when it stands up, it reaches to almost 250 mm. during each motion, standing up and sitting down, center of mass moves forward and backward according to the CoM controller to balance the humanoid to avoid falling or tipping over the foot. Left smaller graphs in graph Figure 7.11a and b show the CoM location change in x direction and y direction during standing up and sitting down.

Humanoid's center of mass has a higher angular velocity during sitting down motion for shorter test. Angular velocity value reaches almost 3.6 rad/s standing up, and it reaches 4.6 rad/s sitting down, see Figure 7.12a and c. With longer motion time (6 sec), center of mass angular velocity decreases to 1.66 rad/sec for both standing up and sitting down. This is an expected behavior because of the time constraints on the tests, humanoid does not need have higher acceleration for slowest test. With shorter time period, humanoid needs to accelerate and decelerate faster, and this increases the overall center of mass dynamics, which increases its own angular velocity.

Figure 7.13 presents the linear velocity of the CoM. Again, with shorter response time from the humanoid, center of mass need to travel faster to a stable position, see Figure 7.13a and c, this requires a faster travel time along the joint trajectories. Longer test time (6 sec) causes less stress on the humanoid robot and this creates lower linear velocity for the center of mass. See Figure 7.13b and d.

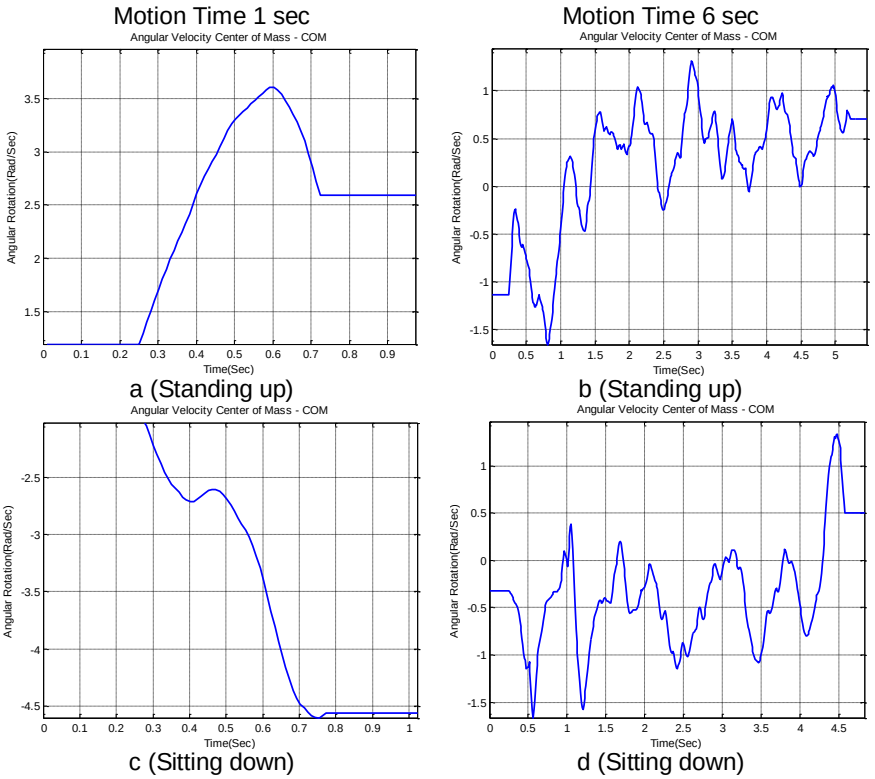

a (Standing up) b (Standing up)

c (Sitting down) d (Sitting down)

Figure 7.12 Angular velocity of CoM

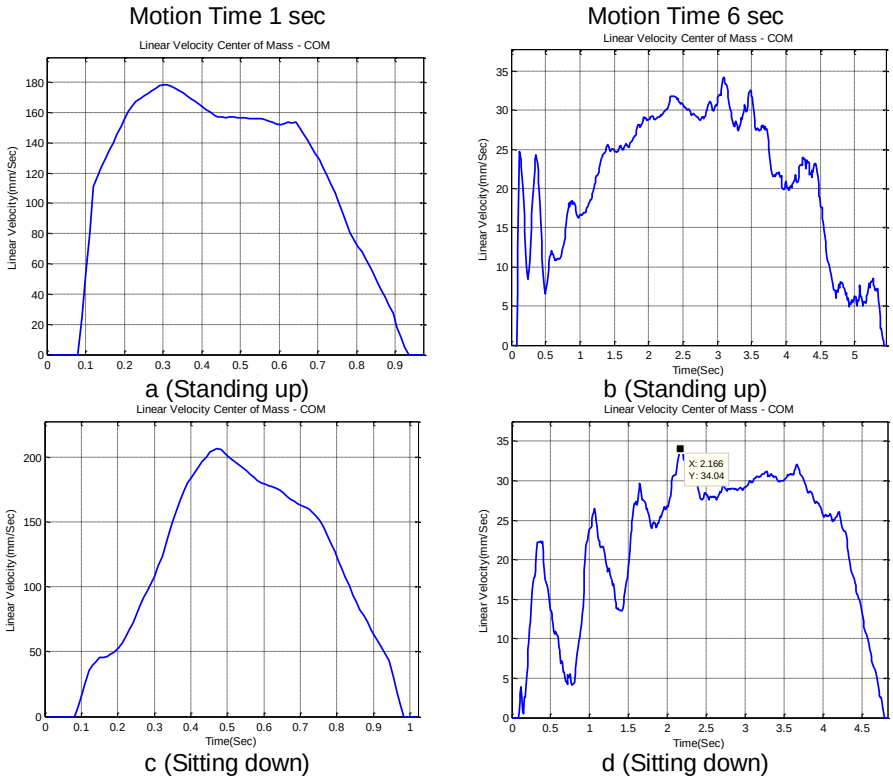

a (Standing up) b (Standing up)

c (Sitting down) d (Sitting down)

Figure 7.13 Linear velocity of the CoM

7.12 Joints Torque Comparisons

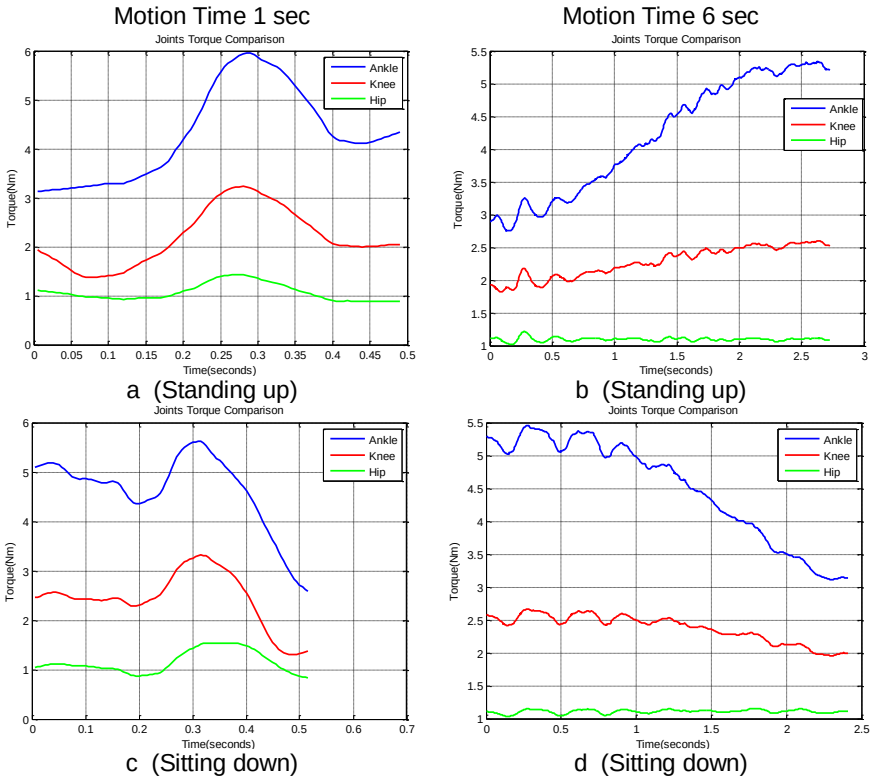

Figure 7.14 Joints torque comparison

Table 7.2 Standing up maximum torque values

Standing up	**Ankle**		**Knee**		**Hip**	
	Min	Max	Min	Max	Min	Max
Motion Time 1 sec	3.13	5.95	1.37	3.22	0.87	1.42
Motion Time 6 sec	2.58	5.62	1.3	3.31	0.84	1.53

Table 7.3 Sitting down maximum torque values

Sitting down	**Ankle**		**Knee**		**Hip**	
	Min	Max	Min	Max	Min	Max
Motion Time 1 sec	2.7	5.32	1.82	2.58	1.01	1.21
Motion Time 6 sec	3.1	5.45	1.95	2.66	1.03	1.14

Figure 7.14 shows the comparison of the torques for ankle, knee and hip for better visibility. Clearly ankle pitch joint will need much bigger torque value in order to keep up with the angular positional trajectory and velocity requirements. Knee pitch joint will have a smaller torque value than ankle joint will have. Hip pitch joint has the smallest torque value. Torque shown in graphs is calculated by the algorithm to identify the applied forces on the every joint. This torque value accounts for humanoid's all dynamical and kinematical information. From above results, knee joint has the biggest positional value compared to other

two joints. This will produce also the biggest angular velocity value among three joints. However, ankle joint will have the highest torque required to manage the standing up and sitting down motion, because, since this joint is coupled with knee joint directly and hip joint indirectly, it is affected more by its own dynamics and dynamics reflected from all other joints. These dynamics include the torque required to manage the ankle position, angular velocity of its own, and torques distributed by knee and hip joints which has totally different angular velocities and trajectories. Generally, effects of coupled joint torques are regarded as external forces, or it can be said that this ankle joint is disturbed by other coupled joints.

7.13 Mechanical Power by Joint DC Motor Comparisons

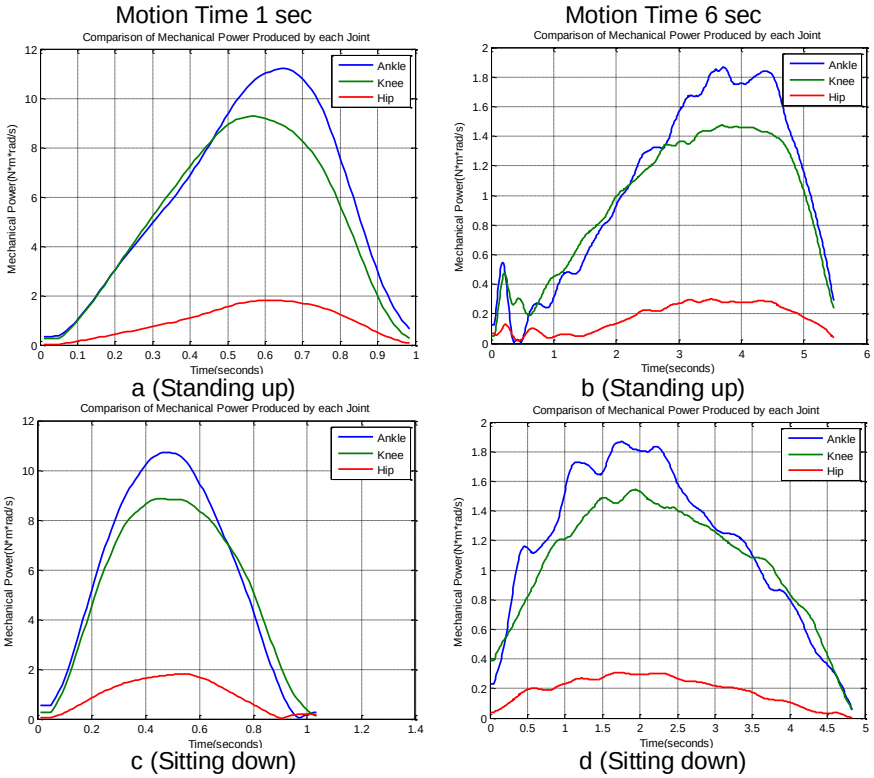

Figure 7.15 Comparison of mechanical power

Table 7.4 Standing up maximum mechanical power values produced by each joint, all values are in Nm.rad/s

Standing up	Ankle	Knee	Hip
Motion Time 1 sec	11.2	9.27	1.8
Motion Time 6 sec	1.86	1.47	0.29

Table 7.5 Sitting down maximum mechanical power values produced by each joint, all values are in Nm.rad/s

Sitting down	Ankle	Knee	Hip
Motion Time 1 sec	10.72	8.86	1.81
Motion Time 6 sec	1.86	1.54	0.3

Figure 7.15, Table 7.4 and 7.5 show the mechanical power produced by every joint to accomplish the positions. Mechanical power is directly related with torque produced and velocity required for the motion. For higher speeds, which causes shorter time to finish motion tasks, mechanical power produced is bigger for joints.

For example with this humanoid NAO during standing up motion, for ankle pitch joint, it requires almost 500% increase in mechanical power, for knee joint, it requires 530% increase in mechanical power, for knee joint, it requires 520% increase in mechanical power. These results are compared between two different test times, 1 sec and 6 sec. In regards of sitting down motion for both test times, ankle joint requires 475% increase, knee joint needs 475% increase, and hip joint needs almost 500% increase when the humanoid goes from very slow speed to very high speed.

If three joints are compared to each other for one particular test, such as for motion time 1 sec, ankle pitch joint will always have the highest mechanical power produced. This is because of its torque and speed requirements. Ankle joint torque handles all the dynamics of the humanoid body as well as all other disturbances caused by the other links during the dynamic motions.

7.14 Comparison of Electrical Input Power Provided to Joints

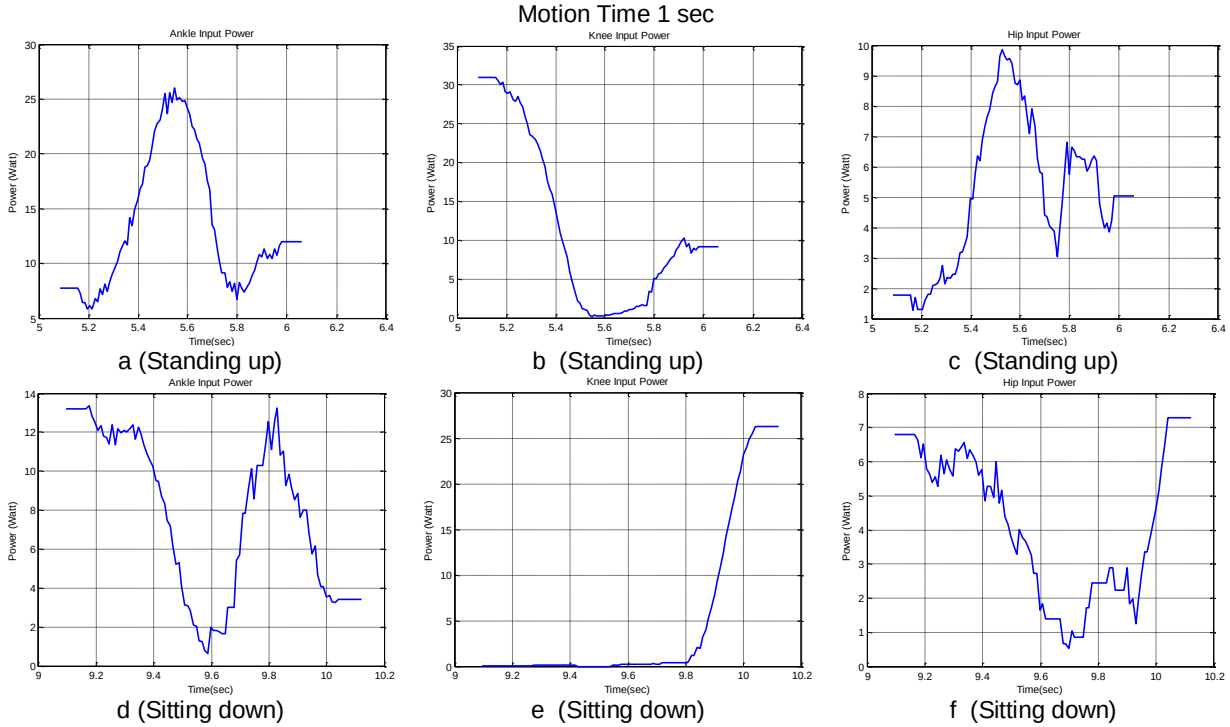

Figure 7.16 Electrical input power comparison with faster motion

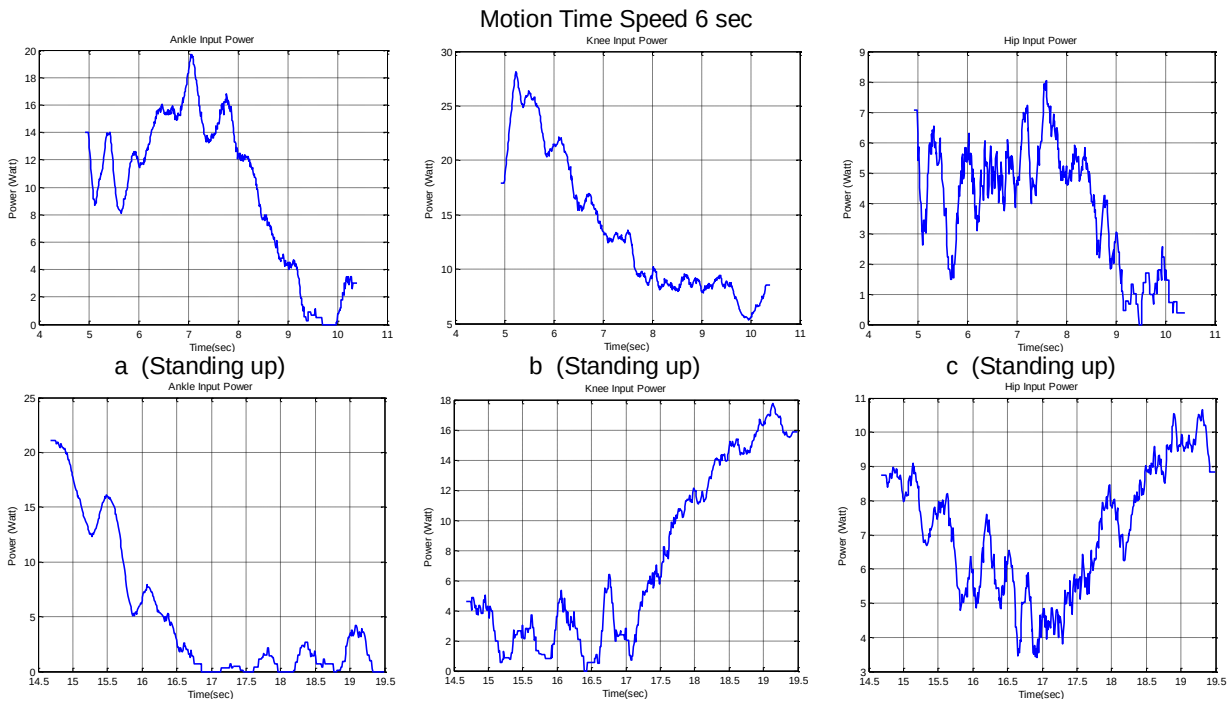

Figure 7.17 Electrical input power comparison with slower motion

Table 7.6 Standing up maximum input electrical power values delivered to each joint

Standing Up	Ankle (W)	Knee (W)	Hip (W)
Motion Time 1 sec	26	30.97	9.85
Motion Time 6 sec	19.71	28.13	8.04

Table 7.7 Sitting down maximum input electrical power values delivered to each joint

Sitting Down	Ankle (W)	Knee (W)	Hip (W)
Motion Time 1 sec	13.36	26.29	7.27
Motion Time 6 sec	21.09	17.74	10.65

All three joints will draw electrical current from the humanoid battery according to the needs of the motions required to accomplish in given time. By looking at the Figure 7.16 and Figure 7.17 above and the Table 7.6 and Table 7.7, during standing up motion, ankle pitch joint uses less input power with slower motion time, knee pitch joint uses more input power with faster motion. Hip pitch joint requires less electrical input with slower motion time. For ankle joint, from low speed motion (0.2 sec) to high speed motion (6 sec), it requires 32% increase. For knee joint, it is 10.1%, for hip joint, it is 22.5%.

For sitting down motion, ankle joint needs more electrical power for slower motions (57% increase). Knee joint needs more power for faster motions (48% increase), and hip joint needs more power for slower motions (46% increase). For the same motion time 1 sec, when standing up and sitting down powers are

compared, ankle joint uses 94% more electrical input power standing up, knee joint uses 19% more power standing up, and hip joint uses 35% more power standing up.

For the same motion time 6 sec, when standing up and sitting down powers are compared, ankle joint uses 7% less electrical input power standing up, knee joint uses 58% more power standing up, and hip joint uses 32% less power standing up.

7.15 Comparison of Loss of Electrical Power in the Joints Motor Armature

DC motors present losses when they operate due to internal electrical losses, friction losses, and torque losses. The electrical loss is caused by motor armature current. This loss is directly related to the electrical current required by DC motor structure to produce the required torque. With higher current values, the losses are expected to increase.

According to the results shown in Figure 7.18, Figure 7.19, Table 7.8 and 7.9, joints present different characteristics. For example, during standing up or sitting down, hip pitch joint loss is the lowest when compared to any other joint losses.

Knee pitch joint loss is the highest with standing up motions for both slow and fast speed. Knee joint has the highest loss when sitting down with high speed. But ankle pitch joint loss is highest with the motion speed is the slowest.

For motion time 1 sec, when standing up and sitting down power loss is compared, ankle has 278% more power loss standing up, knee pitch joint has 38% more power loss standing up, and hip pitch joint has 76% more power loss standing up. For motion time 6 sec, when standing up and sitting down power loss is compared, ankle has 14% less power loss standing up, knee pitch joint has 64% less power loss sitting down, and hip pitch joint has 75% less power loss standing up.

Table 7.8 Standing up maximum electrical power loss values in each joint

Standing up	Ankle (W)	Knee (W)	Hip (W)
Motion Time 1 sec	0.87	1.23	0.12
Motion Time 6 sec	0.5	1.02	0.08

Table 7.9 Sitting down maximum electrical power loss values in each joint

Sitting down	Ankle (W)	Knee (W)	Hip (W)
Motion Time 1 sec	0.23	0.89	0.068
Motion Time 6 sec	0.57	0.4	0.14

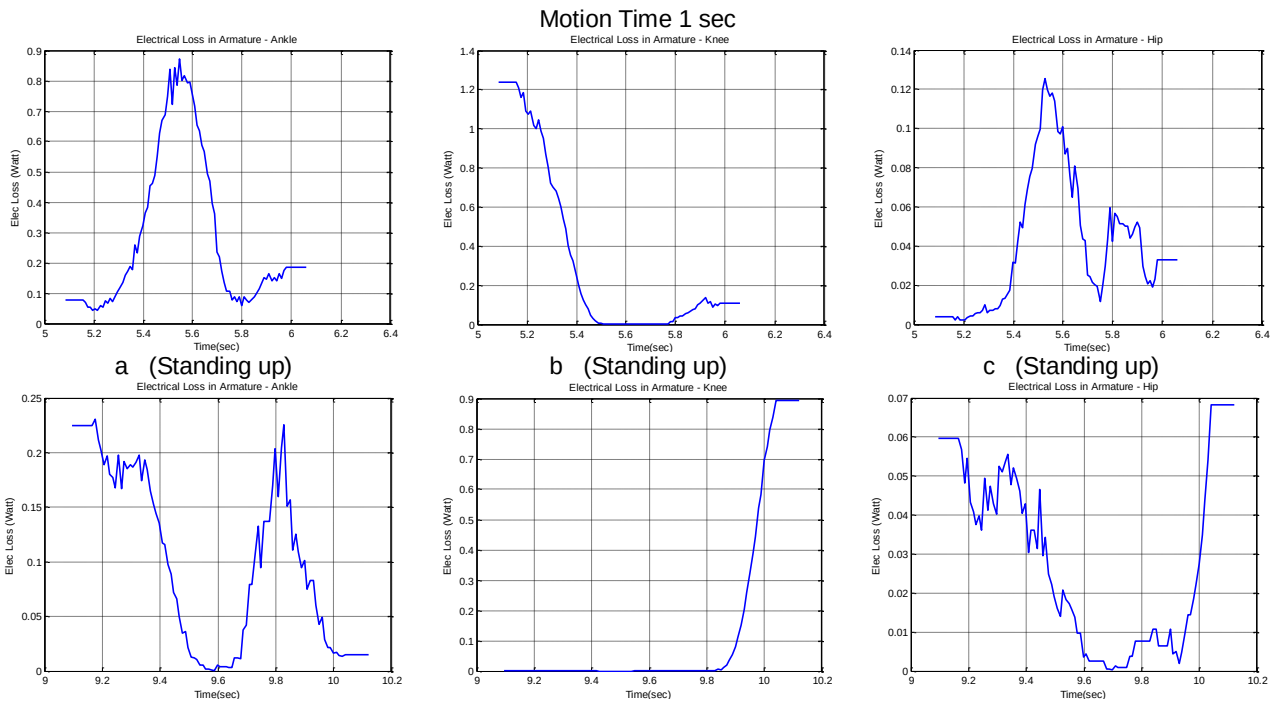

Figure 7.18 Electrical power comparison with test 1

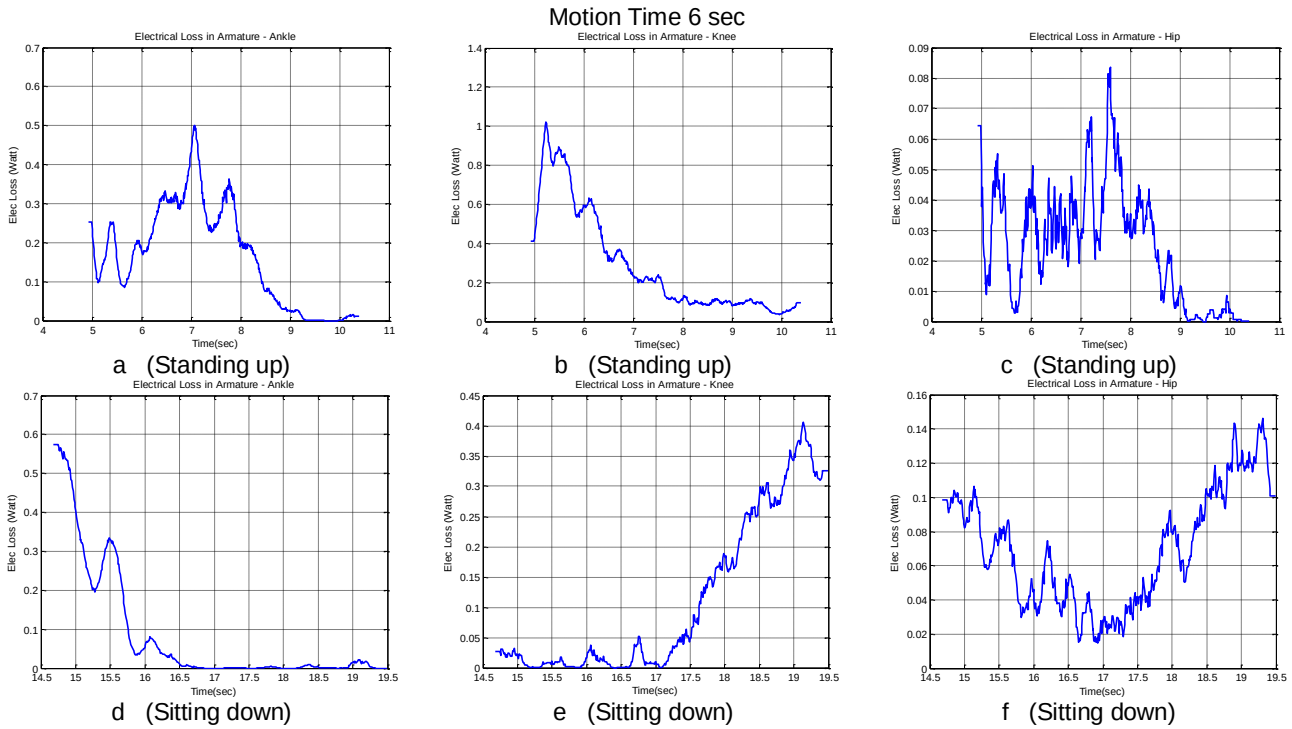

Figure 7.19 Electrical power loss comparison with test 2

7.16 Ankle, Knee and Hip Joint Current Usage Comparisons for Different Angular Speeds

Figure 7.20 and Figure 7.21 show the two different graphs for current demands for different angular velocities for the ankle pitch joint. With higher speed, this joint reaches almost maximum 1.4A current for

standing up, while with slowest speed its current demand reaches maximum 0.85A. For sitting down motion, faster motion time 1 sec has a higher maximum current usage (1A) than slower motion time 6 sec.

For the same motion time 0.2, ankle pitch joint uses more energy for standing up motion. One of the reasons is that ankle pitch joint needs to work against the gravity to apply the control commands.

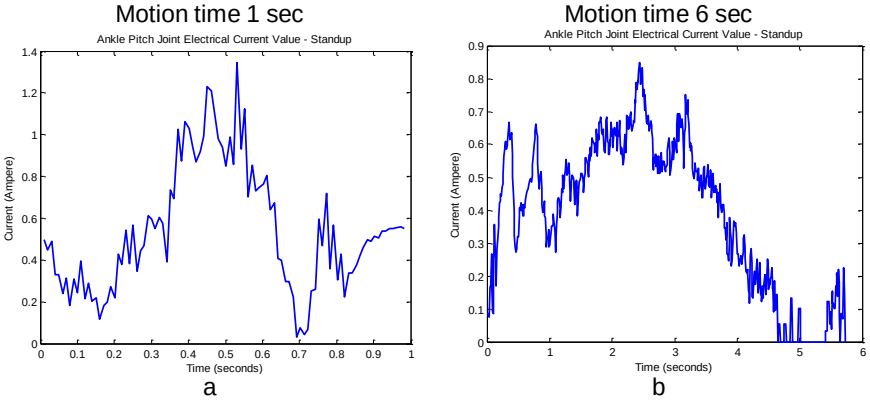

a b

Figure 7.20 Ankle pitch current usage for standing up motion

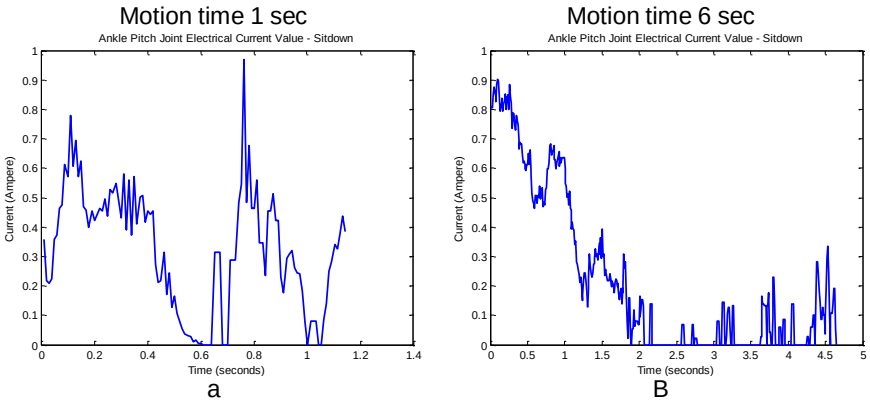

a B

Figure 7.21 Ankle pitch current usage for sitting down motion

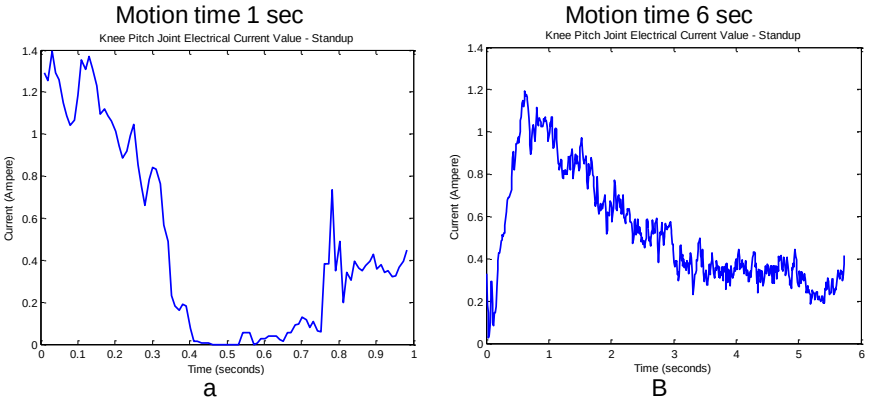

a B

Figure 7.22 Knee pitch current usage for standing up motion

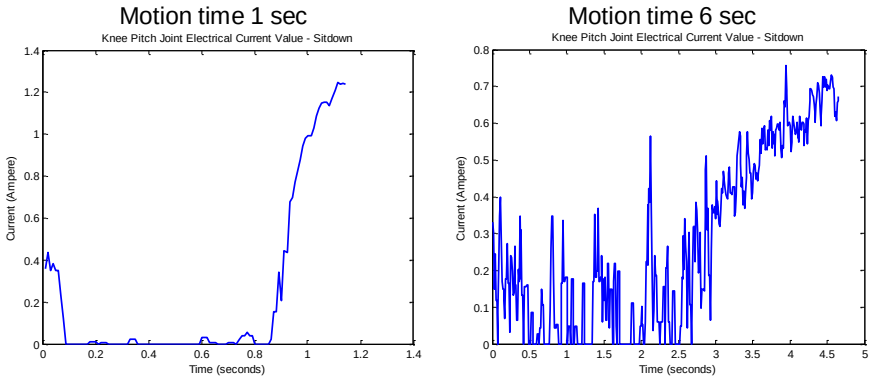

a B

Figure 7.23 Knee pitch current usage for sitting down motion

Knee pitch joint uses more current with faster motion as seen in Figure 7.22 and Figure 7.23. Standing up current reaches almost maximum 1.4A while sitting down current is around maximum 1.2A. Knee pitch joint uses less current with slower speed. For sitting down it reaches maximum 1.2A with slower test motion (6 sec).

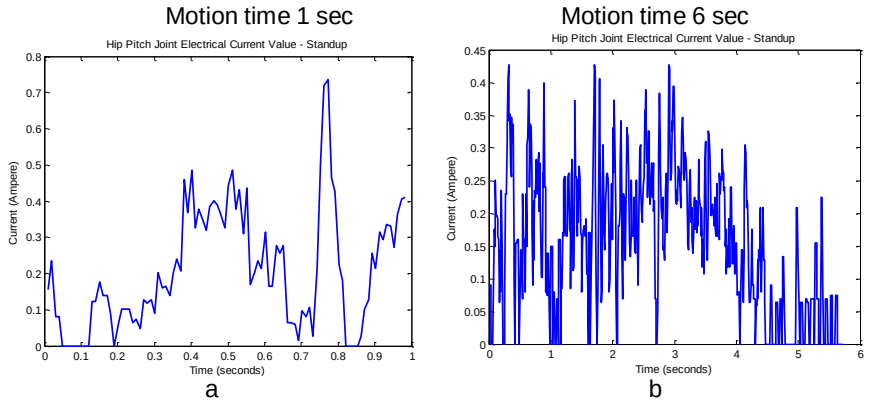

a b

Figure 7.24 Hip pitch current usage for standing up motion

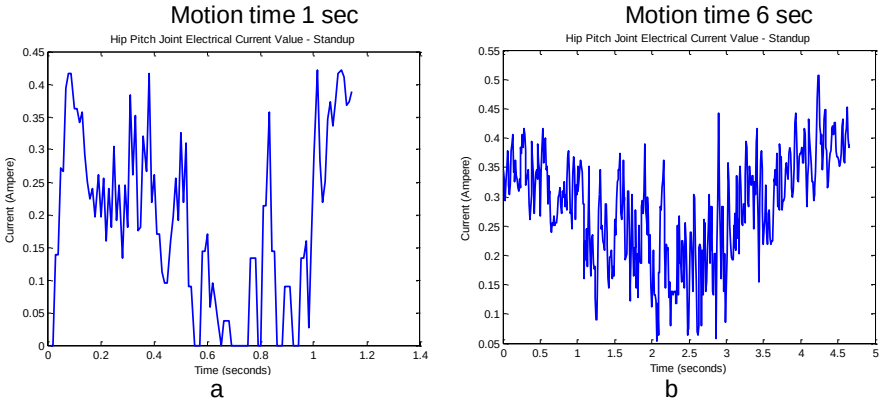

a b

Figure 7.25 Hip pitch current usage for sitting down motion

Similar results are seen in above Figure 7.24 and Figure 7.25 for hip. For faster task accomplishment time during standing up, current values have bigger values when they are compared to

the slower angular speeds. Ankle and knee joints will use higher current for faster speed. Hip joint will have maximum current value less than other joints current values. Knee joint will use almost same current value for the slowest motion. This is because of the control mechanism of the joint, it tries to balance the upper body during the motions, with longer task time, and this joint will have higher current utilization.

7.17 Current, Power Usage Comparisons for Different Angular Speeds in Table Format

Following tables show the current, electrical power loss, electrical input power values for ankle, knee and hip pitch joints. Values are shown for each joint motion time. Values in red show the maximum, green show the minimum.

Table 7.10 Knee standing up results

Motion Time (Seconds)	1	2	3	4	5	6
Maximum Current	1.392	1.296	1.205	1.216	1.301	1.194
Mean Current (Ampere)	0.472	0.505	0.510	0.482	0.534	0.530
Maximum Elect Loss (Joule)	1.550	1.343	1.162	1.182	1.354	1.141
Mean Elect Loss (Joule)	0.345	0.282	0.267	0.239	0.283	0.280
Maximum Input Energy (Watt)	34.660	32.270	30.012	30.278	32.403	29.747
Mean Input Energy (Watt)	11.777	12.581	12.720	12.009	13.317	13.219

Table 7.10 shows the results of standing up motion for knee joint. Knee pitch joint draws minimum current when it finishes its angular rotation in 6 seconds compared other times for standing up.

This speed seems to work best with the knee joint, it is using longer time and not operating at full speed. Joint's mean current usage is better when joint moves faster, with 1 second to finish the rotation.

This joint's electrical loss in the motor is the highest with the fastest joint speed because it would need the high current input to accomplish the motion task. Joint's maximum electrical input power has its highest value when it operates with the highest angular rotation but its slowest motion (4 sec) has the highest mean input value. This is because the slowest angular rotation takes longer time to finish the motion, knee joint is continuously engaged.

Table 7.11 shows the results of sitting down motion for knee joint. Knee joint works best with lower speeds as seen in the table.

With high speeds, joint starts to have very high electrical loses and maximum current usage. With longest task time for sitting down, knee joint has the highest mean values for current usage and input electrical power value.

Table 7.11 Knee sitting down results

Motion Time (Seconds)	1	2	3	4	5	6
Maximum Current	1.248	1.216	1.061	0.842	0.922	0.757
Mean Current (Ampere)	0.243	0.238	0.250	0.235	0.269	0.277
Maximum Elect Loss (Joule)	1.246	1.182	0.901	0.568	0.681	0.458
Mean Elect Loss (Joule)	0.183	0.147	0.129	0.105	0.118	0.105
Maximum Input Energy (Watt)	31.075	30.278	26.427	20.9824	22.974	18.857
Mean Input Energy (Watt)	6.061	5.941	6.226	5.868	6.706	6.915

Table 7.12 Hip standing up

Motion Time (Seconds)	1	2	3	4	5	6
Maximum Current	0.736	0.394	0.453	0.48	0.458	0.426
Mean Current (Ampere)	0.208	0.128	0.146	0.163	0.152	0.156
Maximum Elect Loss (Joule)	0.433	0.124	0.164	0.184	0.168	0.145
Mean Elect Loss (Joule)	0.055	0.020	0.023	0.030	0.027	0.028
Maximum Input Energy (Watt)	18.326	9.827	11.288	11.952	11.420	10.624
Mean Input Energy (Watt)	5.183	3.195	3.659	4.077	3.794	3.885

Table 7.12 shows the results of standing up motion for hip joint. Hip pitch joint has the highest losses and current usage for the fastest motion time (1 sec) for standing up motion. It has the lowest values for motion time 2 sec.

Table 7.13 Hip sitting down

Motion Time (Seconds)	1	2	3	4	5	6
Maximum Current	0.421	0.448	0.469	0.464	0.469	0.506
Mean Current (Ampere)	0.184	0.215	0.2420	0.262	0.293	0.281
Maximum Elect Loss (Joule)	0.142	0.160	0.176	0.1722	0.176	0.205
Mean Elect Loss (Joule)	0.041	0.047	0.055	0.061	0.075	0.069
Maximum Input Energy (Watt)	10.491	11.155	11.686	11.553	11.686	12.616
Mean Input Energy (Watt)	4.600	5.369	6.026	6.531	7.304	7.010

Table 7.13 shows the results of sitting down motion for hip joint. Hip pitch joint uses minimal current with higher speed motion (1 sec). Its mean current usage value remains higher for slower speed motion (6 sec) because of the motion time takes longer to finish.

Hip joint's electrical loss has the highest number when it rotates with slower angular speed (1 sec), but fastest angular speed (1 sec) has the lowest electrical loss value. With highest angular speed (1 sec),

this joint needs the lowest electrical input energy. With lowest angular speed (6 sec), joint needs the highest electrical input energy.

Table 7.14 Ankle standing up

Motion Time (Seconds)	1	2	3	4	5	6
Maximum Current	1.344	0.858	0.8	0.832	0.784	0.848
Mean Current (Ampere)	0.540	0.388	0.435	0.406	0.382	0.387
Maximum Elect Loss (Joule)	1.445	0.589	0.512	0.553	0.491	0.575
Mean Elect Loss (Joule)	0.302	0.167	0.196	0.182	0.155	0.162
Maximum Input Energy (Watt)	33.465	21.380	19.92	20.7168	19.521	21.115
Mean Input Energy (Watt)	13.460	9.674	10.845	10.130	9.527	9.651

Table 7.14 shows the results of standing up motion for ankle joint. Ankle pitch joint has the minimal current usage with slower angular speed (5 sec) but highest current usage with the fastest angular speed (1 sec). Mean current usage is also highest with the fastest angular speed (1 sec).

Joint's electrical loss is minimum with the slower angular speed (5 sec) and maximum with the fastest angular speed (1 sec). It needs the highest electrical input power for the highest angular speed (1 sec).

Slower angular speed (5 sec) needs the minimum electrical power input. Fastest angular speed consumes the highest mean value of electrical input power.

Table 7.15 shows the results of sitting down motion for ankle joint. Ankle pitch joint seem to be efficient with certain angular speeds. At these motion completion times (2 and 3 sec), knee pitch joint uses less current and power. Its current, electrical power usage and electrical loss values have highest values for the fastest test time (1 sec).

Table 7.15 Ankle sitting down

Motion Time (Seconds)	1	2	3	4	5	6
Maximum Current	0.970	0.789	0.832	0.8	0.821	0.901
Mean Current (Ampere)	0.322	0.206	0.196	0.202	0.214	0.220
Maximum Elect Loss (Joule)	0.753	0.498	0.553	0.512	0.539	0.649
Mean Elect Loss (Joule)	0.116	0.081	0.077	0.078	0.089	0.096
Maximum Input Energy (Watt)	24.169	19.654	20.716	19.92	20.451	22.443
Mean Input Energy (Watt)	8.028	5.151	4.888	5.044	5.333	5.499

7.18 Comparison of Maximum Values of Mechanical Power Produced, Standard Deviation Value, and Energy Lost Per Angular Speed

Figure 7.26a shows the comparison between joint maximum current usage during standing up motion. Knee joint has the highest current value, knee and hip joints have the sharp increase with increasing velocity. Each current minimum points are around 0.4 and 0.6 rad/sec. Figure 7.26b shows the mean current usage for standing up motion. Knee joint have declining mean current usage with faster motions. Ankle and hip joints have increasing mean current usage with slower motions.

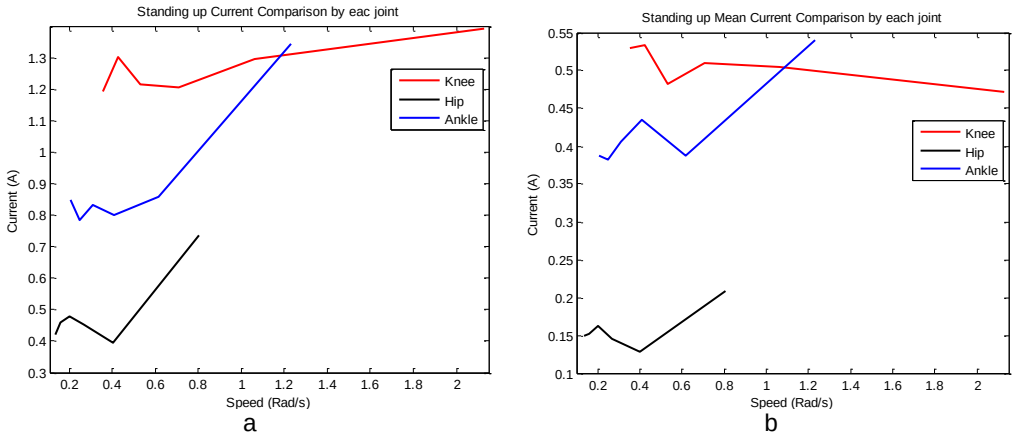

a b

Figure 7.26 Standing up maximum and mean current comparisons

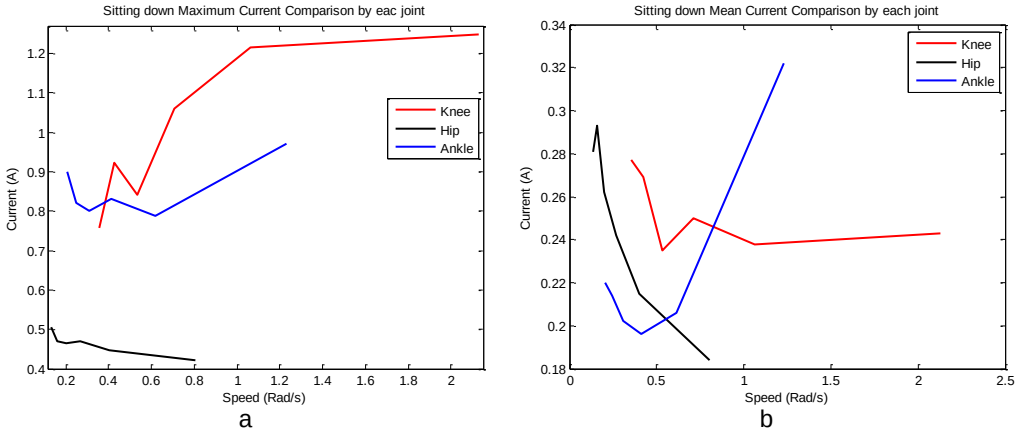

a b

Figure 7.27 Sitting down maximum and mean current comparisons

Figure 7.27a shows the maximum current comparison of each joint for sitting down motion. With increasing sitting down velocity, knee joint has the highest current usage. Since humanoid tries to sit down faster, with the help of gravity its velocity increases rapidly, but by the end of the motion, knee joint needs to stop the inertia built in the humanoid and this effect can be seen with increasing current usage with faster motions. Sitting down mean current usage comparisons are shown in the above right graph. Ankle joint

current usage increases very rapidly with the increasing motion velocity. On the other hand, kneed and hip joints mean current usage decline with faster motions.

Figure 7.28a shows the mean input power to the joints during the sitting down motion. Ankle and knee joint show similar characteristics for increase power demand with increasing motion speed. This is also effected by the gravitational forces and increased momentum of the humanoid in higher speeds.

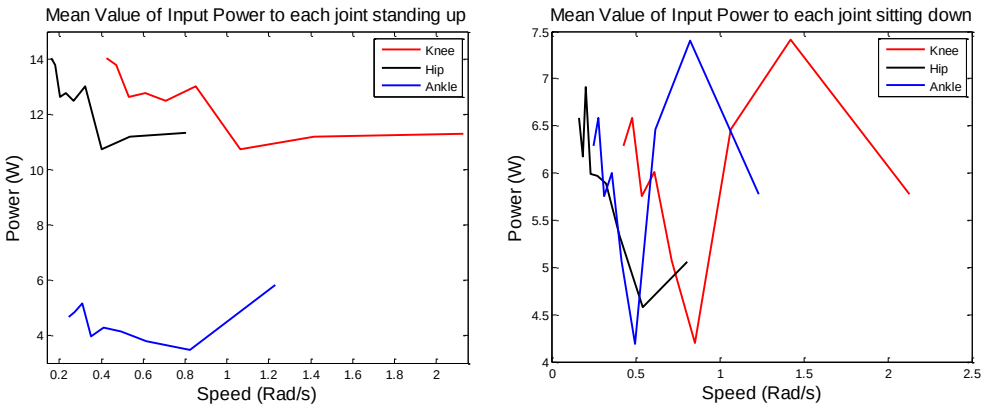

a b

Figure 7.28 Maximum and mean input power comparisons

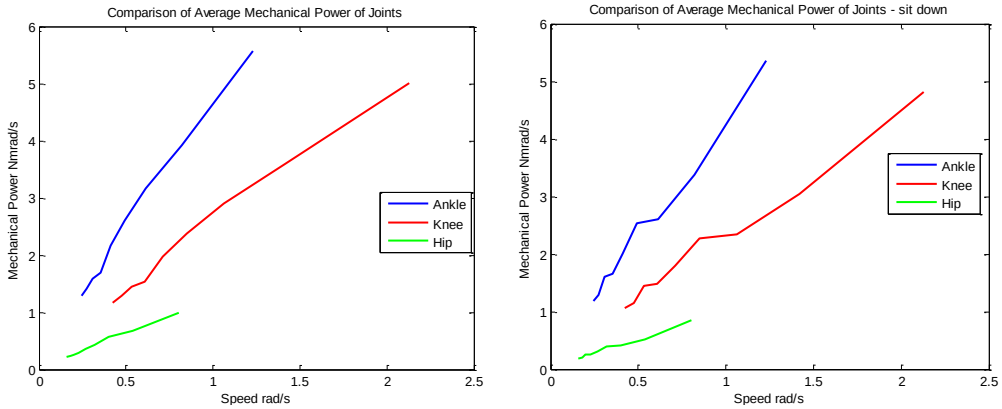

a b

Figure 7.29 Maximum and mean mechanical power comparisons

Figure 7.29a shows the mechanical power produced by each joint in accordance with the angular speed of the joints for standing up motion. With increased velocity, ankle joint produces more mechanical power with a sharp climb. Knee joint response seem as if has almost a linear response to increasing velocity. Above right graph, for sitting down motion, ankle joint produces more mechanical power than other two joints. Ankle joints mechanical power response is very similar to standing up motion response.

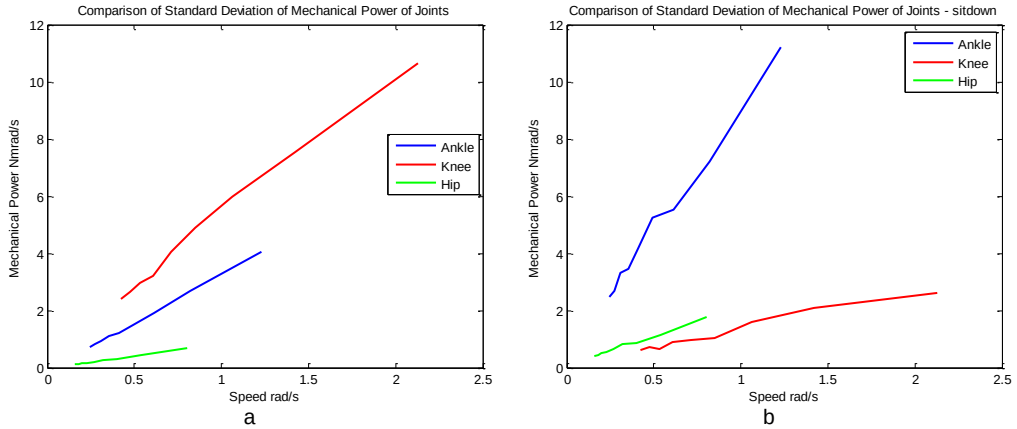

a b

Figure 7.30 Maximum and mean value of standard deviation of mechanical power comparisons

Figure 7.30a shows the standard deviation of the mechanical power produced by each joint. Knee joint has the highest deviation because with increasing speed in the standing up motion, it is required to produce more mechanical power with more speed.

Figure 7.30b shows the sitting down results of standard deviation of mechanical power. Ankle joint causes more deviation of mechanical power during sitting down motion with higher velocities. Ankle joint needs to balance the humanoid and work against the gravity forces, that's why its mechanical power standard deviation is bigger compared to the other two joints.

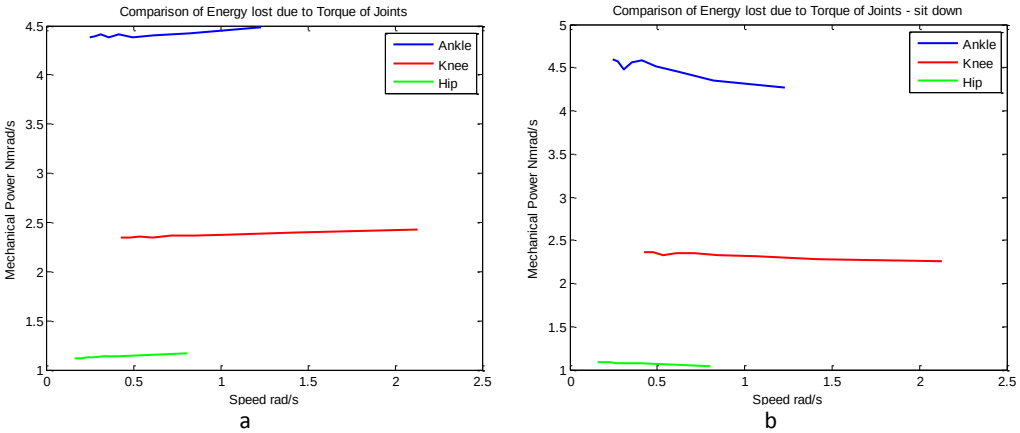

a b

Figure 7.31 Maximum and mean value of energy loss comparisons

Figure 7.31a shows the power losses due to produced torque in each joints. For standing up and sitting down motions, ankle joint loses more energy due to its own torque when compare to the other two joints. Since ankle joint is at the base of the humanoid, it is susceptible to all other coupled dynamic forces from other joints, and gravitational forces. These forces affect ankle joints ability to control the humanoid balance and stability, and this definitely caused energy loss.

7.19 Center of Pressure Location

Center of pressure point is an important indication of the forces applied under each foot. Figure 7.32 shows the fastest (1 sec) and slowest (6 sec) test results for center of pressure. With higher speed, since the dynamic forces and torques of the humanoid is higher compared to the slower speed, center of pressure location spans a larger area as seen on the left graphs. With slower speed, center of pressure is seemed to be more localized around ankle point (shown by x mark).

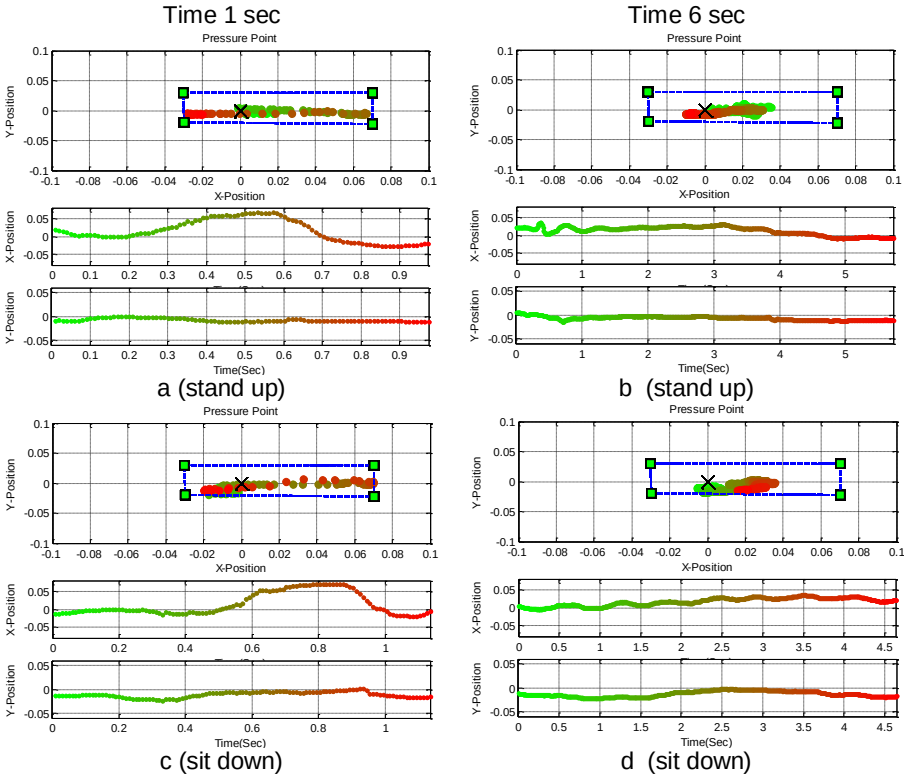

Figure 7.32 Graph shows the foot area and center of pressure location change for the standing up and sitting down motions

7.20 Tilting Forward and Backward by Ankle Joint During Biped Stance

Different experiments are performed with different tilting forward and backward ankle angles. The expectation is that as the vertical body angle changes, total energy consumption for certain joints will be bigger. The purpose of this test is to find the best possible CoM and CoP locations for least minimal energy usage for torso and lower joints using the ankle strategy formulated in previous sections. There are constraints for this motion, such as limits of CoP, CoM, friction between ground and the feet, angular velocity of CoM, and linear velocity of CoM. As long as humanoid avoids violating these constraints, biped will try to find the best vertical angle that will allow the humanoid to stay stable and utilize the minimal energy to

accomplish this task. During this task, knees and hips joints are kept still. Knees and hip joints are engaged with the torque all the time, and ankle joint will be used to control the moment and velocity of the CoM.

Figure 7.33 shows the humanoid center of mass location change. Humanoid body sways back and forth to find the minimum energy required for backward and forward balancing motions.

Humanoid center of mass moves almost 54 mm in positive and 44 mm in negative x direction, it does not change much its location in y direction since the humanoid is standing up and its feet are not moving. All joints are fixed at one position except the ankle joint.

Ankle joint uses the trajectory shown in Figure 10.35. It moves from to 0.15 rad backward and 0.25 rad forward. There are two test with two different motion times to compare the velocity effect on energy consumption, one for 2 sec and another one for 4 sec.

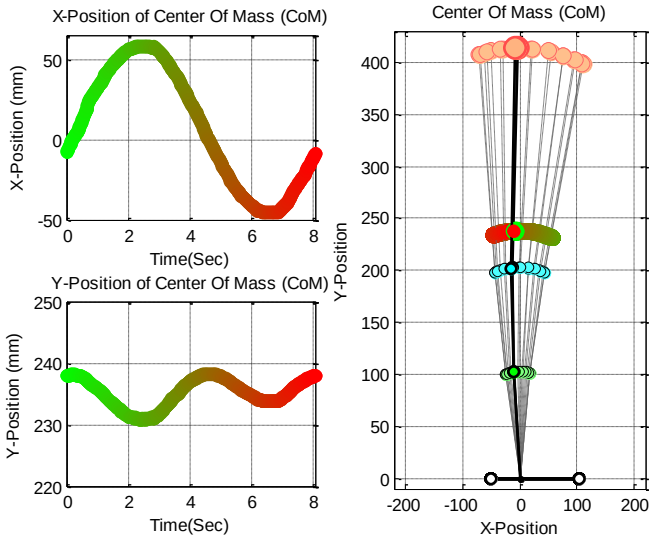

Figure 7.33 Center of mass location change by ankle

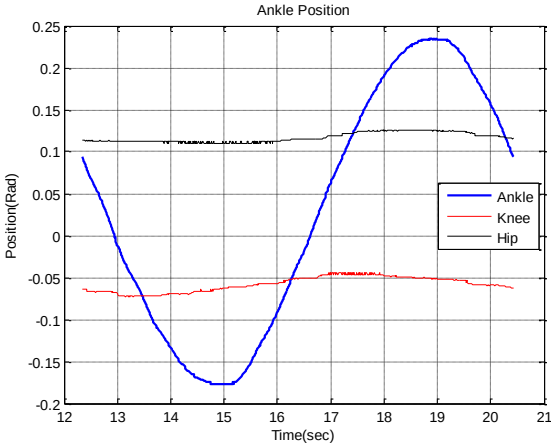

Figure 7.34 Joint angular positions, and ankle pitch joint trajectory shown in blue line

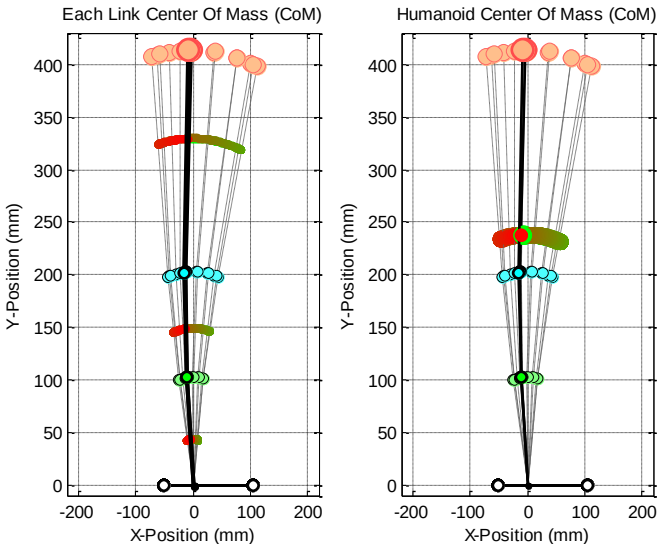

Figure 7.35 Link CoM (left figure) and humanoid CoM (right figure)

Each joint link center of mass move backward and forward, but their trajectories are different as seen in Figure 7.35. Ankle pitch link center of mass does not move much compared to hip joint link center of mass. Hip link center of mass travel between -62 mm and 85 mm, knee link center of mass travel between -31 mm and 29 mm, ankle joint link center of mass travels between -9 mm and 7 mm.

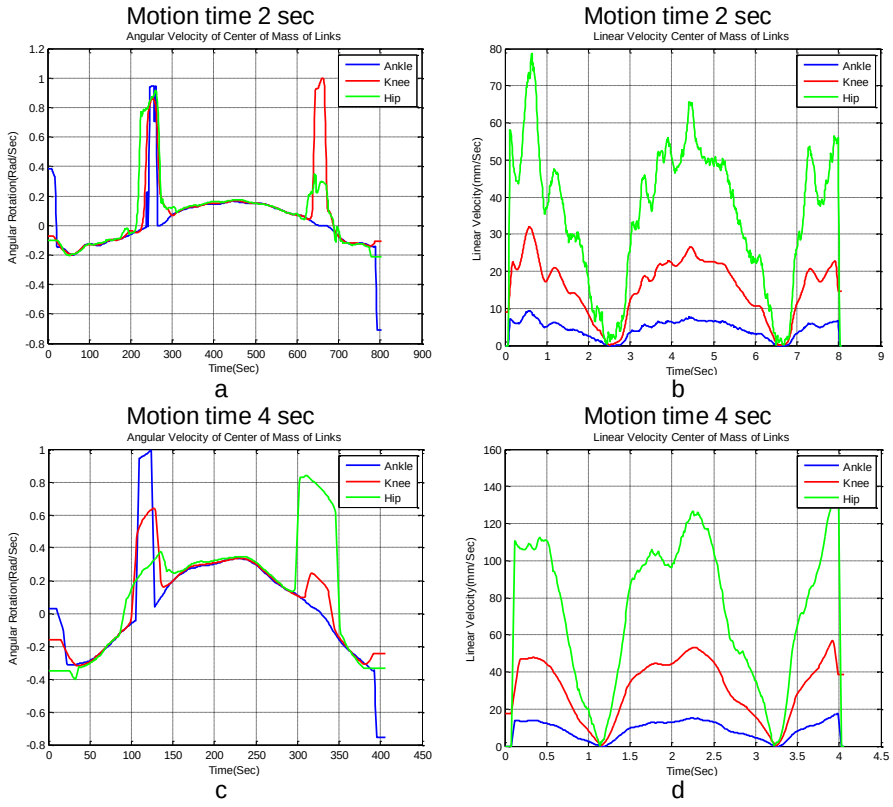

Figure 7.36 CoM of links angular and linear velocities

With shorter time to finish the motion commands given to the joint DC motors, angular and linear velocities of CoM of each link increase as seen in Figure 7.36, which shows the results for two different time, 2 sec and 4 sec. Angular velocity of the ankle joint link center of mass increases, while angular joint of knee and hip center of masses either stay close or change slightly. Over all they are very close to the same value, which is expected for the angular velocity. As for the linear velocity of each center of mass, it is definitely increasing with decrease motion time. See Figure 7.36b and d for the results. Hip link center of mass has the fastest linear velocity since its angular trajectory is bigger than other two center of masses' angular trajectories.

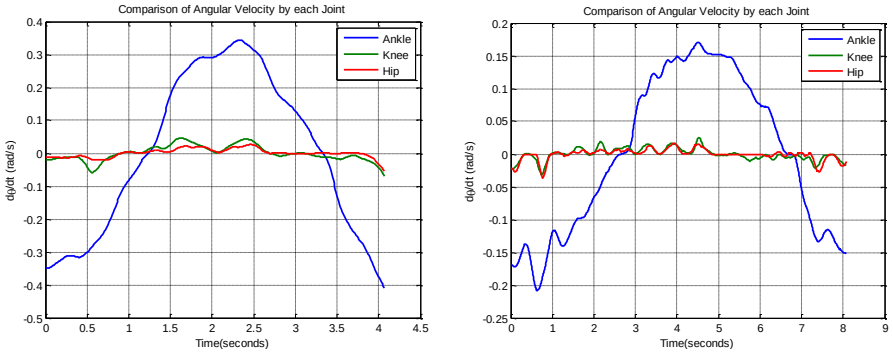

a b

Figure 7.37 Angular velocities of each joint, 2 sec (a) and 4 sec (b)

Ankle joint increases its own angular velocity to finish the motion in shorter time. Results are presented in Figure 7.37. By cutting the motion time in half, ankle joint angular velocity increases by almost 50% while other two joint's angular velocity change slightly.

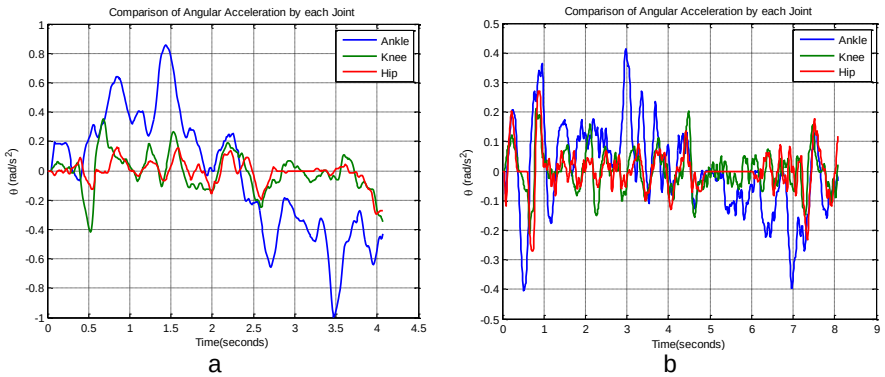

a b

Figure 7.38 Angular acceleration comparisons, 2 sec (a), 4 sec (b)

Angular acceleration is another good indicator for the joint responses to the control commands. As seen in Figure 7.38, with shorter time motion, angular acceleration of ankle joint increases almost 50%, knee joint angular acceleration also increases 50%. Hip joint angular acceleration does not reflect a big

change with motion time difference. As seen in Figure 7.38b, with slower motion time, knee and hip joint angular velocity values stay closer to each other. Figure 7.38a shows that ankle has the biggest acceleration. DC motor input power usage increases with longer motion times. This is seen in Figure 7.39b, with longer motion time, ankle joint is loaded longer which draws more current and power. With short operation time, Figure 7.39a, joint current usage is less. See Table 7.16 for comparison. With 50% less time, ankle is using 4% less input power, knee joint uses 4% less power, hip joint uses 16% less power for this particular test. Ankle joint shows higher electrical losses with longer operation time as seen in Figure 7.40b. Electrical loss value is 0.85W compared to 0.79W in short time motion. So, if angular velocity increases, ankle joint will engage shorter time and loaded shorter time, this will yield less electrical loss. See Table 7.17 for comparisons.

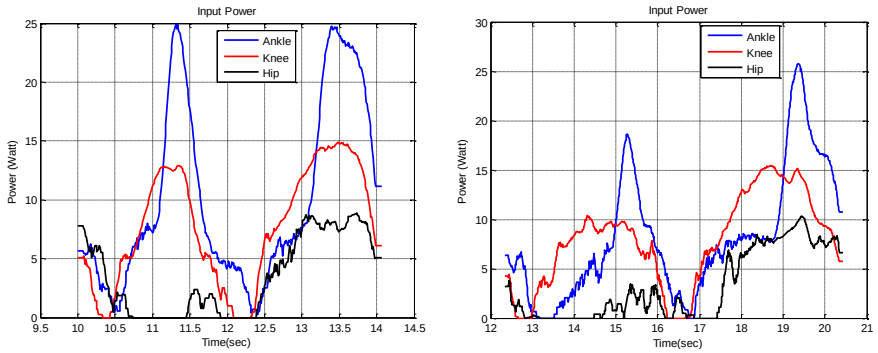

a b

Figure 7.39 Electrical power used, from 0.15 rad to 0.25 rad comparisons, 2 sec (a) and 4 sec (b)

Table 7.16 Maximum values of input power for different motion times

	Motion time 2 sec	Motion time 4 sec
Ankle (W)	24.86	25.76
Knee (W)	14.87	15.48
Hip (W)	8.87	10.33

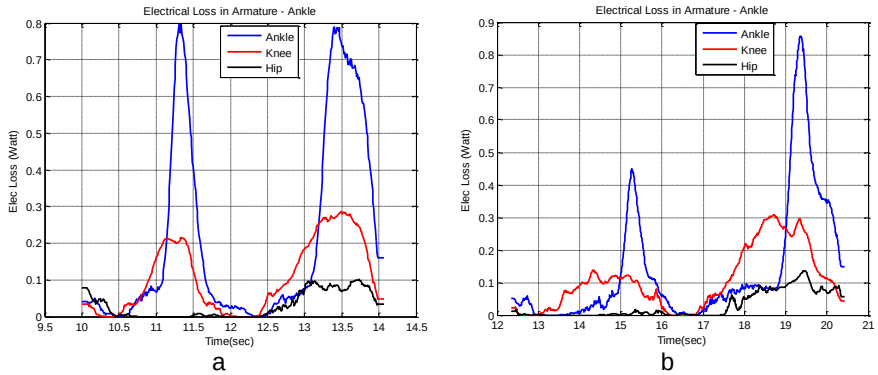

a b

Figure 7.40 Electrical loss for each joint, from 0.15 rad to 0.25 rad comparisons, 2 sec (a) and 4 sec (b)

Table 7.17 Maximum values of electrical loss in each joint for different motion times

	Motion time 2 sec	Motion time 4 sec
Ankle (W)	0.79	0.85
Knee (W)	0.28	0.3
Hip (W)	0.1	0.13

Mechanical torque represents the torque produced by the joint and forces acting on the joint from other external forces which includes the momentum and inertial effects from other body links. Figure 7.41a shows the increased angular velocity effect on the ankle joint torque. This torque has ripples which Figure 7.41b does not have. These ripples are caused by momentum and inertial effects from other joint's acceleration and dynamic motion. This is clearly seen in Lagrange equations. Table 7.18 shows the comparison of torques of each joint for two different motion times. With 50% less time for each motion, ankle joint torque increases by 2.5%. Other two joint torques do not change a lot to mention here.

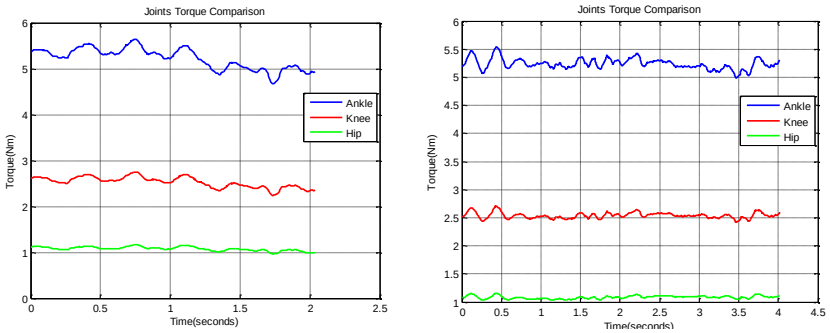

a b

Figure 7.41 Mechanical torque produced by each joint, from 0.15 rad to 0.25 rad comparisons

Table 7.18 Maximum values of torque produced by each joint

	Motion time 2 sec	Motion time 4 sec
Ankle (Nm)	5.64	5.5
Knee (Nm)	2.75	2.7
Hip (Nm)	1.17	1.15

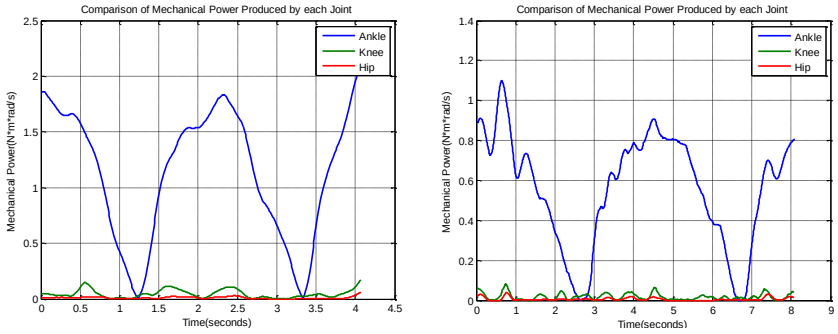

a b

Figure 7.42 Mechanical power produced by each joint, from 0.15 rad to 0.25 rad comparisons

Table 7.19 Maximum values of mechanical power by each joint comparison for two different motion times

	Motion time 2 sec	Motion time 4 sec
Ankle (NmRad/Sec)	2.13	1.1
Knee (NmRad/Sec)	0.17	0.08
Hip (NmRad/Sec)	0.05	0.04

Mechanical power produced by each joint is effected by joint angular velocity and torque produced. Result of increased angular velocity and torque can be seen in Figure 7.42 and Table 7.19.

Ankle joint needs 93% more mechanical power to handle faster motion, knee joint needs 112% more mechanical power and hip joint needs 25 % more mechanical power.

Table 7.20 Power, current, electrical loss comparison

Motion Time (Seconds)	**2**	**3**	**4**
Maximum Current	1.077	1.034	1.098
Mean Current (Ampere)	0.403	0.338	0.325
Maximum Electrical Loss (Joule)	0.928	0.856	0.965
Mean Electrical Loss (Joule)	0.211	0.153	0.139
Maximum Input Energy (Watt)	26.825	25.763	27.356
Mean Input Energy (Watt)	10.039	8.438	8.116

Table 7.20 shows mean and maximum values of the electrical power, current input, and electrical loss for ankle joint.

For highest speed (motion time 2 sec), ankle joint has highest mean current input demand, highest mean electrical losses and highest mean input power. For longer motion time (4 sec), ankle joint has maximum values for input current, electrical loss, and input power. Ankle joint seems to work best with mid-range velocity (3 sec) for balancing the humanoid body.

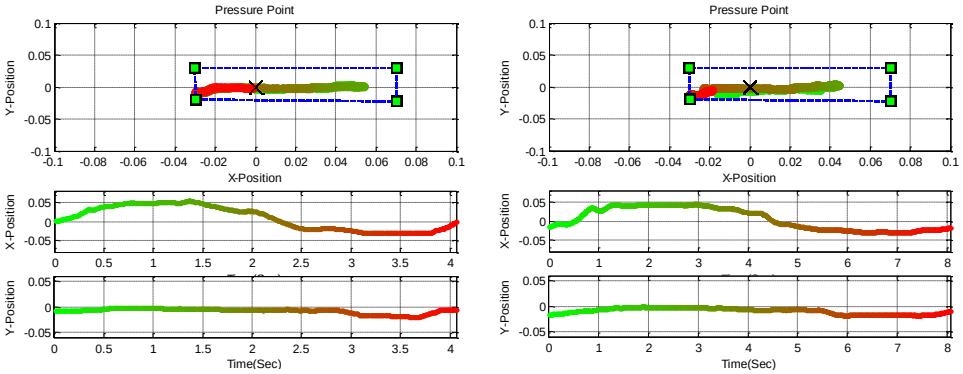

a b

Figure 7.43 Center of pressure comparison for fast and slow motion

Center of pressure location results are seen in Figure 7.43. With faster ankle joint motion, center of pressure points spreads over a wider area because of the increased dynamics of the humanoid. With slower angular speed of ankle joint, center of pressure points are covering less area.

7.21 Tilting Forward and Backward During Biped Stand by Hip Joint

The purpose of this test is to use hip control strategy to balance the robot, increase the stability and find the best possible torso posture for lowest minimal energy usage for torso as well as for the rest of the joints.

In this test, humanoid keeps its stance posture with ankle, knees and hip joints fully actuated. Torso angle which is initially vertical to the ground is changed in order to find the best CoM, CoP projection locations on the ground, and hip position that has minimal energy usage. Hip joints are used to move the torso clockwise and counterclockwise as a strategy for better performance. During this motion, constraints of CoM, CoP, and angular velocity are not violated. All other joints are fixed except hip joints.

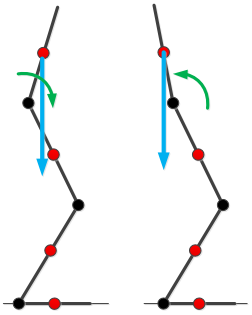

Figure 7.44 Hip joint motion

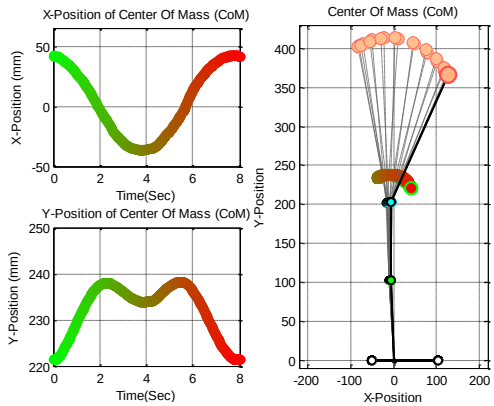

Figure 7.45 Hip joint motion and humanoid center of mass location change

Figure 7.45 shows the humanoid center of mass location change. Humanoid upper body sways back and forth to find the minimum energy required for backward and forward balancing motions by hip joint. Humanoid center of mass moves almost 41 mm in positive and 32 mm in negative x direction, it

changes its location in y direction between 221mm and 238mm while it is standing up and its feet are not moving. All joints are fixed at one position except the hip joint. Hip joint uses the trajectory shown in Figure 10.47. It moves from to -0.4 rad backward and 0.4 rad forward. There are two test with two different motion times, one for 2 sec and another one for 4 sec.

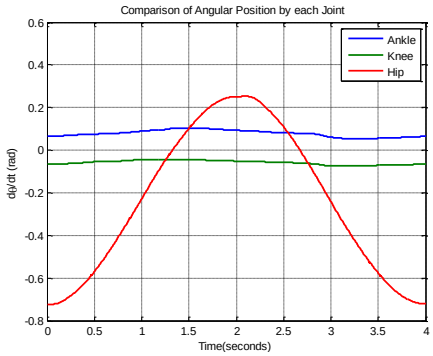

Figure 7.46 Joint angular positions, hip pitch joint trajectory shown in red line

Hip joint center of mass move backward and forward, as seen in Figure 7.47. Ankle pitch link center of mass does not move. Hip link center of mass travel between -54 mm and 74 mm. Knee link center of mass does not.

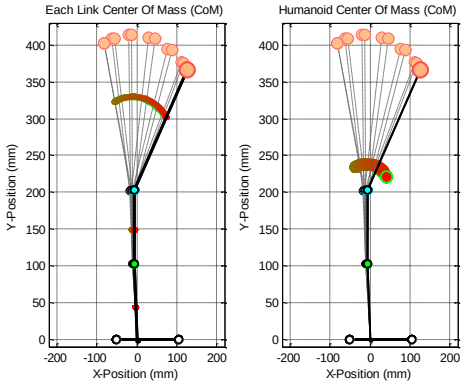

Figure 7.47 Center of mass position of each link (left figure) and center of mass of humanoid (right figure)

With shorter time to finish the motion commands given to the joint DC motors, angular and linear velocity of CoM of hip pitch link increase as seen in Figure 7.48 and in Table 7.21 and 7.22, which shows the results for two different times; 2 sec and 4 sec. Angular velocity of the hip joint link center of mass increases by 56%, while angular joint of knee and hip center of masses either stay close or change slightly as seen in Table 7.21. Over all ankle and knee joint angular velocity are very close to the same value, which is expected for the angular velocity. Only hip pitch joint angular velocity is increasing which is expected. As for the linear velocity of each center of mass, it is increasing with decrease motion time. See Figure 7.48b

and d and Table 7.22 for the results. Hip link center of mass has the fastest linear velocity since its angular trajectory is bigger than other two center of masses' angular trajectories. It is increasing its linear velocity by 70%.

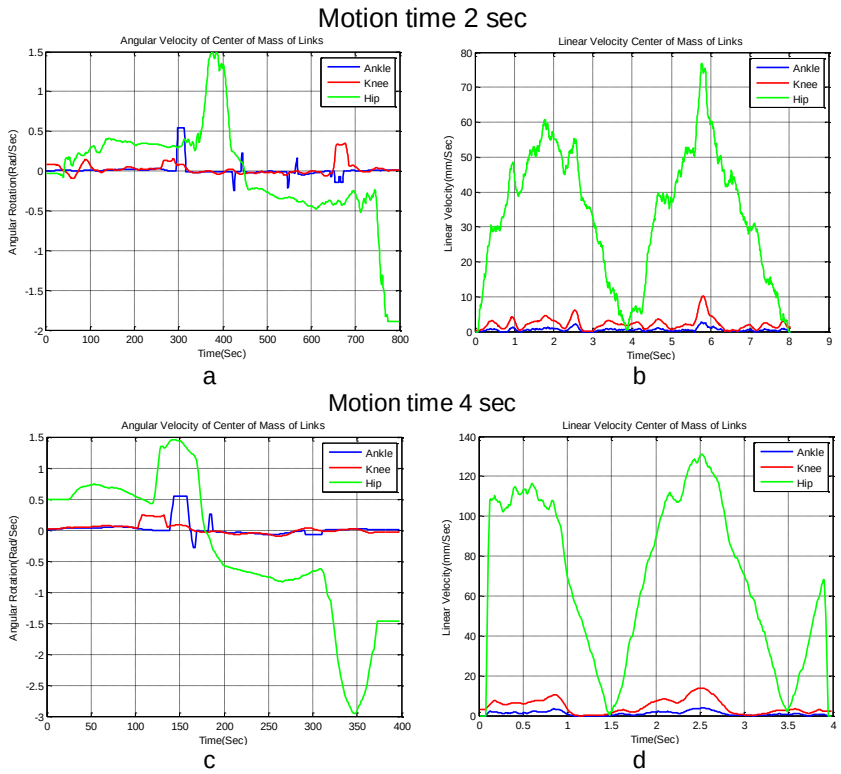

Figure 7.48 CoM of links angular and linear velocities

Table 7.21 Maximum values of angular velocity of center of mass of links

	Motion time 2 sec	Motion time 4 sec
Ankle (rad/sec)	0.22	0.33
Knee (rad/sec)	0.55	0.54
Hip (rad/sec)	2.95	1.89

Table 7.22 Maximum values of link CoM angular velocity

	Motion time 2 sec	Motion time 4 sec
Ankle (rad/sec)	3.1	2.54
Knee (rad/sec)	13.63	10.14
Hip (rad/sec)	131.2	76.91

Hip pitch joint increases its own angular velocity to finish the motion in shorter time. Results are shown in Figure 7.49 and Table 7.23. By reducing the motion time by 50%, ankle joint angular velocity increases by almost 93% while knee joint's angular velocity changes slightly and ankle pitch joint angular velocity increases by 95%.

As seen in Figure 7.50 and Table 7.24, with shorter time motion, angular acceleration of hip joint increases almost 103%, knee joint angular acceleration increases slightly 5%. Ankle joint angular acceleration does reflect a change about 24%. As seen in Figure 7.50b, with slower motion time, knee and ankle joint angular velocity values stay closer to each other. Figure 7.50a shows that hip joint has the biggest acceleration.

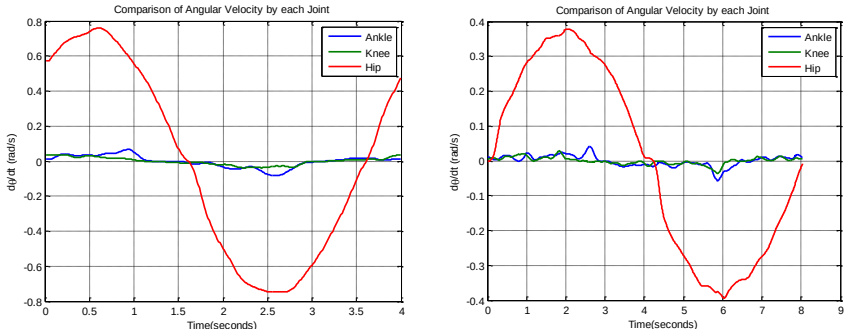

a b

Figure 7.49 Comparison of angular velocities of each joint, 2 sec (a) and 4 sec (b)

Table 7.23 Maximum values of link CoM linear velocity

	Motion time 2 sec	Motion time 4 sec
Ankle (rad/sec)	0.82	0.042
Knee (rad/sec)	0.037	0.036
Hip (rad/sec)	0.76	0.393

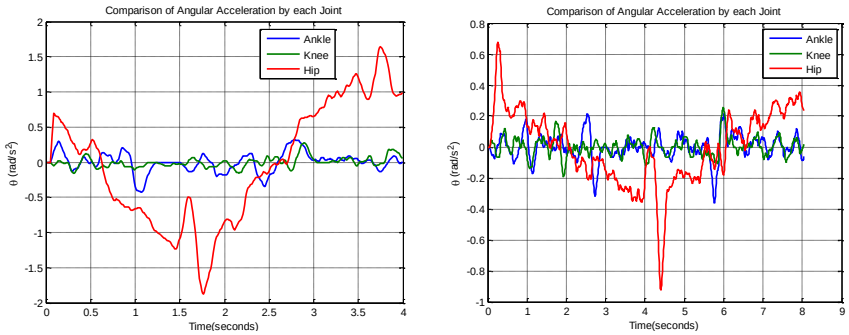

a b

Figure 7.50 Angular acceleration comparisons, 2 sec (a), 4 sec (b)

Table 7.24 Maximum values of angular acceleration of each joint

	Motion time 2 sec	Motion time 4 sec
Ankle	0.424	0.341
Knee	0.267	0.253
Hip	1.876	0.923

Hip control motion shows a different result from the ankle control motion. Figure 7.51 shows that even though the hip pitch joint is moving and other two joints are fixed, hip joint is still using less electrical

input power than ankle pitch joint. Hip and knee pitch joints electrical input power usage are very similar. With increase in speed, hip joint electrical input power only increases by 6%, knee joint electrical input power usage increases by 11%, and ankle electrical input power decreases by 7%. Since ankle joint is still carrying all humanoid weight, it makes sense for it to use more current, and use even more current with extended motion time and extended angular position.

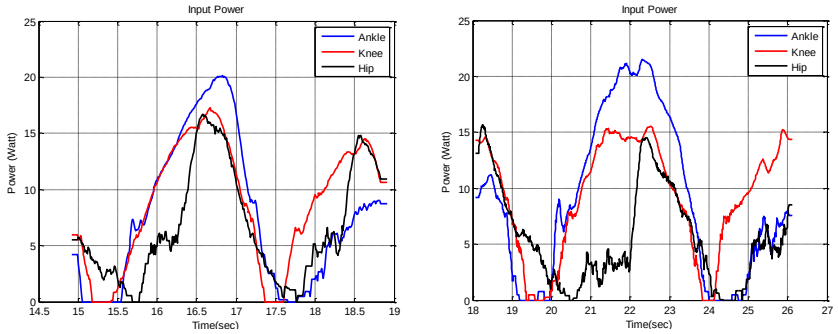

a b

Figure 7.51 Comparison of electrical power used, 2 sec (a) and 4 sec (b)

Table 7.25 Maximum values of input power for different motion times

	Motion time 2 sec	Motion time 4 sec
Ankle (W)	20.08	21.54
Knee (W)	17.24	15.51
Hip (W)	16.63	15.7

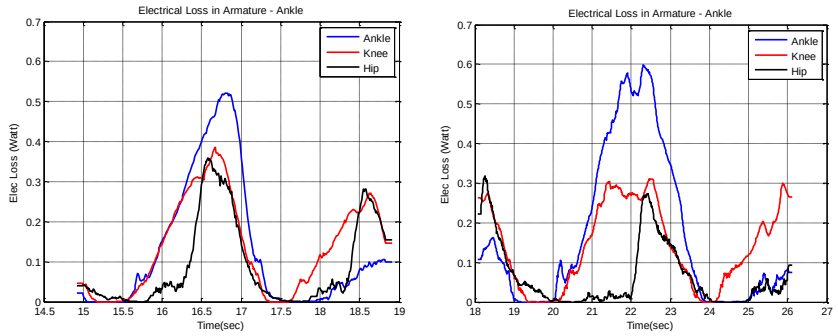

a b

Figure 7.52 Comparison of electrical loss for each joint, 2 sec (a) and 4 sec (b)

Table 7.26 Maximum values of electrical loss in each joint for different motion times

	Motion time 2 sec	Motion time 4 sec
Ankle (W)	0.52	0.59
Knee (W)	0.39	0.3
Hip (W)	0.36	0.31

Ankle joint shows higher electrical losses with extended operation time as seen in Figure 7.52b. Electrical loss value is 0.59W compared to 0.52W in short time motion. So, if angular velocity increases,

ankle joint will engage shorter time and loaded shorter time, this will yield less electrical loss. See Table 7.26 for comparisons. With higher speed, hip joint shows more electrical loss, about 16% more.

Torque required represents the torque produced by the joint and forces acting on the joint from other external forces which includes the momentum and inertial effects from other body links. Figure 7.53a shows the increased angular velocity effect on the ankle joint torque.

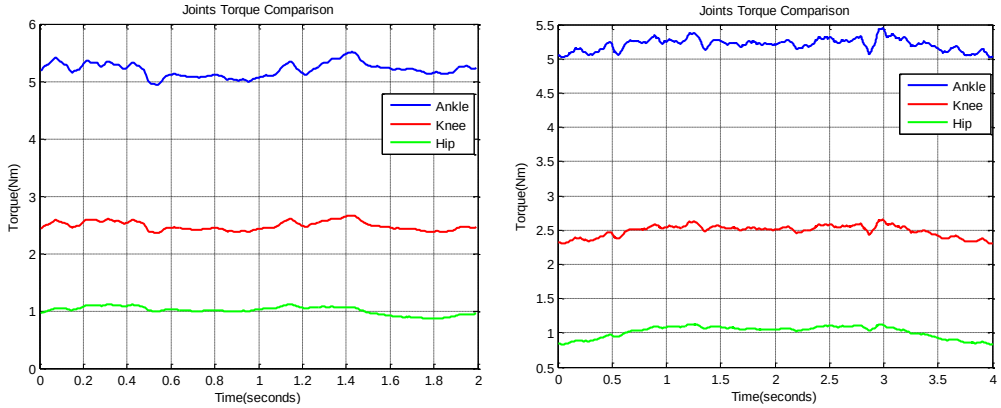

a b

Figure 7.53 Comparison of torque by each joint, 2 sec (a) 4 sec (b)

Table 7.27 Maximum values of torque by each joint

	Motion time 2 sec	Motion time 4 sec
Ankle (Nm)	5.505	5.444
Knee (Nm)	2.66	2.648
Hip (Nm)	1.114	1.129

This torque has bigger ripples, Figure 7.53b have smaller ones. These ripples are caused by momentum and inertial effects from other joint's acceleration and dynamic motion. This is clearly seen in Lagrange equations. Table 7.7 shows the comparison of torques of each joint for two different motion times. With 50% less time for each motion, hip joint torque increases by 1%. Knee joint torques increase by 2%.

Mechanical power produced by each joint is effected by joint angular velocity and torque produced. Result of increased angular velocity and torque can be seen in Figure 7.54 and Table 7.28. Hip joint needs 96% more mechanical power to handle faster motion, knee joint needs 10% more mechanical power and ankle joint needs 46 % more mechanical power.

Table 7.28 Maximum values of mechanical power by each joint comparison for two different motion times

	Motion time 2 sec	Motion time 4 sec
Ankle (NmRad/Sec)	0.44	0.3
Knee (NmRad/Sec)	0.097	0.088
Hip (NmRad/Sec)	0.837	0.426

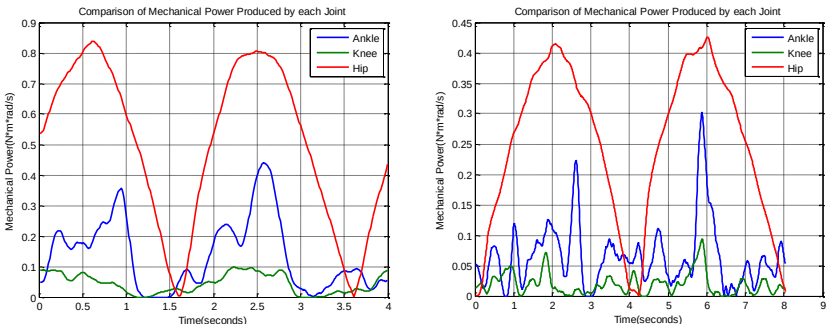

a b

Figure 7.54 Comparison of mechanical power produced by each joint 2 sec (a) 4 sec (b)

Table 7.29 Power, current, electrical loss comparison

Motion Time (Seconds)	2	3	4
Maximum Current	0.72	0.672	0.682
Mean Current (Ampere)	0.269	0.233	0.223
Maximum Electrical Loss (Joule)	0.414	0.361	0.372
Mean Electrical Loss (Joule)	0.093	0.070	0.067
Maximum Input Energy (Watt)	17.928	16.732	16.998
Mean Input Energy (Watt)	6.699	5.802	5.571

Table 7.29 shows mean and maximum values of the electrical power, current input, and electrical loss for ankle joint. For highest speed (motion time 2 sec), hip joint has highest current input, mean current input, highest electrical loss, mean electrical losses, input power and mean input power. For longer motion times (3 and 4 sec), ankle joint has lower losses and current usage. Hip joint seems to work best with mid-range velocity (3 sec) for balancing the humanoid upper-body.

Center of pressure location results are seen in Figure 7.55. With faster hip joint motion, center of pressure points cover area very similar to the area that is covered by slower angular speed of hip joint. Since hip joint does not cause a lot of dynamics in humanoid, center of pressure points for both speed are very similar.

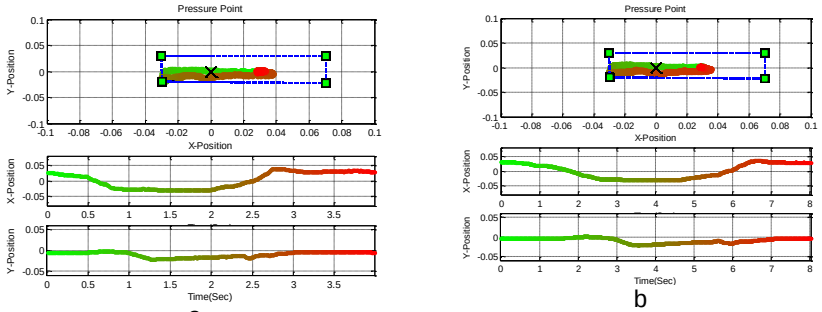

a b

Figure 7.55 Center of pressure comparison for fast and slow motion

CHAPTER 8: MINIMIZING ENERGY CONSUMPTION WITH Q LEARNING

Different reinforcement learning algorithms are applied to the robotic area to optimize the dynamics motions [56]. Walking locomotion has been studied widely by many researchers [57-660]. Study [61] indicated the goal of their research is optimizing the energy usage through reinforcement learning.

The goal of this section is to optimize the standing up motion and humanoid's energy usage by Q-learning reinforcement algorithm, which is used to find joint angular trajectories with reduced energy usage. The torques generated by the simulated controller joints for balancing define the proper location of the CoM. This data is provided to the real robot controller model which keeps the limitations on the CoM and control procedure for standing postures. Q-Learning finds several candidate paths to accomplish the tasks. The goal is to compare the consumed energy of each trajectories of joints and preserve by finding better trajectories and angular and linear velocities, or avoiding frequent accelerations. This model presents a controller for constrained optimal control. In order to prevent the constraint violations, this control changes the motion variables gradually by simulating the system forward by Q Learning.

In order to perform simulated experiments related with the standup process on a real robot, the 4-link humanoid robot model described in chapter 3 is used. The real robot (NAO) has 25 degrees of freedom (DoF), which includes two legs, two arms, a trunk, and a head.

8.1 Motor Model

The joint DC motor model used in simulations was estimated from collected actual motor responses. In order to produce an approximation of each joint motor response during standup motions, this simulation needs three different models, one for each joint motor of ankle, knee, and hip pitch. Transfer function model is shown in equation (8.1), parameters for ankle are $\omega = 0.0098,\ \zeta = 1.4$, for knee are $\omega = 0.0097,\ \zeta = 0.9$ and for hip are $\omega = 0.0021,\ \zeta = 4.95$.

A second order system is used as a process model and Predicting-Error Minimization (PEM) algorithm [82] used as estimation method. In order to increase the correctness of the information given to the estimation algorithm, joint position and target position values were recorded previously while performing

Aldebaran version of the stand-up process. The data was applied to PEM estimation method and the humanoid dynamic model to obtain an individual joint model as close to the real behavior of each motor as possible.

$$G_{(s)} = \frac{1}{\omega^2 s + 2\omega\zeta s + 1} \tag{8.1}$$

8.2 Q-Learning

Q learning is a technique for resolving reinforcement learning challenges which is capable of learning a policy based solely in spurious feedback [63]. This algorithm keeps a Q table that stores the expected outcome of performing an action in a given state. After performing an action *a* in state *s*, the agent receives a reward *r* and arrives to state *s*. Then, the Q table is updated according to equation (8.2), where α is a learning rate parameter between 0 and 1.

$$Q(s,a) = Q(s,a) + \alpha\big(r + max_{a'} Q(s',a') - Q(s,a)\big) \tag{8.2}$$

A policy Π of which action to perform at each state can be derived from the Q table, as shown in equation (8.3).

$$\Pi: s \to a :: \Pi(s) = argmax_a Q(s,a) \tag{8.3}$$

8.3 Standing up Learning Algorithm

The Q-Learning algorithm controlled the ankle and knee joints only, while torso is set to vertical position in reference to the ground. The angular velocities and positions of the ankle and knee joints determined the state. Each joint state-space was discretized using a fixed length discretization. The same fixed length discretization was performed for velocities.

The agent performed one of three possible actions, which changed the ankle and knee velocities by digressing it, leaving it unmodified or incrementing it. The digressions and increments were done by a fixed predefined value.

Equation (8.4) shows how the reward is computed. A negative reward is given whenever the humanoid performs a motion that leaves a joint in an invalid position, according to the NAO robot limits.

A negative reward is also given if the humanoid fails. It is considered to have failed when the location of the hip joint along the sagittal plane is further than a non-return point. A positive reward is given if the humanoid reaches a target stand up position within some error tolerance and all joint angular velocities

are below a threshold. The position requirement is necessary for the humanoid to learn the task of standing up. The velocity constraints, on the other hand, ensure that the final inertia of the standup motion can be accomplished without the robot falling or making a big energy effort to lower it.

The average produced torque is subtracted from the positive reward value. This promotes solutions that minimize torque application, which in turn minimizes energy consumption. Only one non-zero reward is given in each episode, right before the episode terminates.

$$r = \begin{cases} -10 & \text{if jointOutOfConstraints or robotFell} \\ 3 - \text{averageTorque} & \text{if standingUp and notMoving} \\ 0 & \text{Otherwise} \end{cases} \quad (8.4)$$

8.4 Simulator

In order to achieve offline learning, a simulator was programmed using the motor, kinematic and dynamic models previously described.

First, an action is selected by determining the state and querying the Q-Value table. Then, the motor models are used to compute the motor response to the required velocities. After that, kinematic models are applied to find joint positions, angular velocities and angular accelerations. This data is used by dynamic model to compute the performed torques.

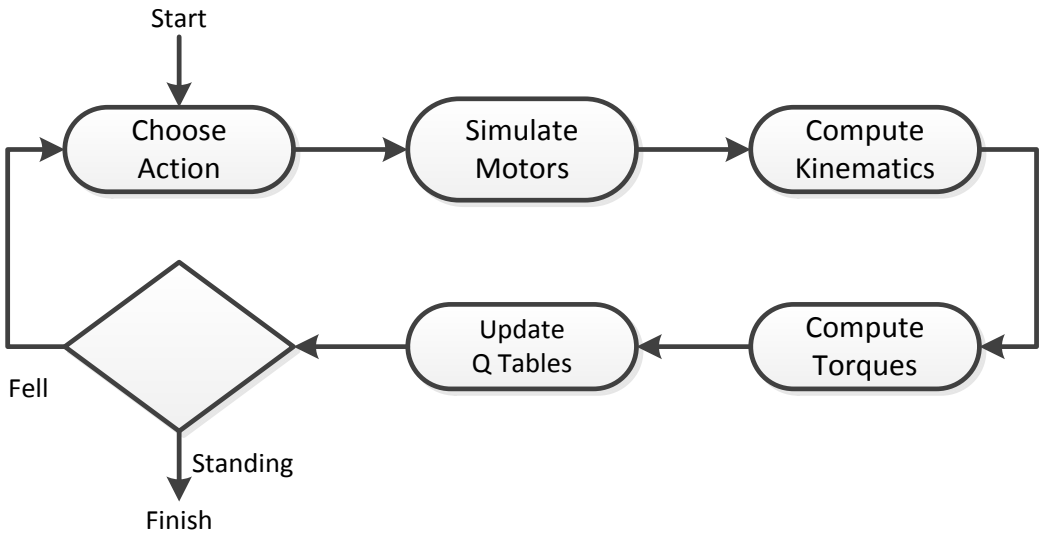

Figure 8.1 The flow of events of a single iteration inside an episode.

Those torques, along with the kinematic information, are in turn used to compute the reward and update the Q-Value table.

A decision process is carried out to determine whether the episode has failed, succeeded, or it should continue. In the latter case, the cycle starts all over again.

8.5 Energy, Power Performance and Evaluation

In order to study the energy and power performance, previously mentioned key considerations equations (5.1 – 5.5) in Chapter 5 are used to analyze this model. Joint power consumption, average mechanical power, power standard deviation, and loss energy values are calculated for each joint.

8.6 Experimental Setup

The robot parameters used in the kinematic and dynamic models, such as link length, link masses and joint angular limits were taken directly from Aldebaran. Additionally, the motor transfer functions were derived from data taken from the real robot while performing standing up motion.

The time step for the motor response computations was set to 10ms, which corresponds to the default control cycle for this robot. Finally the simulator was tailored to the NAO robot. This allowed for the application of joint configuration space paths to be seamlessly applied to the real robot.

8.7 Results

Simulation environment determined the joint trajectories for best energy utilization by using Matlab program and produced the required motions. Motions are applied to the real robot by python language.

A custom made NAO local module (getsensorvalues) is used to collect the joint position and electrical current usage values and dumped the data to a csv file on the robot harddrive. This data is analyzed by Matlab programs later. Robot is controlled over ethernet network.

Results are presented per joints (ankle, knee, and hip) for stand up and sit down motions by comparing Aldebaran and Q Learning routines.

Results include the joint position, velocity, acceleration, torque, mechanical power and current consumption of both routines in the same figure for comparison. Discussion about the analysis of each result will follow the individual figure.

Figure 8.2 shows the joint trajectories performed by both Aldebaran and QL stand up and sit down routines. QL routine shows its difference by reaching its target rotation degree sooner for stand up motion, but it uses almost same time reaching its target but slightly different trajectory, a longer trajectory, for sit down.

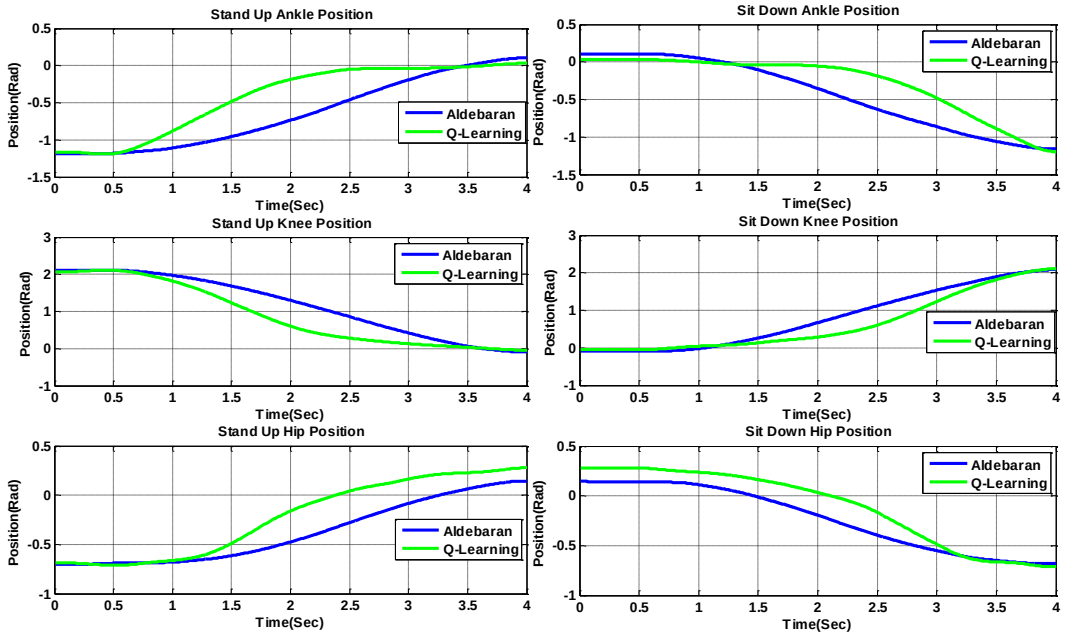

Figure 8.2 Joint position comparisons for stand up and sit down

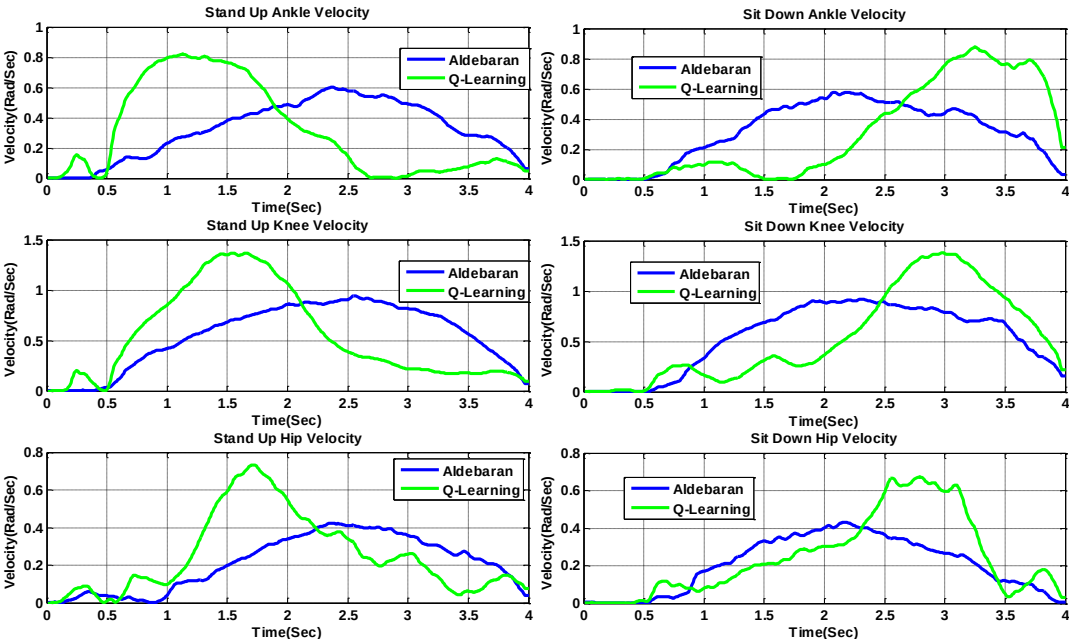

Figure 8.3 Joint velocity comparisons for stand up and sit down

Joint velocity comparisons are shown in Figure 8.3. Q Learning routine reaches higher velocity quicker, at the beginning of the routine, for stand up motion and it reaches its maximum velocity towards the end of the sit down motion. Q Learning builds up more inertial forces at the beginning of the standing up, and it uses gravity force help mostly during the sit down.

Joint acceleration comparisons are shown in Figure 8.4. Q Learning routine has higher ankle and knee joint acceleration than Aldebaran routine at the beginning of stand up and at the end of the sit down

motions. Q Learning hip joint acceleration is higher than Aldebaran hip joint acceleration for both stand up and sit down.

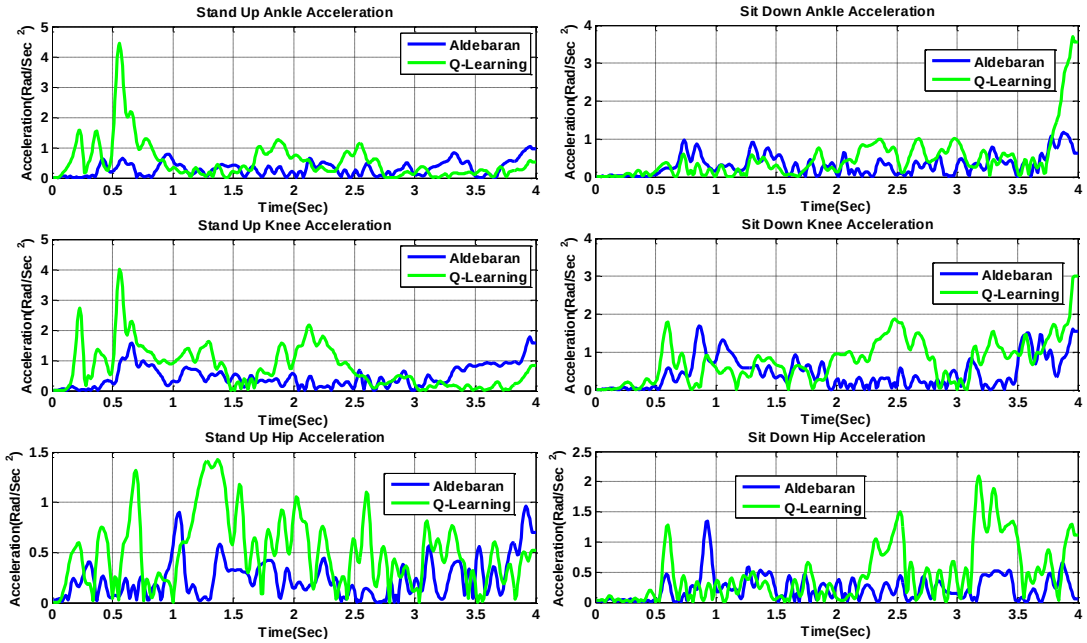

Figure 8.4 Joint acceleration comparisons for stand up and sit down

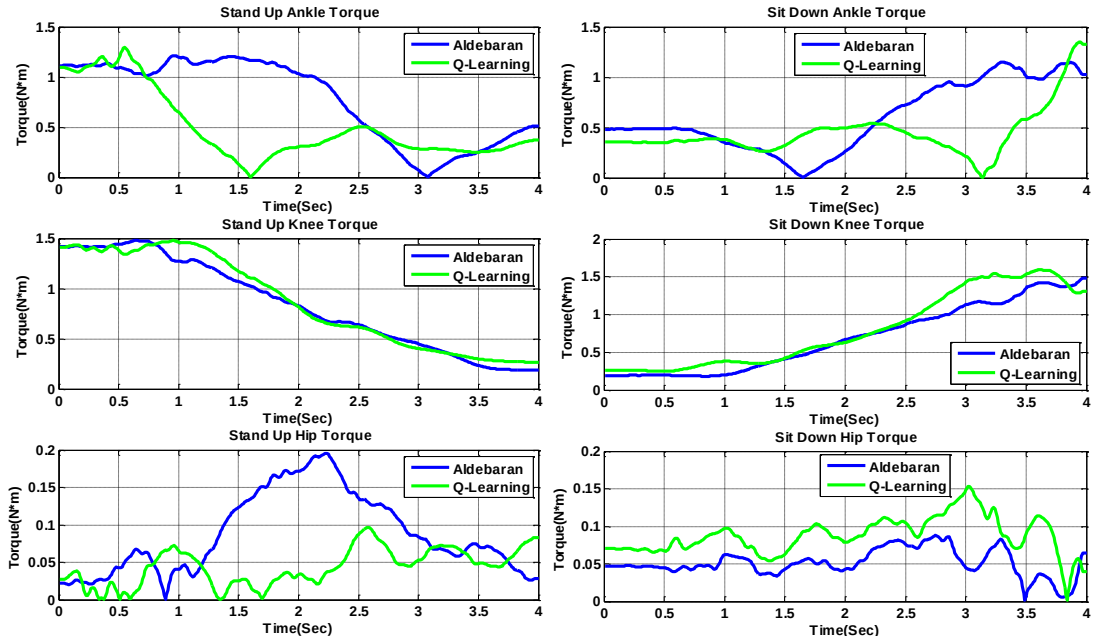

Figure 8.5 Joint torque comparisons for stand up and sit down

Figure 8.5 shows the torque required by each joint for both stand up and sit down motions. By looking at Q Learning routine, ankle joint requires more torque at the beginning, and less torque for the rest of stand up, less torque at the beginning of sit down and more torque at the end of the sit down, knee joint uses slightly more torque for stand up and sit down, hip joint uses more torque for both motions. These

results show the effect of velocity and acceleration on the joint requirements for torque. Table III shows the total torque required by each joint during stand up, ankle and hip joints total torque decreased while the knee joint total torque increased. In Table 8.1 for sit down motion, ankle joint total torque decreased while the knee and hip joints total torque increased.

Table 8.1 Comparison of total torque by each joint

Stand Up Torque (N*m) (Total per joint)			
	Ankle	**Knee**	**Hip**
Aldebaran	311.2507	337.8637	35.0482
Q Learning	199.8457	349.7881	17.421
Change	-111.405	11.9244	-17.6272
Joint Change (%)	-55.745	3.409	-101.183
Total Change (%)	-17.11		

Sit Down Torque (N*m) (Total per joint)			
	Ankle	**Knee**	**Hip**
Aldebaran	241.4009	277.5257	20.4802
Q Learning	177.905	320.0648	34.9446
change	-63.4959	42.5391	14.4644
Joint Change (%)	-35.67	13.291	41.392
Total Change (%)	-12.03		

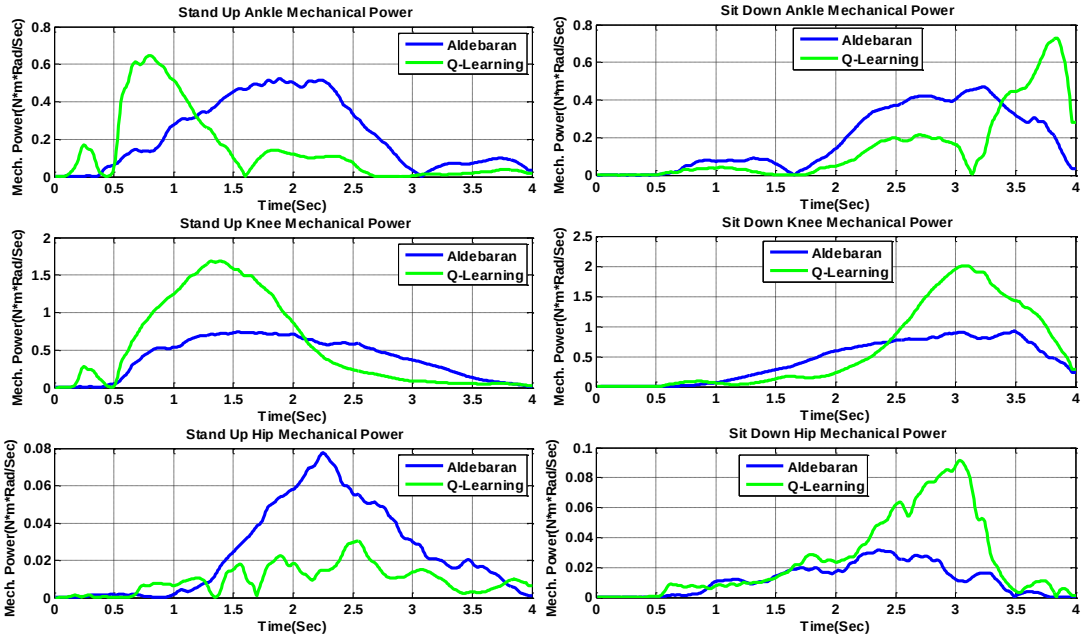

Figure 8.6 Joint mechanical power comparisons for stand up and sit down

Mechanical power produced by each joint is shown in Figure 8.6. Q learning routine needs more mechanical power from three joints at the beginning of the standing up motion, and this power need diminishes towards the end of the motion. This is in accordance with the other results shown in Figure 8.4. Q learning routine uses gravity to its advantage by using minimum mechanical power at the beginning of the sitting down motion, and it requires more power for hip at the end, slightly less power for both ankle and knee joints. Table 8.2 shows the total mechanical power per link for stand up and sit down. Even though

ankle and hip joint used less mechanical power, knee power used more. Percentage change values are presented in the Table 8.2. For sit down motion, while ankle joint uses less mechanical power, knee and hip joints uses more mechanical power.

Table 8.2 Comparison of mechanical power by each joint

Stand Up Mechanical power (N*m*Rad/Sec) (Total)			
	Ankle	Knee	Hip
Aldebaran	89.3364	158.9411	9.8351
Q Learning	56.9992	222.9058	3.8435
Change	-32.3372	63.9647	-5.9916
Joint Change (%)	-56.732	28.695	-155.889
Total Change (%)	9.93		

Sit Down Mechanical power (N*m*Rad/Sec) (Total)			
	Ankle	Knee	Hip
Aldebaran	75.3304	177.3991	4.7311
Q Learning	58.234	247.785	10.0908
Change	-17.0964	70.3859	5.3597
Joint Change (%)	-29.358	28.406	53.114
Total Change (%)	22.77		

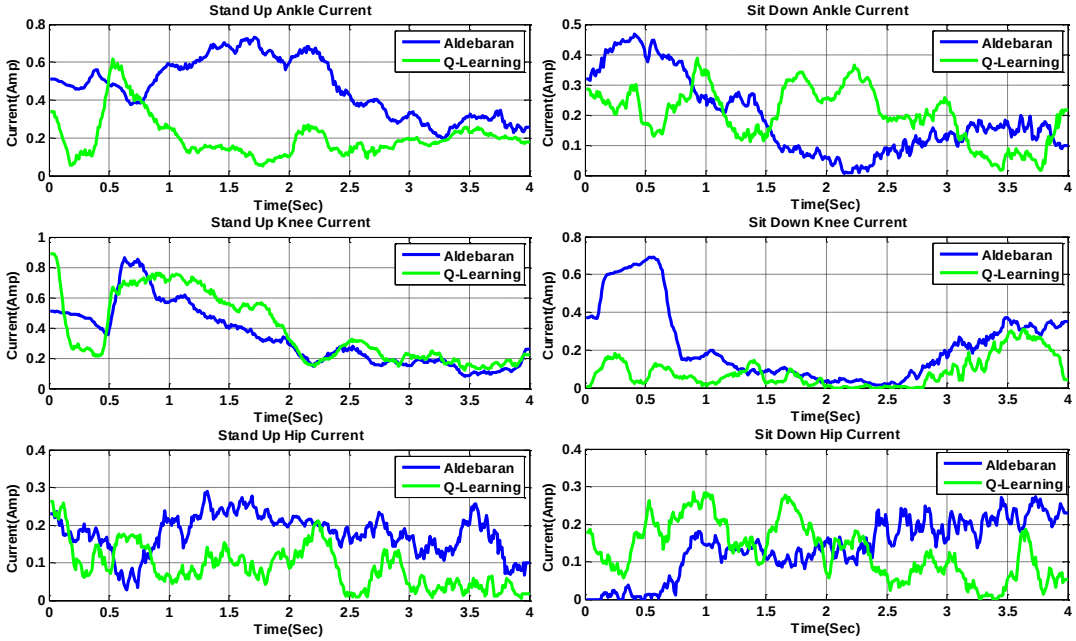

Figure 8.7 Joint current consumption comparisons for stand up and sit down

Electrical current consumption comparison is shown in Figure 8.7. Q Learning routine demand less current usage for ankle and hip during standing up, and slightly more current for knee joint than Aldebaran routine. Sitting down joint current consumption is different than standing up consumption. Q Learning routine uses less current for knee and hip joint, slightly more current consumption for ankle joint than Aldebaran routine. These results are in accordance with the torque requirement for each joint as seen in Figure 8.5. Table 8.3 shows the total current used by each joint for stand up. Ankle and hip joints use less

current while knee joint uses 11% more electrical current. Table 8.3 also shows the total electrical current per joint for sit down motion. Knee and hip joints uses less current while ankle joint uses 4% more current. Total current used for stand up is 45% less and for sit down 33% less.

Table 8.3 Comparison of total electrical current by each joint

Stand Up Total Current (Ampere) per joint			
	Ankle	Knee	Hip
Aldebaran	186.7388	136.7272	70.954
Q Learning	81.148	154.8232	35.6936
Change	-105.5908	18.096	-35.2604
Joint Change (%)	-130.121	11.688	-98.786
Total Change (%)	-31.122		

Sit Down Total Current (Ampere) per joint			
	Ankle	Knee	Hip
Aldebaran	76.068	90.9264	55.3264
Q Learning	80.552	33.452	51.9156
Change	4.484	-57.4744	-3.4108
Joint Change (%)	5.566	-171.811	-6.569
Total Change (%)	-25.369		

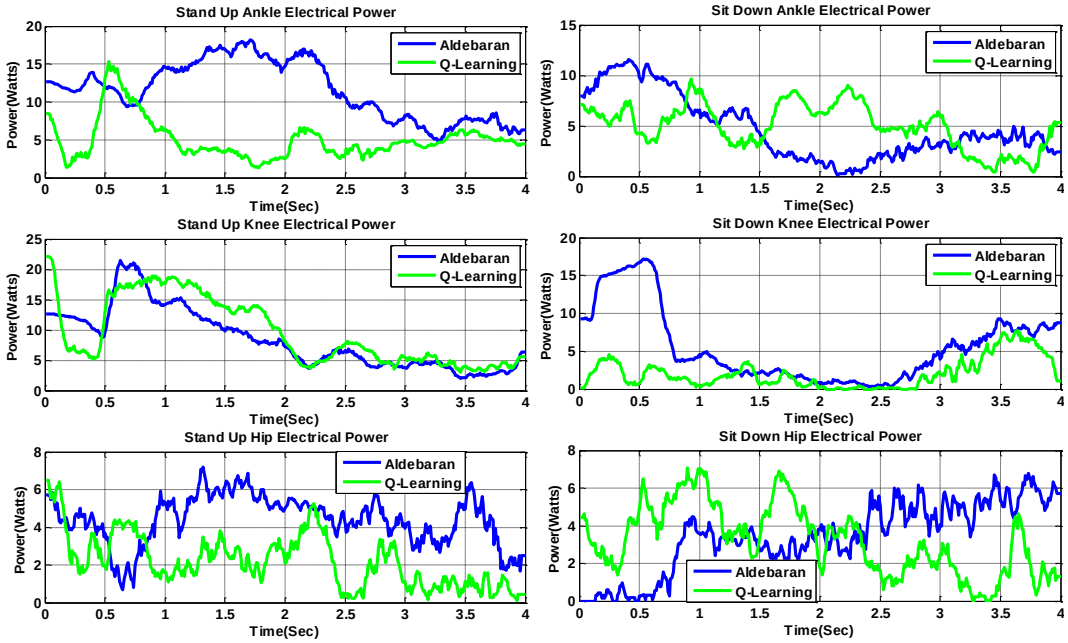

Figure 8.8 Joint input power consumption comparisons for stand up and sit down

Joint electrical input power demand comparisons are shown in Figure 8.8. These results are showing the input power for each joint during standing up and sitting down. By using Q Learning routine, ankle joint uses less input power for standing up and sitting down, knee joint uses more power for standing up, less power sitting down, hip joint uses less input power for both motions than Aldebaran routine. Table 8.4 shows the total electrical power per link for stand up and sit down motions respectively. Ankle and hip joints use less electrical power for stand up task, knee joint uses more. Knee and hip joint uses less

electrical power for sit down task while ankle joint uses less power. Total electrical power saving is 31% for stand up and 25% for sit down.

Table 8.4 Comparison of total electrical power by each joint

Stand Up Total Electrical Power (Watts) per joint			
	Ankle	Knee	Hip
Aldebaran	4631.221	3390.834	1759.659
Q Learning	2012.4704	3839.615	885.2012
Change	-2618.7506	448.781	-874.4578
Joint Change (%)	-130.126	11.688	-98.786
Total Change (%)	-31.123		

Sit Down Total Electrical Power (Watts) per joint			
	Ankle	Knee	Hip
Aldebaran	1886.486	2254.974	1372.094
Q Learning	1997.689	829.6096	1287.506
Change	111.203	-1425.3644	-84.588
Joint Change (%)	5.566	-171.811	-6.569
Total Change (%)	-25.369		

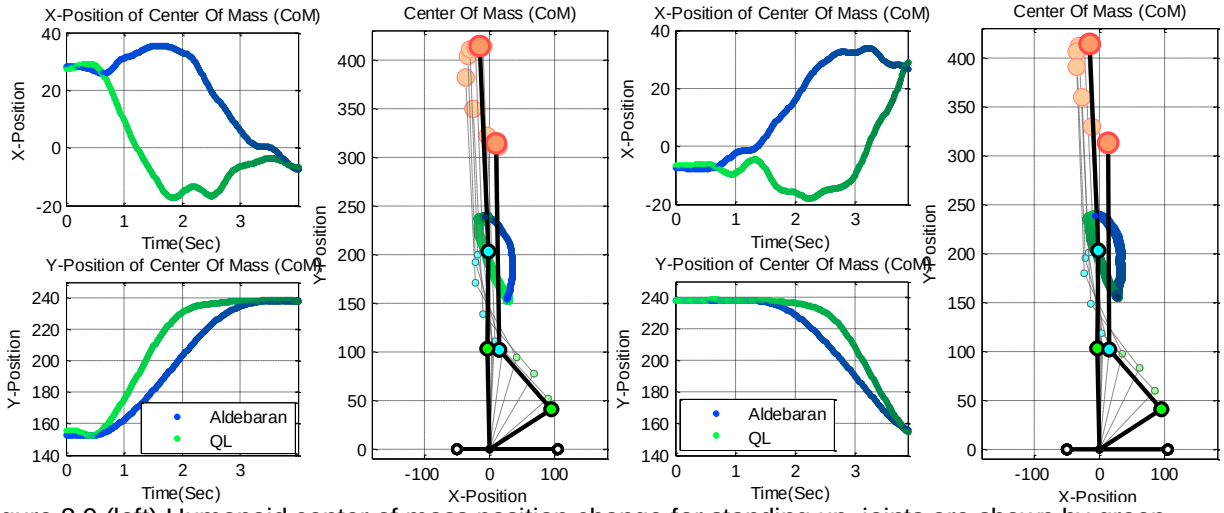

Figure 8.9 (left) Humanoid center of mass position change for standing up, joints are shown by green circles, head is shown by orange circle, (right) for sitting down, joints are shown by green circles, head is shown by orange circle

Figure 8.9 show the center of mass position change for standing up and sitting down motions respectively. By looking at the Q Learning routine, it puts the center of mass above the ankle joint sooner in both motions than the Aldebaran routines does.

Aldebaran routines lean forward to stand up and sit down, whereas Q Learning routine leans towards the back and align the vertical center of mass with ankle joint. Figure 8.10 shows the center of pressure for Aldebaran motion. Pressure point starts at the front of the ankle joint and stays mostly in the front area until motion is finished.

Figure 8.10 shows the center of pressure point for Q Learning standing up motion, where pressure point start from the front side of the ankle and ends very close to a point behind the ankle joint.

Figure 8.11 shows the pressure of Aldebaran motion for sitting down motion, where pressure points are mostly in the front side of the ankle joint from start to the finish. Figure 8.11 shows the pressure points for Q Learning sitting down motion. Pressure points start from the behind of the ankle and end at the front of the ankle.

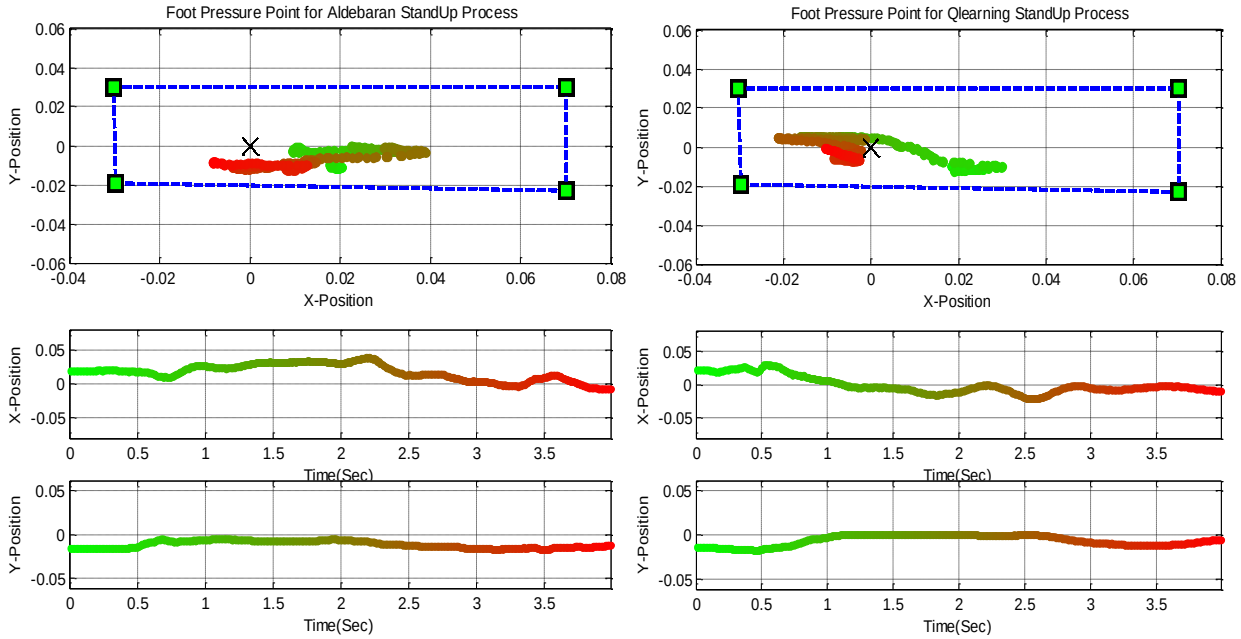

Figure 8.10 (left) Center of pressure for Aldebaran standing up, green squares and blue line defines the foot pressure area, (right) for Q learning standing up, green squares and blue line defines the foot pressure area

Table 8.5 shows the mechanical power performance of Q Learning (Q-L) and Aldebaran (Ald.) routine. Mechanical power, standard deviation of mechanical power, energy lost due to torque requirement and the change percentage between two routines are shown.

Average mechanical power of ankle is lower for standing up and sitting down with Q Learning, knee joint mechanical power is higher than Aldebaran routine. Hip Q learning result is lower for standing up and higher in sitting down. Q Learning ankle joint lost energy is lower for both standing up and sitting down but ankle joint energy lost is higher for both motions. Q Learning hip joint energy loss is lower for standing up and higher for sitting down.

Results show individual joint energy saving as well as overall humanoid energy consumption decrease for both motions.

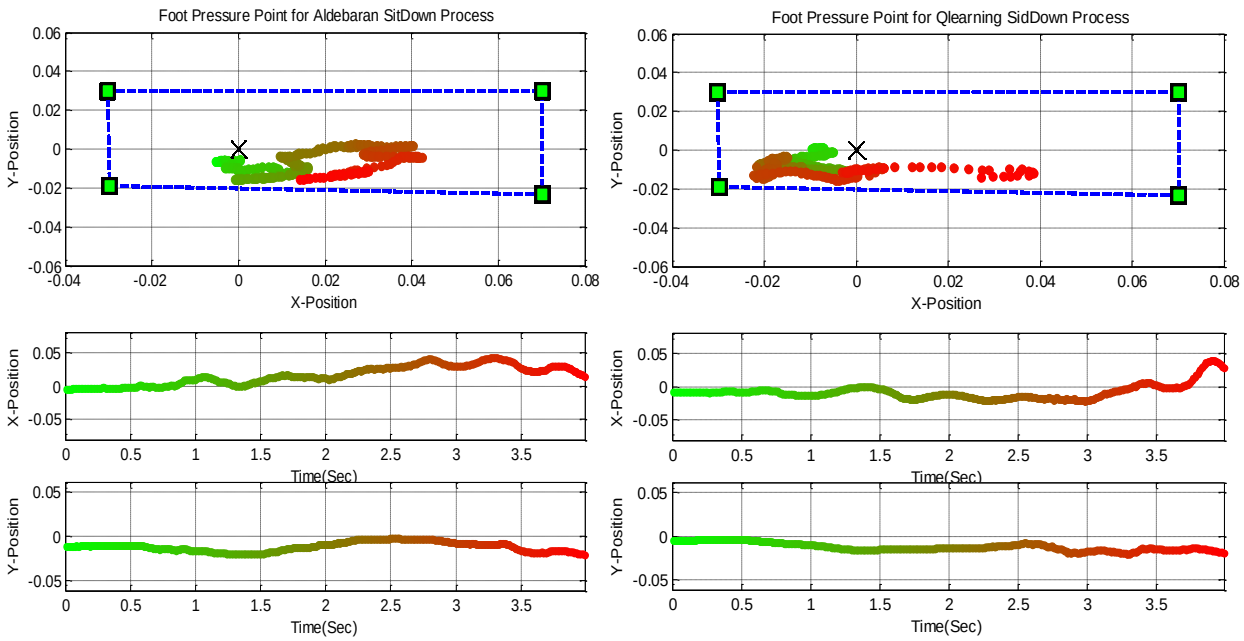

Figure 8.11 (left) Center of pressure for Aldebaran sitting down, green squares and blue line defines the foot pressure area, (right) for Q learning sitting down, green squares and blue line defines the foot pressure area

Table 8.5 Comparison average mechanical power by each joint

Stand Up			Sit Down		
Mechanical Power Average			Mechanical Power Average		
	Q-L	Ald.		Q-L	Ald.
Ankle	0.1425	0.2233	Ankle	0.1456	0.1883
Knee	0.5573	0.3974	Knee	0.6195	0.4435
Hip	0.0118	0.0246	Hip	0.0252	0.0096
Mechanical Power Standard Deviation			Mechanical Power Standard Deviation		
	Q-L	Ald.		Q-L	Ald.
Ankle	0.1942	0.183	Ankle	0.3472	0.4106
Knee	1.2459	0.8371	Knee	0.6778	0.3324
Hip	0.0257	0.0236	Hip	0.057	0.0075
Lost Energy			Lost Energy		
	Q-L	Ald.		Q-L	Ald.
Ankle	0.6047	0.8771	Ankle	0.5041	0.6922
Knee	0.9868	0.9562	Knee	0.9364	0.8209
Hip	0.0543	0.1025	Hip	0.0907	0.0499

Electrical input power for ankle and hip joints is reduced for standing up and electrical input current for knee and hip joints is reduced for sitting down by using Q Learning trajectories. Knee joint electrical input power increased slightly for standing up and ankle joint electrical input power increased slightly for sitting down by using Q Learning trajectories. Overall less electrical power is used by Q Learning routine for stand up and sit down motions.

CoM and CoP results are shown for both Aldebaran and Q Learning algorithm. Q Learning routine tends to keep the center of pressure close to ankle joint and most of the time around a point behind the ankle joint, while Aldebaran routine keeps it in a position away from the ankle joint. Center of mass location is moved over to ankle joint quickly with Q Learning, whereas Aldebaran routine kept the location in front of the ankle. Q Learning caused the energy saving for both standing up and sitting down by choosing better location for CoM and CoP. As a result of these, joint torque requirements, and mechanical power requirements are changed.

CHAPTER 9: CONCLUSION

Research on energy consumption and analysis is one of the major objectives of humanoid robotics study. In order for autonomous humanoids to be useful for a practical time, they need to reach a definite level of independence. If new generation of humanoid battery technology supply longer operational time, it is very important to control humanoid robots to be energy efficient.

Even with a simplified model, a humanoid robot model can still be very difficult to analyze. In this study, standing up and sitting down motions are accomplished and all joints are analyzed per angular velocities for the best energy consumption level. Each individual joint electrical power consumption, electrical power losses are analyzed for standing up and sitting down per different joint angular velocities.

Produced mechanical power, mechanical power standard deviation, and energy lost due to produced torque for each joint are analyzed for the best energy saving points. Ankle, knee and hip joints have very different dynamics, energy usage characteristics and electrical power losses for standing up and sitting down even with the same robot speed. These joints also have very different motion characteristics, energy usage, and mechanical power production for different angular speeds.

In order to find the best possible energy usage per joint, produced torque, produced mechanical power, external forces applied on each joint and effect of angular speed and acceleration of joints on humanoid should be considered. There will be some velocities that some joint will use less energy while others will use more and there will be a velocity value that a joint will perform very badly. Trade off point for the best energy usage and performance will be a critical point to decide depending on the robot application.

Results have shown the influence of the motion parameters on the energy efficiency. The approach that is proposed to analyze the motions for better energy efficiency is different. For a general humanoid robot, a path is given to follow. Joint trajectories are obtained from the model robot uses, such as CoM trajectory or foot trajectory. Individual joint trajectories might create peaks of current usage, large standard deviation of mechanical power, and torque. The approach in this research is to analyze the individual joints

and their contribution to overall energy consumption. This information can be used for better trajectories with minimal energy usage. This approach presented effective results.

Dependable motion control is essential to permit humanoid robots to adapt a dynamic environment, maintain a balance and decrease energy consumption. Chapters 4-8 provided the model for balance, walking and constraints for the humanoid model. In order to reach a satisfying performance in humanoid motion task, it is essential to have a model of the control and use the energy consumption of each joint and overall humanoid as feedback. Because the effectiveness of the results succeeded in one model affects the quality of the other model.

REFERENCES

[1] Yongguo Mei; Yung-Hsiang Lu; Hu, Y.C.; Lee, C.S.G., "A case study of mobile robot's energy consumption and conservation techniques," Advanced Robotics, 2005. ICAR '05. Proceedings., 12th International Conference on , vol., no., pp.492,497, 18-20 July 2005

[2] Haruna, M.; Ogino, M.; Hosoda, K.; Asada, M., "Yet another humanoid walking - passive dynamic walking with torso under simple control," Intelligent Robots and Systems, 2001. Proceedings. 2001 IEEE/RSJ International Conference on , vol.1, no., pp.259,264 vol.1, 2001

[3] Yongguo Mei, Yung-Hsiang Lu, Y. Charlie Hu, and C.S. Georg,e Lee, Energy-Efficient Motion Planning for Mobile Robots, Robotics and Automation, 2004. Proceedings. ICRA '04. 2004 IEEE International Conference, 2004

[4] Kazuya OGAWA, Hyonju KIM, Makoto MIZUKAWA, Yoshinobu Ando, Development of the Robot Power Management System Adapting to Tasks and Environments-The design guideline of the Power Control System Applied to the Distributed Control Robot-, SICE-ICASE International Joint Conference 2006, Oct. 18-2 1, 2006 in Bexco, Busan, Korea

[5] M. Mistry, A. Murai, K. Yamane, and J. Hodgins, “Sit-to-stand task on a humanoid robot from human demonstration,” in Humanoid Robots (Humanoids), 2010 10th IEEE-RAS International Conference on. IEEE, 2010, pp. 218–223.

[6] Sven Behnke, Michael Schreiber, Jorg Stuckler, Reimund Renner, and Hauke Strasdat, See, walk, and kick: Humanoid robots start to play soccer, Humanoid Robots Group, Computer Science Institute, 2006

[7] Lesperance, E.; Desbiens, A.L.; Roux, M.-A.; Lavoie, M.-A.; Fauteux, P., "Design of a small and low-cost power management unit for a cockroach-like running robot," Intelligent Robots and Systems, 2005. (IROS 2005). 2005 IEEE/RSJ International Conference on , vol., no., pp.2387,2392, 2-6 Aug. 2005

[8] Wei Zhang; Jianghai Hu, "Low power management for autonomous mobile robots using optimal control," Decision and Control, 2007 46th IEEE Conference on , vol., no., pp.5364,5369, 12-14 Dec. 2007

[9] Kulk, J., and Welsh, J.S., A low power walk for the NAO robot, Proceedings of the Australian Conference on Robotics and Automation, Dec 3-5, Canberra, Australia (2008)

[10] Tokekar, Pratap; Karnad, N.; Isler, V., "Energy-optimal velocity profiles for car-like robots," Robotics and Automation (ICRA), 2011 IEEE International Conference on, vol., no., pp.1457,1462, 9-13 May 2011

[11] Silva, F.M.; Machado, J.A.T., "Energy analysis during biped walking," Robotics and Automation, 1999. Proceedings. 1999 IEEE International Conference on , vol.1, no., pp.59,64 vol.1, 1999

[12] Yamasaki, F.; Hosoda, K.; Asada, M., "An energy consumption based control for humanoid walking," Intelligent Robots and Systems, 2002. IEEE/RSJ International Conference on , vol.3, no., pp.2473,2477 vol.3, 2002

[13] Yamasaki, F.; Endo, K.; Kitano, H.; Asada, M., "Acquisition of humanoid walking motion using genetic algorithm-Considering characteristics of servo modules," Robotics and Automation, 2002. Proceedings. ICRA '02. IEEE International Conference on , vol.3, no., pp.3123,3128, 2002

[14] J. Morimoto and K. Doya, “Acquisition of stand-up behavior by a real robot using hierarchical reinforcement learning,” Robotics and Autonomous Systems, vol. 36, no. 1, pp. 37–51, 2001.

[15] Xu-Sheng Lei; Jing Pan; Jian-Bo Su, "Humanoid robot locomotion," Machine Learning and Cybernetics, 2005. Proceedings of 2005 International Conference on , vol.2, no., pp.882,887 Vol. 2, 18-21 Aug. 2005

[16] Kuo, A.D., "An optimal control model for analyzing human postural balance," Biomedical Engineering, IEEE Transactions on , vol.42, no.1, pp.87,101, Jan. 1995

[17] Q. Wu, N. Sepehri, A. B. Thornton-Trump and M. Alexander, Stability and control of human trunk movement during walking, Comput. Meth. Biomech. Biomech. Eng. 1 (1998) 247–259.

[18] Hemami, H.; Stokes, BradFord T., "A Qualitative Discussion of Mechanisms of Feedback and Feedforward in the Control of Locomotion," Biomedical Engineering, IEEE Transactions on , vol.BME-30, no.11, pp.681,689, Nov. 1983

[19] A. D. Kuo, D. M. Donelan and A. Ruina, Energetic consequences of walking like an inverted pendulum: Step to step transitions, Exercise Sports Sci. Rev. 33 (2005) 88–97.

[20] T. McGeer, Passive dynamic walking, Int. J. Robotics Res. 9 (1990) 62–82.

[21] R. Goddard, H. Hemami, and F. Weimer, “Biped side step in the frontal plane,” IEEE Transactions on Automatic Control, vol. 28, no. 2, pp. 179–187, February 1983.

[22] S. Kajita and K. Tani, “Study of dynamic biped locomotion on rugged terrain-derivation and application of the linear inverted pendulum mode,” in Proceedings of the IEEE International Conference on Robotics and Automation, vol. 2, April 1991, pp. 1405–1411

[23] J. Pratt and R. Tedrake, “Velocity based stability margins for fast bipedal walking,” in First Ruperto Carola Symposium in the International Science Forum of the University of Heidelberg entitled “Fast Motions in Biomechanics and Robots”, Heidelberg Germany, September 7-9 2005.

[24] D. Winter, “Human balance and posture control during standing and walking,” Gait and Posture, vol. 3, no. 4, pp. 193–214, December 1995.

[25] F. Horak and L. Nashner, “Central programming of postural movements: adaptation to altered support-surface configurations.” Journal of Neurophysiology, vol. 55, no. 6, pp. 1369–1381, 1986.

[26] B. Makai andW. McIlroy, “The role of limb movements in maintaining upright stance: the ”change-in-support” strategy,” Physical Therapy,vol. 77, no. 5, pp. 488–507, May 1997.

[27] M. Vukobratovic, A. A. Frank, and D. Juricic, “On the stability of biped locomotion,” IEEE Transactions on Biomedical Engineering, pp. 25–36, January 1970.

[28] C. Galliday and H. Hemami, “Postural stability of the two-degree of-freedom biped by general linear feedback,” IEEE Transactions on Automatic Control, vol. 21, no. 1, pp. 74–79, February 1976.

[29] H. Hemami and B.-R. Chen, “Stability analysis and input design of a two-link planar biped,” The International Journal of Robotics Research, vol. 3, no. 2, pp. 93–100, 1984

[30] S. Kajita, F. Kanehiro, K. Kaneko, K. Fujiwara, K. Harada, K. Yokoi, and H. Hirukawa, “Biped walking pattern generation by using preview control of zero-moment-point,” in Proc. IEEE Int. Conf. Robot. Auton., Taipei, Taiwan, Sep. 14–19, 2003, vol. 2, pp. 1620–1626.

[31] T. Sugihara, Y. Nakamura, and H. Inoue, “Real-time humanoid motion generation through ZMP manipulation based on inverted pendulum control,” in Proc. IEEE Int. Conf. Robot. Auton., Washington, DC, USA, May 2002, pp. 1404–1409.

[32] C. Zhu and A. Kawamura, “Walking principle analysis for biped robot with ZMP concept, friction constraint, and inverted pendulum model,” in Proc. IEEE/RSJ Int. Conf. Intell. Robots Syst., Las Vegas, CA, USA, Oct. 27–31, 2003, vol. 1, pp. 364–369.

[33] B. Vanderborght, V. Verrelst, R. V. Ham, M. V. Damme, and D. Lefeber, “Objective locomotion parameters based inverted pendulum trajectory generator,” Robot. Auton. Syst., vol. 56, no. 9, pp. 738–750, 2008.

[34] A. Albert and W. Gerth, “Analytic path planning algorithms for bipedal robots without a trunk,” J. Intell. Robot. Syst., vol. 36, no. 2, pp. 109–127, 2003.

[35] Tzuu-Hseng S. Li, Yu-Te Su, Shao-Hsien Liu, Jhen-Jia Hu, and Ching-Chang Chen, “Dynamic Balance Control for Biped robot walking using sensor fusion, Kalman filter, and Fuzzy Logic,” IEEE Transactions on Industrial Electronics, Vol. 59, No. 11

[36] Hsin-Yu Liu, Wen-June Wang, Rong-Jyue Wang, “A Course in simulation and demonstration of humanoid robot motion,” IEEE Transactions of Education, Vol. 54, No. 2, 2011.

[37] K. Harada, S. Kajita, K. Kaneko, and H. Hirukawa, “An analytical method on real-time gait planning for a humanoid robot,” in Proc. IEEE /RAS Int. Conf. Human. Robot. Los Angeles, CA, USA, Nov. 10–12, 2004, vol. 2, pp. 640–655.

[38] M. Morisawa, K. Harada, S. Kajita, K. Kaneko, F. Kanehiro, K. Fujiwara, S. Nakaoka, and H. Hirukawa, “A biped pattern generation allowing immediate modification of foot placement in real-time,” in Proc. IEEE /RAS Int. Conf. Human. Robot. (Humanoids), Genova, Italy, Dec 4–6, 2006, pp. 581–586.

[39] S. Kajita, F. Kanehiro, K. Kaneko, K. Yokoi, and H. Hirukawa, “The 3D Linear inverted pendulum mode: A simple modeling for a biped walking pattern generation,” in Proc. IEEE /RSJ Int. Conf. Intell. Robots Syst., Oct. 29–Nov. 03, 2001, vol. 1, pp. 239–246

[40] A. Goswami, “Postural stability of biped robots and the foot-rotation indication (fri) point,” International Journal of Robotics Research, vol. 18, no. 6, pp. 523–533, June 1999.

[41] K. Hirai, M. Hirose, Y. Haikawa, and T. Takenaka, “The development of honda humanoid robot,” in Proceedings of the 1998 IEEE International Conference on Robotics and Automation, vol. 2, May 1998, pp. 1321–1326.

[42] Kajita, S.; Tani, K.; "Experimental study of biped dynamic walking in the linear inverted pendulum mode," Robotics and Automation, 1995. Proceedings., 1995 IEEE International Conference on , vol.3, no., pp.2885-2891 vol.3, 21-27 May 1995

[43] Masaki Ogino, Embodiment Approaches to Humanoid Behavior –Energy efficient walking and visuo-motor mapping, Ph.D. Thesis, Osaka University, 2005

[44] Honda Motor Co. ASIMO. http://world.honda.com/ASIMO/technology/walking_02.htm

[45] HRP-2 [AIST. HRP-2. http://www.kawada.co.jp/global/ams/hrp_2.html, 1998-2002

[46] The University of Tokyo. UT-Theta. http://www.ynl.t.u-tokyo.ac.jp/research/theta/theta.html, since 2001

[47] T. Sugihara and Y. Nakamura, “Whole-body cooperative balancing of humanoid robot using cog jacobian’,” 2002 IEEE/RSJ International Conference on Intelligent Robots and Systems, pp. 2575–2580, 2002

[48] C. Ott, D. Lee, and Y. Nakamura, “Motion capture based human motion recognition and imitation by direct marker control,” IEEE-RAS International Conference on Humanoid Robots 2008, pp. 399–405, 2008.

[49] J. P. Scholz and G. Sch¨oner, “The uncontrolled manifold concept: identifying control variables for a functional task,” Exp Brain Res, vol. 126, no. 3, pp. 289–306, Jun 1999.

[50] M. H. P. Dekker, “Zero-moment point method for stable biped walking,” Internship report, Eindhoven, 2009

[51] Tzafestas, S., Raibert, M., and Tzafestas, C., 1996, Robust Sliding-mode Control Applied to a 5-Link Biped Robot, Journal of Intelligent and Robotic Systems, Vol. 15, pp. 67-133.

[52] AGonzalez-Fierro, M.; Balaguer, C.; Swann, N.; Nanayakkara, T., "A humanoid robot standing up through learning from demonstration using a multimodal reward function," Humanoid Robots (Humanoids), 2013 13th IEEE-RAS International Conference on , vol., no., pp.74,79, 15-17 Oct. 2013

[53] Aguilar-Ibaez, C.; Gutierrez, O.F.; Sossa-Azuela, H., "Control of the Furuta Pendulum by using a Lyapunov function," Decision and Control, 2006 45th IEEE Conference on , vol., no., pp.6128,6132, 13-15 Dec. 2006

[54] Dragomir N. Nenchev, Akinori Nishio, “Experimental Validation of ankle and hip strategies for balance recovery with a biped subjected to an impact,” International Conference on Intelligent Robots and Systems, San Diego, CA, 2007

[55] M. Nahon and J. Angeles, “Minimization of power losses in cooperating manipulator,” J. Dyn. Syst. Meas. Control (Trans. ASME), vol. 114, no. 2, pp. 213–219, 1992.

[56] J. Kober, J. A. Bagnell, and J. Peters, “Reinforcement Learning in Robotics: A Survey,” Int. J. Robot. Res., p. 0278364913495721, Aug. 2013.

[57] R. Tedrake, T. W. Zhang, and H. S. Seung, “Learning to walk in 20 minutes,” in Proceedings of the Fourteenth Yale Workshop on Adaptive and Learning Systems, 2005, vol. 95585.

[58] G. Endo, J. Morimoto, T. Matsubara, J. Nakanishi, and G. Cheng, “Learning CPG-based Biped Locomotion with a Policy Gradient Method: Application to a Humanoid Robot,” Int. J. Robot. Res., vol. 27, no. 2, pp. 213–228, Feb. 2008.

[59] T. Geng, B. Porr, and F. Wörgötter, “Fast biped walking with a reflexive controller and real-time policy searching,” in Advances in Neural Information Processing Systems, 2005, pp. 427–434.

[60] E. C. Whitman and C. G. Atkeson, “Control of Instantaneously Coupled Systems applied to humanoid walking,” in 2010 10th IEEE-RAS International Conference on Humanoid Robots (Humanoids), 2010, pp. 210–217.

[61] S. Kuindersma, R. Grupen, and A. Barto, “Learning dynamic arm motions for postural recovery,” in 2011 11th IEEE-RAS International Conference on Humanoid Robots (Humanoids), 2011, pp. 7–12.

[62] L. Ljung. System Identication - Theory for the User. Prentice-Hall, Upper Saddle River, N.J., 2nd edition, 1999.

[63] R. S. Sutton and A. G. Barto, Reinforcement learning: an introduction. Cambridge, Mass: MIT Press, 1998.

[64] Power Usage Reduction of Humanoid Standing Process using Q-Learning, Ercan Elibol, Juan Calderon, Martin Llofriu, Wilfrido Moreno, and Alfredo Weitzenfeld, RoboCup 2015, Robot Soccer World Cup XIX . China, 2015 (accepted)

ABOUT THE AUTHOR

Ercan Elibol graduated from Istanbul University with a Bachelor of Science in Electronics Engineering. After completion of his undergraduate studies, his graduate study began at Indiana State University, where he earned his Master of Science degree in Electronics and Computer Technology in 2002. After his graduate study, he worked in the IT industry in Turkey as a network analyst for about a year. After working in IT, he returned to academia to start his graduate study again to complete his doctoral degree requirements at the University of South Florida in 2015.